INFORMATION TO USERS

This manuscript has been reproduced from the microfilm master. UMI films the text directly from the original or copy submitted. Thus, some thesis and dissertation copies are in typewriter face, while others may be from any type of computer printer.

The quality of this reproduction is dependent upon the quality of the copy submitted. Broken or indistinct print, colored or poor quality illustrations and photographs, print bleedthrough, substandard margins, and improper alignment can adversely affect reproduction.

In the unlikely event that the author did not send UMI a complete manuscript and there are missing pages, these will be noted. Also, if unauthorized copyright material had to be removed, a note will indicate the deletion.

Oversize materials (e.g., maps, drawings, charts) are reproduced by sectioning the original, beginning at the upper left-hand corner and continuing from left to right in equal sections with small overlaps.

UMI®

Development of Zeolite based Acid Catalysts for the Hydroisomerization of *n*-Paraffins

Mohammad Ali Saberi

A Thesis

in

The Department

of

Chemistry & Biochemistry

Presented in Partial Fulfilment of the Requirement

for the Degree of Doctor of Philosophy at

Concordia University

Montreal, Quebec, Canada

August 2002

© Mohammad Ali Saberi

0-612-73338-6

Canada

ABSTRACT

Development of Zeolite based Acid Catalysts for the Hydroisomerization of *n*-Paraffins

Mohammad Ali Saberi, Ph. D

Concordia University, 2002

There are some abundant long chain *n*-alkanes in refinery stream fuels which have a lower octane number and a higher pour point. It would be thus desirable to convert these normal paraffins to their branched isomers (which have higher octane number). Novel classes of cation incorporated Pt-M-HY (M being cations such as Zn^{2+}, Al^{3+}, Cd^{2+}, Ni^{2+}, Cr^{3+} and some others) and bifunctional Pt-HY zeolite catalysts have been prepared and tested for hydroisomerization of *n*-Paraffins (*n*-heptane as a model). The modified zeolite catalysts showed superiority to that of the parent bifunctional Pt-HY zeolite catalyst in term of isomerization of *n*-heptane. This is due to the desorption-transfer promoting behavior of the mentioned cations which cause fast removal of intermediate alkylcarbocation from Brønsted acid sites (decreasing the residence time of these species on acid sites). By decreasing the residence time of the intermediate alkylcarbocations on Brønsted acid sites, these species did not undergo further cracking reactions. As a result the isomerization products increased significantly and cracked products decreased. Such behavior was ascribed to the formation of new desorption-transfer promoting sites.

A triangular "acid/dehydro-hydrogenation/desorption-transfer promoting" site configuration (trifunctional catalyst) was proposed. The data obtained from characterization studies such as BET, XRD, FTIR and NH_3-TPD show that cationic species do not effect: pore size distribution, surface area, crystallinity, dehydrogenation-hydrogenation (Pt) site, and Brønsted acid site density and strength. No significant ion-exchange was observed upon Zn^{2+}, Al^{3+}, Cd^{2+}, Ni^{2+} and Cr^{3+} loading at the reaction conditions. These species only create some Lewis acid sites of which the acid character appeared to play an important role in the enhancement of the isomerization activity. Our concept of trifunctional catalyst suggests that Zn^{2+} and other ions behave as sorption competitors to the zeolite Brønsted acid sites. As a result, the isomerization activity of zeolite increased where the effect of Zn^{2+} was higher than the other cations. In addition the simultaneous incorporation Zn^{2+} or the other cations with Pt species gave better results than that of the sequential loading.

With increasing reaction temperature more acid sites were activated and became involved in the reaction, thus, each reaction temperature needed a specific Zn^{2+} loading in order to provide the best isomerization activity, and a higher amount of zinc was required at higher reaction temperature where the cracking activity is stronger.

The kinetic studies showed that the behavior of the trifunctional Pt-Zn_y-HY was significantly different than that of the bifunctional Pt-HY zeolite catalyst. All kinetic data showed a drastic reduction of cracking (β-scission) within the temperature range of 195 °C - 240 °C.

ACKNOWLEDGMENTS

I wish to express my sincere gratitude to my thesis supervisor Dr. Raymond Le Van Mao for his precious guidance and direction throughout the course of this research work and preparation of this thesis.

I would also like to thank the members of my research committee, Dr. O. S. Tee, Dr. G. Dénès and Dr. P. H. Bird for their time and helpful suggestions during research.

I wish to give my special thanks to Dr. P. B. M. Joyce for his helpful suggestions and for his patience in reading this manuscript.

I would like to give my special thanks to Dr. T. Si Le for his great help during my research work.

I am greatly indebted to my aunts Shahrbano, Tokaz, to Dr. M. Naersefat, Mrs Hoorieh, A. Esmaiely, to my brothers A. Asgar, Abolfazl, Hossein, to my sisters Fatemeh, Masomeh, Zakieh, Zahra and Batol for their precious support and continuous encouragement.

I also thank to my friends who helped me during my research works, studying and their friendship, Dr. S. Y. Xiao, Dr. A. Muntasar, Dr. B. Alijani, Dr. A. Owlia, Dr. I. Bayat, Dr. F. Alavimogadam, Dr. M. Kasrai, Dr. P. Sioshansi, Mr. B. Nabardi, Mr. Meysami Mr P. Kletnieks Mr. N. Al-yassir.

I also wish to express my sincere thanks to Mrs Carole Coutts for giving me good advices during my study.

Finally, I dedicate this thesis to my wife V. Nadersefat my son Aydin and my daughter Ayda for their love, understanding and believing in me.

In precious memory of my father Mr. Ali H. Saberi

And my mother Mrs Fatemeh B. Shahmoradi

Table of Contents

Appendices   221

List of Figures

Chapter II

Chapter III

List of Tables

LIST OF ABBREVIATIONS

AAS	Atomic Absorption Spectroscopy
ACl	Acid Site
$\mathbf{A_{crk}}$	Preexponential Factor of Cracking
$\mathbf{A_{iso}}$	Preexponential Factor of Isomerization
AFSY	Ammonium Fluorosilicate Treated Y Zeolite
BET	Brunauer, Emmett and Teller
BTX	Benzene, Toluene and Xylene
$\mathbf{C_{cr}}$	Conversion to Cracked products
$\mathbf{C_{mo}}$	Conversion to Mono-Branched Heptanes
$\mathbf{C_{mu}}$	Conversion to Multi-Branched Heptanes
$\mathbf{C_t}$	Toal n-Heptane Conversion
CPCP	Corner Protonated Cyclopropane
DES	Desorption-Transfer Promoting Site
DHY	Dehydro-Hydrogenation Site
DRIFTS	Diffuse Reflectance Infrared Fourier Transform Spectroscopy
$\mathbf{\Delta E_{iso}}$	Apparent Activation Energy of Isomerization
$\mathbf{\Delta E_{crk}}$	Apparent Activation Energy of Cracking
$\mathbf{(E_a)_{bi}}$	Apparent Activation Energy of Bifunctional (Pt-HY) Catalyst
$\mathbf{(E_a)_{tri}}$	Apparent Activation Energy of Trifunctional (Pt-Zn-HY) Catalyst
EPCP	Edge Protonated Cyclopropane
FID	Flame Ionization Detector
FPCP	Face Protonated Cyclopropane
ETBE	Ethyl Tertiary Butyl Ether

FTIR	Fourier Transform Infrared Spectroscopy
GC	Gas Chromatograph
IR	Infrared Spectroscopy
Iso/Crk	Composite Selectivity ratio
k_{crk}	Rate Constant of Cracking Reaction
k_{iso}	Rate Constant of Isomerization Reaction (Branched Heptanes)
k_{cr}^{0}	Cracking Rate Constants at Zero Contact Time
k_{mo}^{0}	Mono-Branched C_7 Rate Constants at Zero Contact Time
k_{mu}^{0}	Multi-Branched C_7 Rate Constants at Zero Contact Time
k_{t}^{0}	Total Rate Constants at Zero Contact Time
MASNMR	Magic Angle Spinning Nuclear Magnetic Resonance
mo	Mono-Branched Heptane
mu	Multi-Branched Heptane
MON	Motor Octane Number
MTBE	Methyl Tertiary Butyl Ether
M^{y}-**Pt-HY**	Sequential Incorporation of Pt and Cation
NMR	Nuclear Magnetic Resonance
Pt-M$_y$-HY	Simultaneous Incorporation of Pt and Cation
Pt-Al$_{ey}$-HY	External Configuration
R	Product Selectivity
r_{cr}	Rate of Formation of Cracking Products
r_{mo}	Rate of Formation of Mono-Branched Heptanes
r_{mu}	Rate of Formation of Multi-Branched Heptanes
r_{t}	Total Reaction Rate
RC	Relative Crystallinity

RE	Rare Earth
RON	Research Octane Number
S_{C7}	Selectivity to C_7 Isomers
S_{crk}	Selectivity to Cracking Products
S_{iso}	Selectivity to Branched Heptanes
S_{mo}	Selectivity to Mono-Branched C_7 Products
S_{mu}	Selectivity to Multi-Branched C_7 Products
TAME	Tertiary Amyl Methyl Ether
TCD	Thermal Conductivity Detector
TEL	Tetraethyllead
TGA	Thermogravimetric Analysis
TML	Tetramethyllead
TPD	Temperature Programmed Desorption
τ	Contact Time
USY	Ultrastable Y zeolite
WHSV	Weight Hourly Space Velocity
XRD	X-Ray Powder Diffraction
Y_{iiso}	Yield of $(C_5\text{-}C_7)$ branched paraffins

CHAPTER I

INTRODUCTION

AND

CRITICAL REVIEW OF LITERATURE

1.1 Petroleum and Petroleum Refining

Petroleum or crude oil can be regarded broadly as a mixture of hydrocarbons and hydrocarbon derivatives that occurs naturally in the earth. On a molecular basis, petroleum is a complex mixture of hydrocarbons plus organic compounds of sulphur, oxygen, and nitrogen, as well as compounds containing metallic constituents, particularly, vanadium, nickel, iron and copper. Hydrocarbons can account for more than 75% of the constitutions of crude oil, and are of three classes: the alkanes (or paraffins), the cycloalkanes (or naphthenes), and the aromatic compounds [1].

Petroleum products derived from crude oil are a convenient source of energy (about 90%) and raw chemicals (about 10%). The separation of petroleum into fractions and the subsequent treating of these fractions to make them into petroleum products is called petroleum refining. Distillation is the key operation in this process [2] and straight run gasoline is generated from the distillation of crude oil, without any other chemical treatments. However, the quality (lower octane number) and total yield of straight run gasoline from crude oil is not adequate to meet market demands for gasoline [3]. Figure 1.1 shows the processing sequence in a modern refinery of high complexity, indicating major process flows between operations [4].
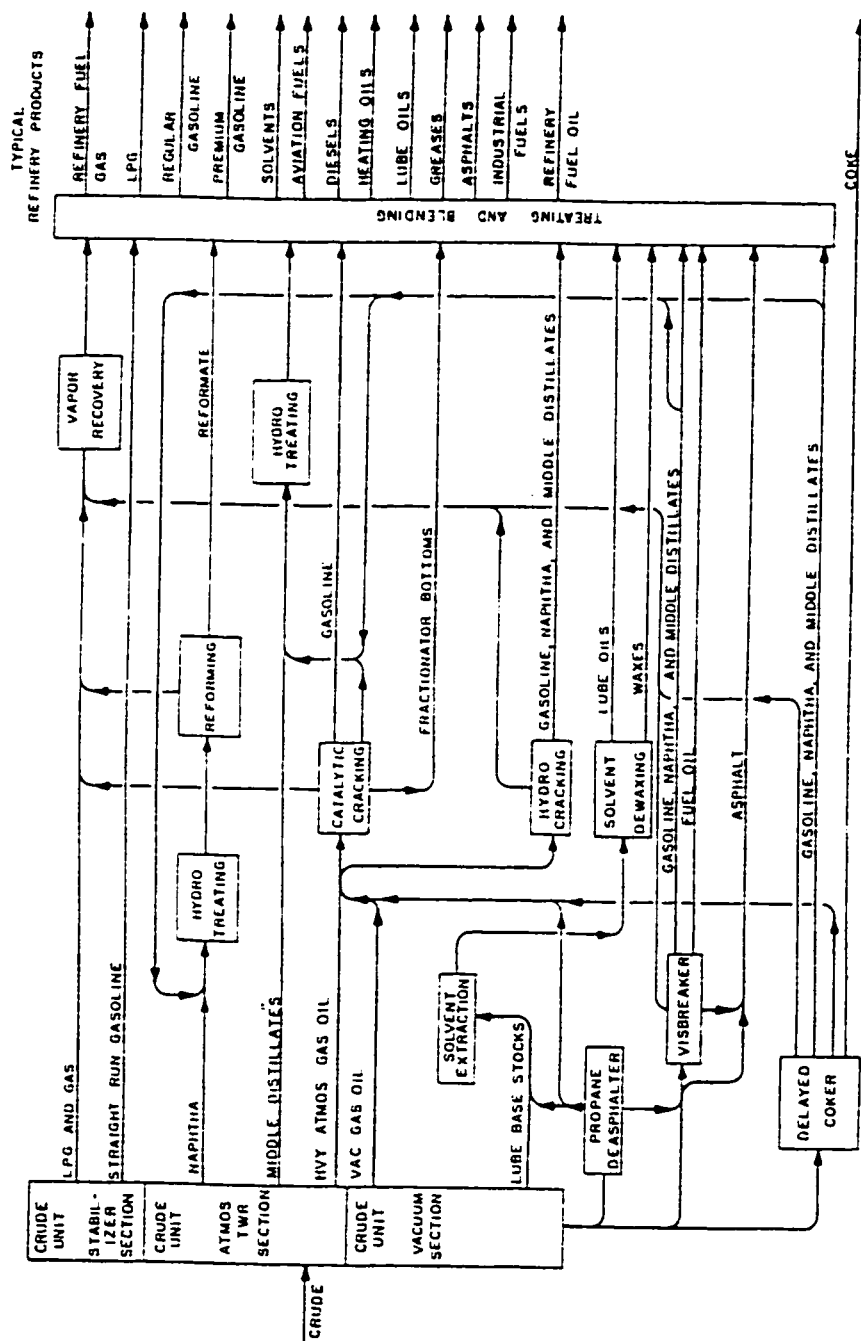
Figure 1.1. Refinery flow diagram (ref. 4).

1.2 Gasoline and its antiknocking properties

The gasolines are colorless blends of volatile liquid-petroleum fractions which boil within the temperature range of about 30 to 200 °C. Generally, motor gasolines cover the whole of this distillation range, with a typical relative density of about 0.73 g/ml. In contrast the distillation range for aviation gasolines is limited to between 50 and 170 °C. Most refiners produce gasoline in two or three grades (unleaded regular, premium and super-premium), with the principal difference among them being their antiknock performance [5]. As mentioned before, the combustion performance of straight run gasoline in modern automobile engines is not satisfactory. Ideally in a well-tuned engine there will be no instant of time during the combustion stroke when some portion of the air-fuel mixture is not burning, so that the energy from the fuel is released uniformly and not violently. However, it is possible that the unburned air-fuel mixture be compressed to a point at which the temperature and density are high enough to cause all of the remaining unburned mixture to ignite at once. The resulting explosion is severe enough that it is audible to the driver, and is the phenomenon known as engine knock. The octane number of gasoline is related to its antiknock tendency. Importantly the octane numbers of the individual hydrocarbons are not the same. After much development work, iso-octane (2,2,4-trimethylpentane) and n-heptane were selected, and given arbitrary ratings of 100 and 0, respectively. Two octane numbers are used to define octane quality: 1) Research Octane Number (RON), measured at low speed under relatively mild driving conditions. 2) Motor Octane Number (MON), measured at high speed under high-severity conditions [6] The octane number of some pure hydrocarbons are shown in (Table 1.1) [7].

Hydrocarbon	Actual		Blending*	
	RON	MON	RON	MON
Paraffins				
n-Butane	93		113	114
n-Pentane	62	62	62	67
2-Methylbutane	92	90	99	104
2,2-Dimethylpropane	85	80	100	90
n-Hexane	25	26	19	22
2,2-Dimethylbutane	92	93	89	97
n-Heptane	0	0	0	0
2,2-Dimethylpentane	93	96	89	93
2,2,3-Trimethylbutane	>100	>100	113	113
2,2,3-Trimethylpentane	100	100	105	112
2,2,4-Trimethylpentane	100	100	100	100
Olefins				
1-pentene	91	77	152	135
2-Methyl-2-butene	97	85	176	141
3-Methyl-2-pentene	97	81	130	118
4-Methyl-2-pentene	99	84	130	128
2,2,4-Trimethyl-1-pentene	>100	86	164	153
2,2,4-Trimethyl-2-pentene	>100	86	148	139
Aromatics				
Benzene	>100	>100	99	91
Toluene	>100	>100	124	112
O-Xylene	>100	>100	120	103
m-Xylene	>100	>100	145	124
p-Xylene	>100	>100	146	127
Ethylbenzene	>100	98	124	107
1,3,5-Trimethylbenzene	>100	>100	171	137
Propylbenzene	>100	98	127	129
Isopropylbenzene	>100	99	132	124
Naphthenes				
Cyclopentane	101	85	141	141
Methylcyclopentane	91	80	107	99
Cyclohexane	83	77	110	97
Methylcyclohexane	75	71	104	84
o-Dimethylcyclohexane	81	79	85	83
m-Dimethylcyclohexane	67	64	67	65
p-Dimethylcyclohexane	68	65	66	63

*) Blending octane numbers are obtained by blending 20 vol% of the specific hydrocarbon in 80 vol% of 60/40 iso-octane/n-heptane mixture.

Table 1.1. Octane number of pure hydrocarbons (ref. 7).

The lower octane number of the straight run gasoline leads to its low antiknock performance. Therefore it is necessary to blend the higher octane number hydrocarbons or other chemicals into the straight run gasoline to increase its octane number and suppress engine knock. In the early 1920's it was discovered that the antiknock behavior of gasoline could be improved by adding tetraethyllead, $(C_2H_5)_4Pb$ [3]. Since that time tetraethyllead (TEL) and other lead compounds such as tetramethyllead (TML) have been widely used for their remarkable effectiveness in suppressing knock. However, due to their detrimental effects on human health such as lower IQ, hyperactivity, reducing learning ability as well as their deactivating action on catalytic mufflers such as catalyst surface coverage, the use of lead compounds in gasoline has been banned in most developed countries. For many years aromatic compounds mostly benzene, toluene and xylene (BTX) have been used as substitutes to lead. Recently, even BTX content in gasoline has been reduced as some of them are carcinogen, ozone-forming or toxic [8]. As alternate sources of octane additives refiners have suggested oxygenates with high octane number such as alcohols (ethanol, methanol) and ethers such as methyl tert-butyl ether (MTBE), ethyl tert-butyl ether (ETBE) and tert-amyl methyl ether (TAME) [8,9,10]. The use of MTBE and ETBE are at risk of ban starting from state of California (USA) because they have a higher solubility in ground water as compared to regular gasoline, and because the emission of CO_2 and CO is higher using ETBE [11,12]. Other ways to increase the octane number of gasolines may include alkylation of isobutane with butenes to yield of branched C_8 octane-boosting additives [13,14] or the isomerization of n-paraffins to isoparaffins, so that less polluting gasolines can be produced [15,16,17].

1.3 Cracking processes for the production of gasoline

As mentioned before, the total yield of straight run gasoline is not adequate to meet today's demands for gasoline. Cracking of heavier molecules is a method that can be used to increase the yield of products in the gasoline range from crude oil at the expense of other less desirable petroleum fractions [18].

Cracking in the petroleum chemistry refers to the breakdown of high-molecular weight hydrocarbons to lower-molecular weight ones through the chemical cleavage of C-C bonds.

1.3.1 Thermal Cracking

Thermal cracking is the process by which heat is applied so that the higher molecular weight materials are broken down into smaller molecules in the absence of a catalyst. This radical type process was developed shortly before World War I [19,20].

1.3.2 Catalytic Cracking

Catalytic cracking is the process of heating the higher molecular weight materials under pressure and in the presence of an acidic catalyst [21,22]. Fixed bed catalytic cracking was first developed commercially in 1936 as a result of work done by Eugene Houdry in the late 1920's [18]. Significantly, cracked

gasoline has less tendency to knock than straight-run gasoline and gasolines obtained from catalytic cracking have even higher antiknock value than those generated by thermal cracking [23].

1.4 Zeolites and their new developments

Zeolites are solid materials, which have been used as catalysts for many reactions in recent decades, especially as bifunctional catalysts. In contrast to monofunctional catalysts, a synergism exists between the two sets of sites in bifunctional catalysts leading to an enhanced catalytic activity, suppressed deactivation, and higher yields of products with tertiary and quaternary C atoms. Several innovations in applied catalysis developed since 1980 which a substantial number of them are based on zeolites and related solids is shown in (Table 1.2) [24,25]. Specially, for the purposes of this discussion many types of zeolite catalysts have been developed and used for hydrocarbon conversion processes in the petroleum refining industry. Processes involving zeolites include, for example, dewaxing, hydrodewaxing, alkylation, isomerization, cracking, aromatization, disproportionation, and the like [26,27,28].

Indeed, some breakthroughs have gone beyond the "old" definition of zeolite. Zeolites have always been defined as crystalline aluminosilicate materials that are constructed from TO_4 tetrahedra (T= tetrahedrally coordinated atom, e.g., Si, Al); each apical oxygen atom is shared with an adjacent tetrahedron. So the framework ratio of O/T is always equal to 2.

Process	Catalyst
conversion of ethane and benzene to ethyl benzene	**H-ZSM-5**
methanol to gasoline (petrol)	**H-ZSM-5**
conversion of ethane and acetic acid to vinyl acetate	Pd
oxidation of tert-butyl alcohol to methylmethacrylate	Mo oxide
improved means of liquefying coal	Co, Ni sulfide
production of diesel fuel from CO+H₂ (syngas)	Co
hydrotreating of hydrocarbons	**Pt Or Ni/Zeolite**
catalytic distillation (in MTBE production)	acidic ion exchange resins
vitamin K₄ production	Pd membrane
dehydrocyclization ('Cyclar process') of alkanes	**Ga-ZSM-5**
conversion of light alkanes to aromatics	**Ga-ZSM-5**
oxidation of methacrolein, hydration of isobutene	Mo-V-P heteropolyacid
polymerization of tetrahydrofuran	Phase-transfer catalysis
production of dimethylcarbonate from acetone	CuCl
conversion of phenol to hydroquinone and catechol	**Ti-silicalite**
isomerization of but-1-ene to 2-methylpropene	**H-ferrierite,H-teta-1(zeolite)**
isomerization of oxime of cyclohexanone to ε-caprolactam	**SAPO-11**
ammoxidation of cyclohexanone to its oxime using H₂O₂	**Ti-silicalite**
production of acrylamide from vinyl cyanide	immoblized nitrile hydratase
complete combustion of natural gas (at ca.1300 °C)	noble oxides
sweetening of natural gas by selective oxidation of H₂S to S	mixed oxides
oxidation of benzene to phenol via cyclohexene	**zeolites**
methanol to light alkenes	Silico-alumino-phosphate
olefin oligomerization ("Shell" process)	**Zeolites**
production of L-aspartic acid and L-analine from NH₄ fumarate	immobilized micro-organisms
toluene cis-1,2-dihydroxy-3-methylbenzene from toluene	pseudomonas pudita
production of 2,6-diiopropylnaphthalene using propene	**mordenite**
decomposition of hypochlorite	NiO
dehydration of alkanols	heteropolyacid salts
conversion of hydrocarbons	**X,Y,ZSM-5,ZSM-20,β-zeolite**
dehydroisomerization of n-butene	**Pt-ZSM-5 zeolite**
cyclohexane to cyclohexanol and cyclohexanone	microporous alumino-phophates
adipic acid by aerial oxidation of cyclohexane	FeAlPO-5, FeAlPO-31
aerial oxidation of n-hexane to adipic acid	molecular sieve catalyst

Table 1.2. Innovations in applied catalysis since 1980 (ref. 24-28).

Zeolites maybe represented by the empirical formula [29].

$$M_{x \cdot n} [(AlO_2)_x \ (SiO_2)_y] \cdot wH_2O \tag{1.1}$$

where M is an n-valent cation, w is the number of water molecules and y/x is called the Silicon-Aluminum (Si/Al) ratio whose value depends on the framework structure of zeolite .

The primary building block of the zeolite structure is a tetrahedron of four oxygen atoms surrounding a central silicon $-(SiO_4)-$ or aluminum atom, $-(AlO_4)-$, as illustrated (Figure 1.2a). A secondary building unit is produced by the joining of these tetrahedra together through shared apical oxygen atoms (Figure 1.2b). By interconnecting of these secondary building units, a wide range of polyhedra is formed (Figure 1.2c), which in turn connect to form the infinitely extended frameworks of the various specific zeolite crystal structures (Figure 1.2d). In these structural diagrams the corners of the polyhedra represent Si or Al atoms, and the connecting lines to the corners represent the shared oxygen atoms [30]. As shown (Figure 1.2), different combinations of the small secondary units give numerous distinctive zeolites.

a

b   4R   6R

c   D4R   D6R

d   Type A   Sodalite   Faujasite
(Type X, Y)
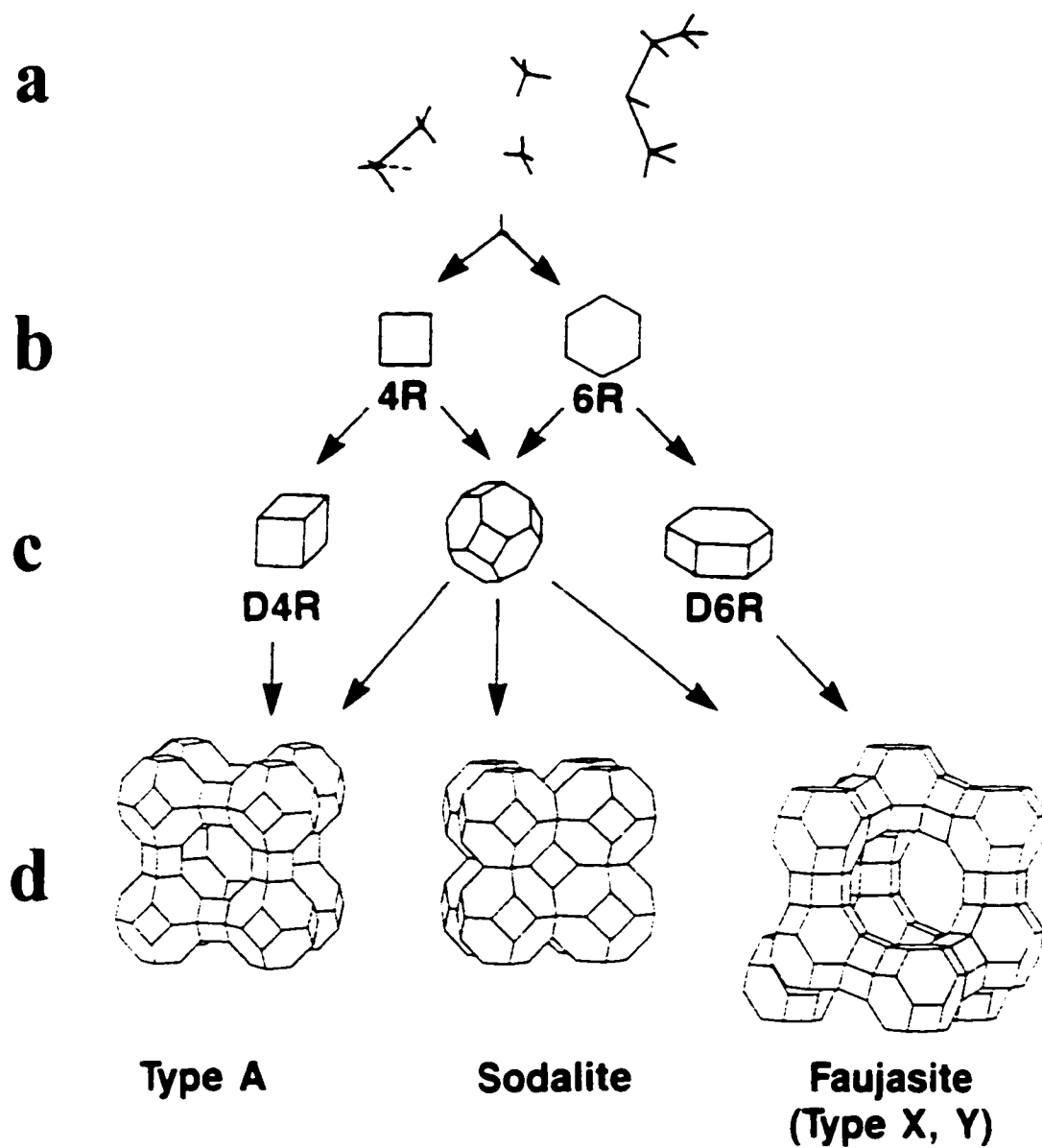
Figure 1.2. The production process of zeolite framework structure (ref. 30).

(a) Primary units; (b) Secondary units;

(c) Tertiary units (polyhedra); (d) Zeolite structure.

Zeolites are crystalline microporous solids containing cavities and channels of molecular dimensions (3 to 10 Å) and are sometimes called molecular sieves. Although as recently as 1982 they would be restricted largely to aluminosilicates in a chemical sense, recent developments suggest that the frameworks of zeolite are no longer constructed solely of the AlO_4 and SiO_4 tetrahedra combinations. The frameworks can contain other metals. Elements such as Ga, Ge, Fe, P, Co, Mn and a few others can be incorporated into the framework structure of this zeolites. Also in some zeolite-like solids, for example, the large family of microporous aluminum phosphates (AlPOs, MAPOs), there are no SiO_4 terahedra [31,32,33,34]. Moreover, in other types of zeolites like titanium-substituted high silica ZSM-5 (TS-1), AlO_4 tetrahedra are absent [35]. In addition, the inorganic oxides no longer exclusively contribute to the framework of zeolites. Recently, it has been reported that some organic solid materials with wide channels have been successfully synthesized [36]. For example, strongly acidic organic polymers such as Amberlyst-15 which contains macropores surrounded by micropores are widely used as catalysts in modern etherification technology [37]. Although these organic zeolite-like structures are fragile compared to inorganic materials, they may be suitable as low-temperature molecular sieves and in specialized catalyst applications.

Finally, the framework of zeolites might possess positive charge in nature, but recently, microporous boron-aluminum chloride with a cationic framework (possess negative charge) has been successfully synthesized [38].

Although to make a positively charged zeolite framework appears difficult using conventional thermal-crystallization methods it could be approached by modification of existing zeolites through insertion or removal of some elements of their framework. These methods have been well developed and desired frameworks such as $ZrPO_4$ and $AlSiPO_4$ have been obtained using these methods [39,40]. Overall, strictly speaking, a zeolite is an aluminosilicate. Thus, molecular sieves with framework atoms other than aluminum and silicon should not be called zeolites. Attention is given only to aluminosilicate type zeolites in this thesis.

The network of linked cavities or pores which form a system of channels throughout the structure is the most important structural feature of zeolites. The windows to these channels and pores form a molecule-sized sieve, hence the well-known name of molecular sieve. The pores are classified in different classes depending on their size: ultramicropores (size < 7 Å or 0.7 nm), micropores (size < 20 Å or 2 nm), mesopores (20 Å or 2 nm< size < 500 Å or 50 nm) and macropores (size > 500 Å or 50 nm) [41]. A pore can have a regular or more commonly, an irregular shape. The selectivity of zeolite catalysts depends on pore dimensions. The dimensions of these pores govern the size and shape of the reactant molecules that may enter, the nature of the reaction intermediates that can form within the cavities and the product molecules may exit. The evolution of zeolite and molecular sieve materials with different pore sizes is shown in (Figure 1.3) [42,43].
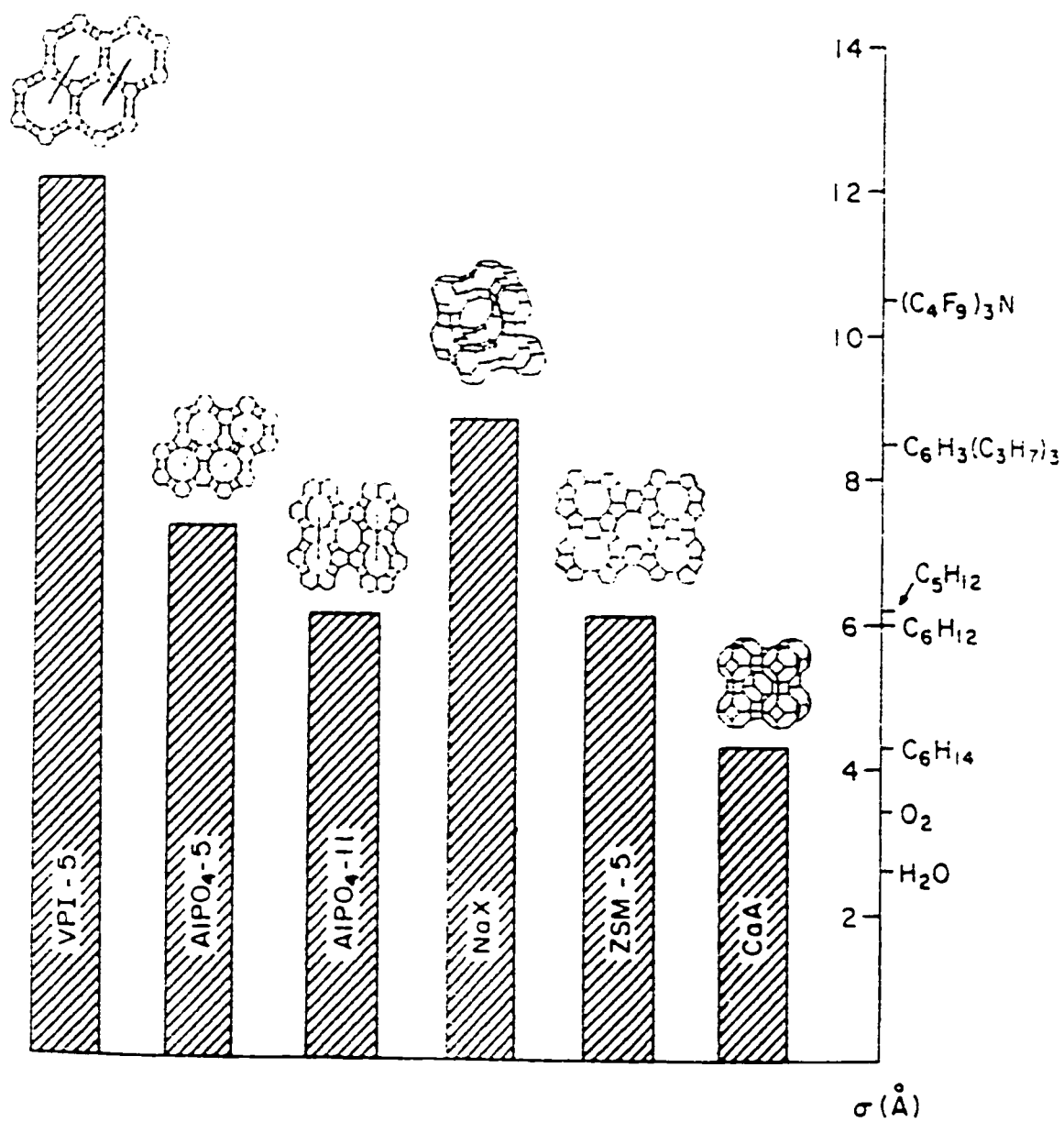
Figure 1.3. Evolution in zeolite and molecular sieve materials (ref. 42,43).

1.4.1 General properties of zeolites

Zeolites share the following properties [44]:

i) zeolites have well defined crystalline structure (X, Y zeolites are cubic with a unit cell dimension of 25 Å) with uniform micropores with one or more discrete sizes

ii) they have high internal surface area (> 600 m²/g)

iii) they show a good thermal stability

iv) zeolites have ability to selectively sorb (sieving effect), and they have ion-exchange capability, producing highly acidic sites when ion-exchanged with protons.

1.4.2 Surface acidity of zeolites

In heterogenous catalytic processes usually three major performance characteristics are considered: activity, selectivity toward one or several products and stability of operation. These performance features are complex, a mixture of various functions for several basic catalytic properties: sorption energies for feeds and products, rates of transport of molecules to and from the active sites, the residence time of intermediates on active sites and intrinsic activities specific for various reactions. The reactivity and selectivity of molecular sieve zeolites as catalysts are determined by active sites generated by an imbalance in charge between the silicon and the aluminum ions in the framework. Since Al is +3, for every aluminum containing tetrahedron there is a net -1 charge which must be balanced by a nearby positive ion.

These compensation cations are relatively mobile and can, in many cases, be easily exchanged for other cations such as proton [45]. Thus, each aluminum atom contained within the framework structure induces a potential active acid site. At these solid surface acid sites, catalyzed reactions exhibit feature similar to reactions catalyzed by mineral acids [46]. It is postulated that the primary requirement for catalytic activity is that the solid be acidic and capable of forming carbenium ions by reactions with unsaturated hydrocarbons [47]. The classical Brønsted and Lewis acid models of acidity have been used to define the active sites on zeolites. Brønsted acidity (proton-donor acidity) occurs in the zeolites when the protons (H$^+$) are balancing the framework anionic charge. Lewis acid (electron acceptor acidity) occurs when a trigonally coordinated aluminum atom and trigonally coordinated Si$^+$, for example, are electron-deficient and accept an electron pair, and thus behave as a Lewis acid as shown in (Figure 1.4) [48]. The compensating cation in the majority of as-synthesized commercial zeolites is either an organic cation or an alkali metal cation. A zeolite surface is illustrated in (Figure 1.5) [49], showing possible types of structures expected to be present at various stages of treatment of a silica rich zeolite. Part (a) shows the as-synthesized material. M$^+$ represents the organic cation or a metal cation (typically Na$^+$). By decomposition of organic cation some protons are produced [50]. Part (b) represents the NH$_4^+$ form of zeolite which is obtained from the sodium form using the ammonium exchange method. Part (c) illustrates the active proton-exchange sites generated by deammoniation using calcination method. The aluminum site with its associated bridged Si-O-H (silanol) is a classical Brønsted acid site and exists in equilibrium with the site depicted in part (d) [51,52,53].
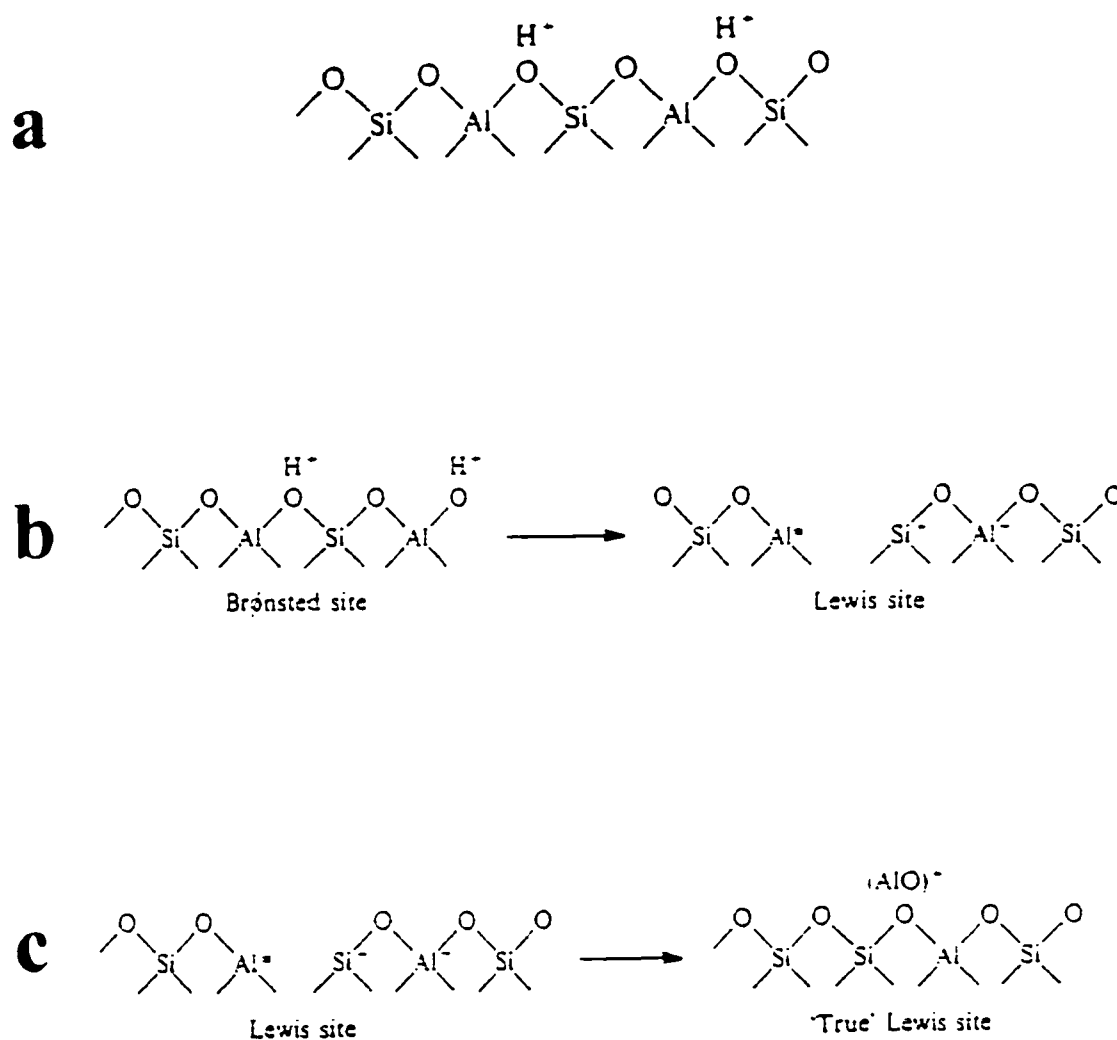
Figure 1.4. The acid site on the surface of zeolite (ref. 48).

(a) Brønsted acid site.

(b) formation of Lewis acid site from Brønsted acid site.

(c) formation of "true" Lewis acid site.
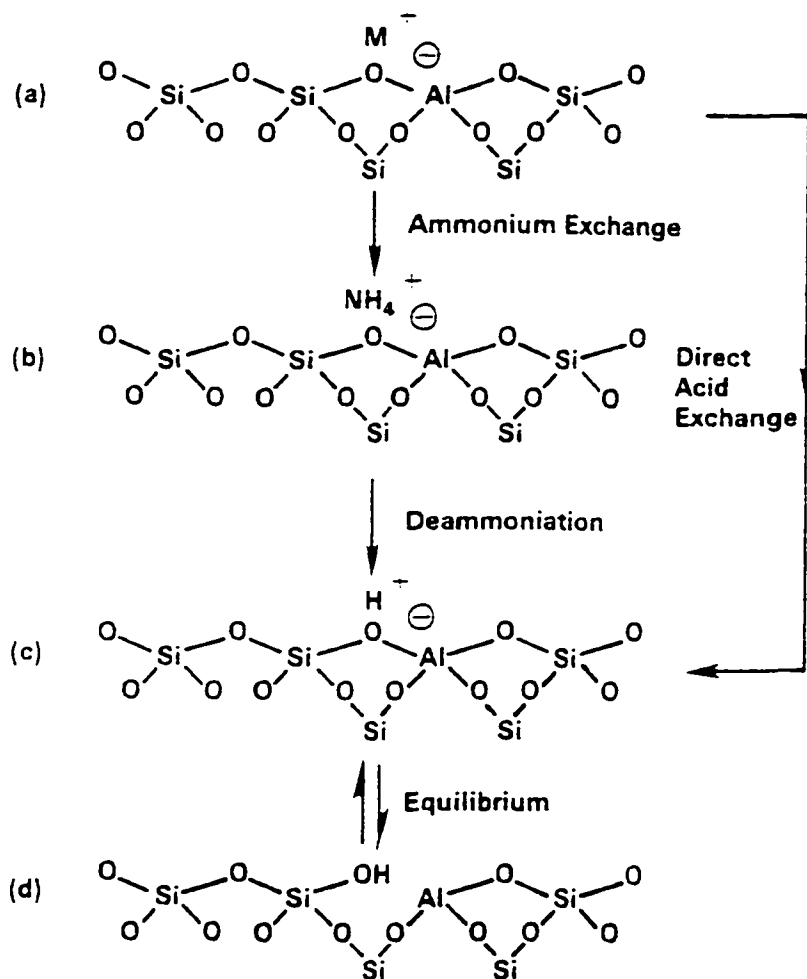
Figure 1.5. Diagram of the surface of zeolite framework (ref. 49).

(a) as-synthesized form, M^+ is either an organic cation or an alkali metal cation.

(b) NH_4^- form, is produced by ion exchanged.

(c) H^-, acid form, is produced by removal of ammonia.

(d) the acid form, is in equilibrium with the form shown in (c).

The major use of zeolite catalysts is as acid catalysts in which the Brønsted and/or Lewis acid sites are catalytically active centers. The acid sites on zeolite catalysts are of considerable interest because it is generally accepted that the surface acidity of zeolite catalysts is responsible for the transformation of various hydrocarbons. Thus, some characterization techniques have been developed to understand the relationship between the catalytic behavior of zeolite and its surface acidity. These techniques include atomic absorption spectroscopy (AAS) [54,55], infrared spectroscopy (IR) [56] and magic angle spinning nuclear magnetic resonance (MASNMR) [57,58,59].

In addition, the catalytic activity of zeolites is also determined by: (i) acid density on the surface of the zeolite, (ii) acid site strength and (iii) acid site accessibility. A wide range of acidity strengths exist in zeolite surface and they are commonly classified as strong, medium and weak acid sites. Acid density is related to the Si/Al ratio in the zeolite structure. If the Si/Al ratio increases the acid density decreases, however, the acid strength increases.

The surface acidity of zeolites is comparable to the inorganic oxyacids $XO_n(OH)_m$. Their acidity strength increases with increasing n and does not depend significantly on the value of m. For example the acid strength of oxyacids containing chlorine increases as the following sequence:

$$Cl(OH) > ClO(OH) > ClO_2(OH) > ClO_3(OH)$$
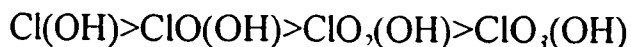
In order to anticipate the acid strength of zeolite the formula of these

materials can be written in the form of $TO_n(OH)_m$ with T being Al+Si. With increasing of Si/Al ratio n increases and m decreases, as a result the acid strength increases with decreasing of acid density [60]. It is worth noting that with increasing of Si/Al ratio some of the lower electronegative Al (1.61) atoms replace with higher electronegative Si (1.9) atoms in the zeolites structure.

Zeolite acidities have been extensively studied using various techniques such as titration, NMR spectroscopy [61], temperature-programmed desorption (TPD) with NH_3 [62], and some other methods using specific probe molecules [63]. CO can be considered as a convenient spectroscopic probe to study the nature of Brønsted acid and Lewis acid sites in zeolites by FTIR-spectroscopy because it combines the softness of a specific probe molecule with a small molecular size [64]. Thus, by using CO adsorption, extensive studies have been devoted to the determination of the acidity in zeolite and aluminophosphates [65,66,67,68]. The interaction of CO molecules via the carbon end with cationic centers which shifts the CO stretching frequency to a higher wave number as compared to that of a free molecule (2143 cm^{-1}). In assaying acidity, probes are needed that measure Brønsted acidity while excluding Lewis acidity. In many cases, such as amine adsorption, both types of acid sites are measured. In special cases, infrared spectroscopy and NMR can differentiate between the two, but the best probes are those that involve the reaction of the surface protons with the probe molecule to form products such as H_2O. Also a combination of the temperature-programmed desorption and thermogravimetric analysis (TPD/TGA) methods measures the total number of Brønsted acid sites to the exclusion of Lewis acids using simple amines. It is well known that

simple amines adsorb as quaternary ammonium ions on Brønsted sites. The best probe molecules are ethylamine and isopropylamine [61]. On the other hand, the term acidity implies both acid density and acid strengths. Nowadays, pyridine and ammonia are routinely used as probes of the acid sites. The FTIR spectroscopy of adsorbed pyridine on zeolite surface shows three bands [69]:

(i) An IR adsorption band near 1540 cm^{-1} characteristic of pyridinium ion (Brønsted-bound pyridine)

(ii) an IR band near 1450 cm^{-1} attributed the coordinated pyridine at Lewis acid sites

(iii) an IR band near 1485 cm^{-1} due to both Lewis and Brønsted-bound pyridine

The surface proton density can be measured using titration of chemisorbed ammonia or using a carbonate solution which liberates CO_2 and acid strength can be determined using the TPD method [61] or FTIR spectroscopy of the low-temperature adsorption of carbon monoxide [64]. An IR study of ZSM-5 zeolite shows two hydroxyl (OH) stretching bands at about 3605 cm^{-1} and 3720 cm^{-1} which have been identified as the hydroxyl stretching associated with the bridging Al-O(H)-Si which characterizes strong Brønsted acid sites [69,53], and the terminal silanol SiOH groups on the crystalline surface respectively [69,50].

1.4.3 Shape selectivity of zeolites

Shape selectivity in molecular sieve catalysis plays a very important role and effects the conversion process. The concept of shape selectivity originated from a consideration of the size of the pore openings in the zeolites in relation to critical dimensions for organic molecules. Shape-selective properties play a key role in enhancing gasoline octane rating when zeolites are used as catalytic additives in gas oil cracking. The size and shape of the molecules diffusing into and out of the zeolite pore network is controlled by shape selectivity. Pore geometry and diffusion limitations are often controlling factors determining catalytic activity and selectivity. The intracrystalline pores and aperture of zeolites have dimensions approximately equal to those of many of the molecules converted in these types of catalytic reactions. As shown in Table 1.3, zeolites are commonly lumped into three pore size classes (small, medium and large) with 8, 10 and 12 tetrahedra in a pore, respectively [70]. Zeolites with more than one pore system are classified according to their largest accessible pore. Moreover, due to the size limitation of zeolite pores only a few relatively small guest molecules can be effectively accommodated in the zeolite cage. The average pore size of some zeolites and the critical molecular dimensions of a number of hydrocarbons that are potential reactants in zeolite-catalyzed reactions are shown in (Figure 1.6) [70]. From this figure it is clear that linear paraffins with molecular dimensions (0.4 nm) and isoparaffins with molecular dimension (0.5-0.6 nm) are accommodated very well in the cavity (0.7 nm) of faujasite type zeolites.

Zeolite	Number of Tetrahedra (or Oxygen) in the Ring	10 × Aperture Dimension, nm (Å)
Charbazite	8	3.6×3.7
Erionite	8	3.6×5.2
Zeolite A	8	4.1
ZSM-5 (or silicalite)	10	5.1×5.5; 5.4×5.6
ZSM-11	10	5.1×5.5
Heulandite	10	4.4×7.2
Ferrierite[a]	10	4.3×5.5
Faujasite	12	7.4
Zeolite L	12	7.1
	12	7.0
Mordenite	12	6.7×7.0
Offretite	12	6.4

a) There are also apertures with eight-membered rings in this zeolite.

Table 1.3. Zeolites and their pore (aperture) dimensions (ref. 70).
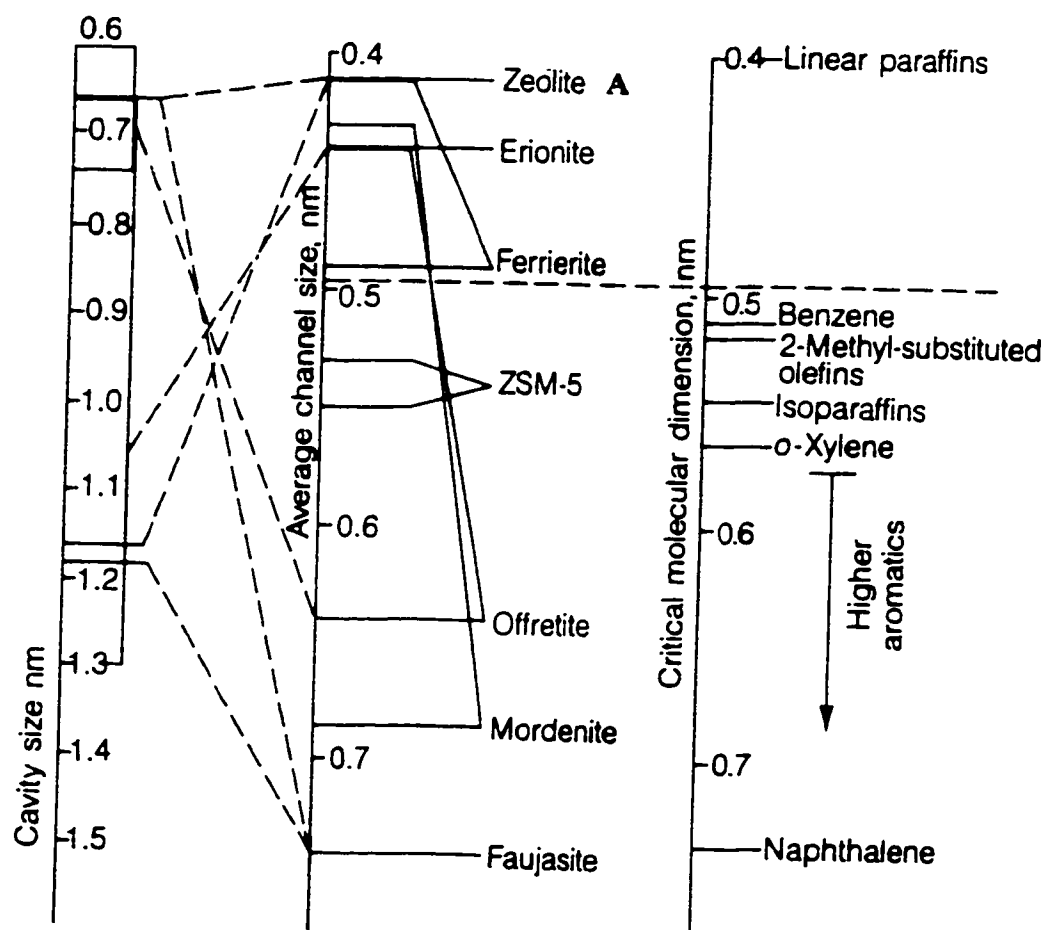
Figure 1.6. Pore dimensions of zeolites and critical dimensions of some hydrocarbons (ref. 70).

Often the controlling factors determining selectivity and catalytic activity are the pore geometry and diffusion limitations. The pore size and shape in a zeolite catalyst may affect the reaction selectivity in the following ways [71,72]: (a) reactant shape selectivity which occurs when the size of molecule is too large compared to the size of zeolite pore such that in a mixture effectively only smaller molecules can diffuse into the pores and react. (b) product shape selectivity which occurs when the formed product molecules are too bulky, cannot diffuse out from the pore, and are converted to smaller molecules, or to carbonaceous deposits within the pore which may cause pore blockage, (c) transition-state shape selectivity which occurs when the corresponding transition state for certain reactions requires more space than is available in the pores so that these reactions are prevented. (d) molecular traffic control [73] which occurs when a zeolite contains two types of channel systems (e.g. in ZSM-5), with different pore openings and geometry. In this case the reactant molecules enter the zeolite preferentially through one type of channels while the products leave the zeolite through another type of channels due to size or shape limitation, (Figure 1.7) [74].
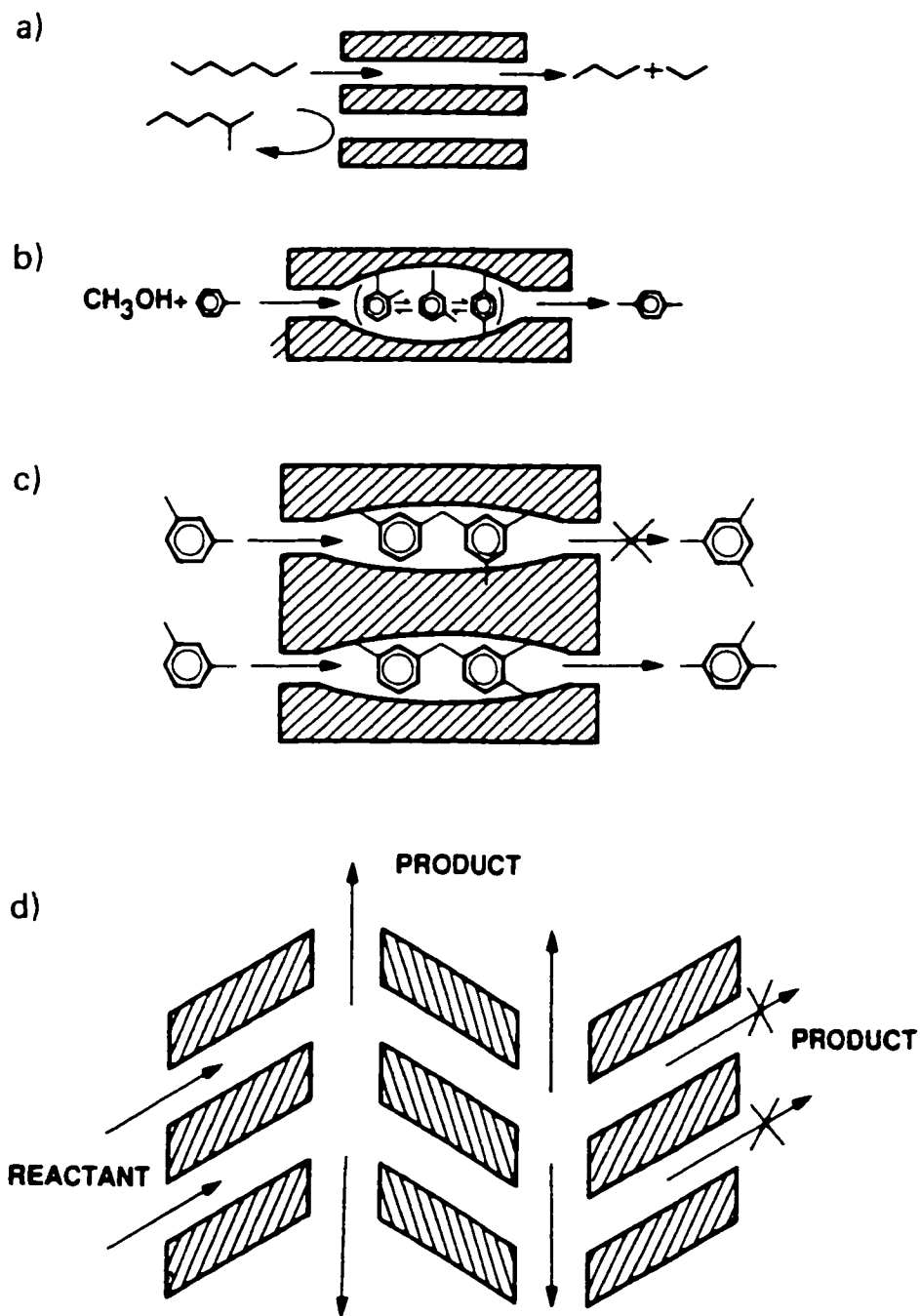
Figure 1.7. Schematic representation of molecular shape selectivity effects:
(a) reactant selectivity, (b) product selectivity, (c) restricted
transition state selectivity, (d) molecular traffic selectivity (ref.74).

The ion exchange capacity of a zeolite depends on its chemical composition: at lower Si/Al ratios a higher exchange capacity is observed with zeolites. In addition, exchange capacities of zeolites vary with the exchange cation. Cation exchange in zeolites is accompanied by a dramatic alteration of catalytic properties such as stability, adsorption behavior, selectivity and catalytic activity. Since many of these properties depend upon controlled cation exchange with particular cation species, detailed information on the cation exchange equilibria is important. The ion exchange property of zeolites provides a route for the introduction of catalytically active metal cations into the zeolite. These cations can subsequently be reduced to metal particles. As a result, a bifunctional zeolite catalyst can be generated [75]. The ion exchange capacities of some zeolites are shown in (Table 1.4) [76].

1.4.5 Surface area of zeolites

As discussed earlier, zeolites are highly porous materials with channels and cavities in their structure and therefore, possess a large specific surface area. The area of the rough surface is regarded as the *external* surface area, whereas the area of the pore walls is the *internal* surface area [77]. The external surface area only represents a few percent of the total surface area [78]. In spite of its theoretical limitations [79,80], the Brunauer-Emmett-Teller (BET) method [81] continues to be widely used for the evaluation of the surface area via physisorption isotherm data [82,83]. The approximated surface areas of some zeolite are listed in (Table 1.4) [76].

Zeolite	Si/Al	Exchange Capacity (milliequiv/g)	Surface area (m²/g)
Zeolite A	1	7.0	≈ 650
Zeolite X	1.25	6.4	≈ 650
Zeolite Y	2.0	5.0	≈ 750
ZSM-5	10-∞	1.5-0	≈ 400

Table 1.4. Exchange Capacity and approximated surface areas of Various Zeolites [ref. 76].

1.5 Major industrial applications of zeolites as catalysts

Zeolite materials are finding widespread applications for many industrial catalytic processes because of their ion exchange capacity with different cations, their shape and size selectivity, the ability to precisely control their acidity as well as the wide range of zeolites existing with different structures and properties such as high internal surface area and high thermal stability. These applications include separation, purification, ion exchange, adsorption and mostly in catalytic reactions such as reforming, isomerization, cracking, dewaxing, and aromatization.

The first application of zeolites as catalysts began in 1959 with an isomerization process at Union Carbide using Y zeolite [48,84]. In 1962 X zeolite was used as cracking catalyst [48]. This process of catalytic cracking was based upon earlier work done by Plank and Rosinski who reported that a small amount of zeolite incorporated into the then-standard silica/alumina or silica/clay catalysts significantly improved the cracking performance of crude oil. Zeolite catalysts have been widely used in both refineries and petrochemical industries in recent decades. Maximizing the yield of gasoline range products especially those with high octane ratings such as high olefin generated from crude oil is the clear aim of a refinery, and it is in this area that the develpment of new zeolite catalysts continues to take place. The major use of zeolite catalysts are in the acid form, and world wide consumption of zeolite materials for this purpose is about 400,000 tons annually, of which 350,000 tons are used for cracking [48].

1.6 Y Zeolite

The family of faujasites, including X zeolite and Y zeolite are finding the largest-scale application in catalysis. Having a three-dimensional pore structure with 0.74-nm apertures (12- membered oxygen rings), this family of zeolites admit hydrocarbon molecules even larger than naphthalene. Their main application is in the catalytic cracking of petroleum molecules to give smaller molecules (in the range of gasoline) [70]. The Faujasite framework structure is closely related to that of zeolite A. However, in the faujasite framework the sodalite cages are in an array with greater spacing than that of zeolite A. Each sodalite cage in the faujasite structures is connected to four other sodalite cages with six bridging oxygen ions linking the hexagonal faces of two sodalite units, as shown in (Figure 1.8) [85]. The bridging oxygens form a smaller cage namely hexagonal prism. The larger cage (1.2 nm diameter) in the faujasite structure is called a supercage. The supercage is surrounded by 10 sodalite units and is large enough to admit reactant molecules such as hydrocarbons in gas oil [86]. The cation sites in the faujasite are illustrated in (Figure 1.8). Type I sites are located at the centers of the hexagonal prisms, while type I' sites are located in the sodalite cages across the hexagonal faces from the type I site. Type II sites are located outside of the sodalite cages and lie within the supercages opposite the II' sites. Type II' sites are located inside of the sodalite cages. Type III sites refer to the positions in the walls of the supercages [85,87]. Since cations such as H^+ are largely responsible for the catalytic activity of zeolites, their locations are important in determining the accessibility and acidity strength. Therefore, it is the type II, II' and III sites that are responsible for catalytic activity.
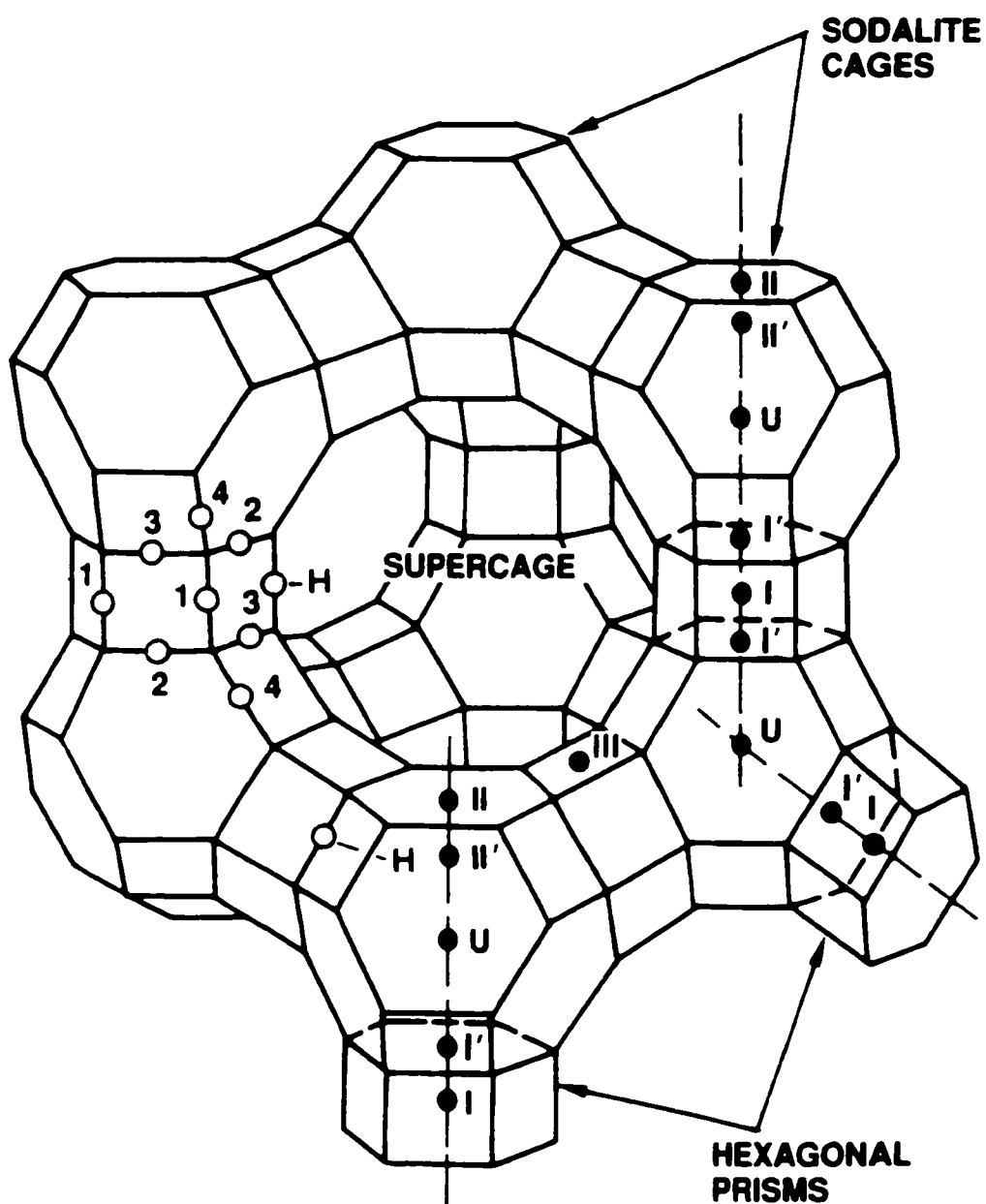
Figure 1.8. Faujasite framework showing oxygen type (O), nonframework
locations (●), and Brønsted acid sites (ref. 85).

The structural composition of Y zeolite is characterized by a Si/Al molar ratio of about 2.5 and for X zeolite this ratio is about 1.3. Structurally modified Y zeolites in which some aluminum has been removed from the framework (dealuminated or high-silica Y zeolite) are frequently used in octane enhancing catalysts [88]. These catalysts usually are ultrastable Y (USY) zeolite which is used in an acid-leached form and ammonium fluorosilicate treated Y (AFSY) zeolite which is used in the rare earth exchanged form. The presence of rare earth elements in the Y zeolite increases its stability and catalytic activity [89]. RE (rare earth) exchanged HY zeolites have good thermal and hydrothermal stability. The presence of polynuclear cations in the sodalite cages of zeolites, containing oxygen-bridge rare earth cations increases their stability [90]. Also thermal treatment of RE, HY results in the formation of additional acid sites, due to the hydrolysis of partially hydrated rare ions [91].

In addition, modified Y zeolites are extensively used for the isomerization of long chain paraffins. A major difficulty in the isomerization of long chain alkanes is their pronounced tendency for cracking. High selectivities for the isomerization of long chain paraffins could be achieved using platinum loaded catalysts such as Pt/HY, Pt/CaY and Pt/USY up to medium level of conversion [92,93]. These platinum loaded catalysts containing acid sites are called bifunctional catalysts. More information on bifunctional catalysts follows (see section 1.7). Because the pore size of HY zeolite (0.74 nm) is much larger than the cross-section of an n-heptane molecule (0.42 nm) [70], the hydroisomerization of n-heptane on HY zeolite has been chosen for this research work.

1.7 Isomerization

In petroleum chemistry isomerization of long chain n-paraffins refers to the conversion of linear (normal) alkanes to branched alkanes. The objective of this process is to increase the octane number of the treated gasolines, or naphthas. In fact, the branched paraffins when blended into gasoline improve its octane number and when added to diesel fuel increase its low-temperature performance [94,7].

There are some abundant long chain n-alkanes in refinery stream fuels which have a lower octane number and a higher pour point. It would be thus desirable to convert these normal paraffins to their branched isomers. Therefore, the isomerization of n-paraffins plays an important role in the petroleum industry and is very attractive to a large number of researchers in both the industrial and academic sectors.

There are actually two categories of skeletal isomerizations of n-paraffins in accordance with their molecular lengths. Research works show that the process for the isomerization of C_6 or lower n- paraffins (the first category) can not be used on C_7 or higher n-paraffins (the second category) because undesired reactions (cracking) occur under such conditions [95,96,97,98].

1.7.1 Isomerization of C_6 and lower n-paraffins (the first category)

In petroleum chemistry the purpose for production of branched isomers of light paraffins such as C_5 and C_6 is to increase the octane number of gasoline which the isomerization of butane produces isobutane. The isomerization reaction converts the low-octane-number normal paraffins with 5 and 6 carbon atoms into higher-octane-numbered isoparaffins (Table 1.1) [99]. The obtained isomers are as follow:

From the isomerization reaction of n-pentane, isopentane with octane number of over 90 is obtained, and neopentane is practically never formed with the catalysts that are commonly in use.

From the isomerization reaction of n-hexane, two types isomers of mono-branched and double-branched are obtained. Mono-branched isomers include to 2-methylpentane and 3-methylpentane with a relatively low octane number of 75. Double-branched isomers include to 2,2-dimethylbutane and 2,3-dimethylbutane with a high octane number of over 90.

From the isomerization reaction of n-butane, isobutane is produced. The isobutane is required for the production of alkylates such as 2,2,4-trimethylpentane and 2,2,3-trimethylpentane [100] and MTBE (methyl tert-butyl ether) as gasoline additives [101,102].

1.7.2 Isomerization of C$_7$ and higher n-paraffins (the second category)

In spite of undesired cracking reactions, isomerization of this category can produce multi-branched isomers (desired because they have high octane numbers and are liquids) in higher yields than the isomerization of first category [103,104,105,106].

Kinetically speaking, the reaction of isomerization is slow. In order to lower the activation energy and increase the rate of the isomerization, it is necessary to use catalysts in the isomerization process. The history of developing catalysts for isomerization of n-paraffins has lasted for more than half a century.

During World War II, there was a great need of high octane rating fuels. Some isomerization plants were built, and usually aluminum chloride was used as the catalyst. However, this process was very expensive and disposal of the sludge formed during isomerization raised a very serious problem [107]. These early processes were replaced by newer versions using bifunctional catalysts. These catalysts were composed of a metal on a classical acidic support such as chlorinated alumina or silica-alumina [108].

In the 1960's, liquid acid catalysts, such as hexafluoroantimonic acid (SbF$_5$-HF), a superacid, were used at low temperature and showed good activity as liquid-phase catalysts [109]. These catalysts however, were easily contaminated and were extremely corrosive, so the plants needed special

construction materials to resist the corrosion. Since that time, many researchers have reported the high activity and selectivity of zeolitic catalysts for the isomerization [110]. These zeolites are loaded with noble metals (bifunctional catalysts) to stabilize the activity. By both chemical and structural modifications of the zeolites, the physicochemical and catalytic properties of the catalyst can be properly adjusted.

However, bifunctional catalysts (hydrogenation-dehydrogenation and Brønsted acid functions) such as zeolites have found more and more applications in the new catalytic systems [111,112].

1.8 Bifunctional Catalysts

These catalysts possess two types of active sites having hydrogenation-dehydrogenation and acid functions, respectively [113]. The cooperation of these sites results in increase of catalytic properties [114,115]. The hydrogenation-dehydrogenation (Pt) sites not only produce olefinic species from paraffins but also by adsorbing back of the olefinic species and then hydrogenating them into isoparafinic products, thus, preventing excessive oligomerization and polymerization reactions leading to coke species.

The hydrogenation-dehydrogenation function is provided by the presence of a metal (in some catalysts more than one type of metal is used). This metal must be active and stable at a reaction temperature of about 500 °C (reforming reaction). Moreover its content must be controlled to prevent or minimize the

demethanation reaction. Metals used in these types of catalysts include Pt, Pd, Cr, Ni, Co among others.

The acid function, provided by the support (with or without impregnation of a halogenated compound) favors the isomerization and cyclization reactions. The acidity must be controlled to moderate hydrocracking, the catalytic competitor of isomerization or dehydrocyclization (aromatization).

Bifunctional catalysts, such as metal-supported zeolites play an important role in petroleum refining and petroleum chemistry. Such zeolite catalysts are used in processes such as isomerization, hydrocracking, and catalytic dewaxing [113,116]. One application of bifunctional catalysis is the catalytic reforming process used to produce high octane rating hydrocarbons, through the following reactions:

(a) dehydrogenation of naphthenes (alkylcyclohexanes) to aromatics, (b) dehydrocyclization of paraffins and isoparaffins to aromatics, and (c) isomerization of paraffins to isoparaffins and of alkylcyclohexanes. A number of side reactions such as coke formation, cracking and demethanation also take place.

1.8.1 Reaction mechanism over bifunctional catalysts

The conventional reaction mechanism for the conversion of an alkane

on a bifunctional catalyst was described originally by Coonradt and Garwood [114] and Weisz [115] and is shown in (Figure 1.9).

The metal function dehydrogenates the alkanes into alkenes which are then protonated on the Brønsted acid function, yielding alkylcarbenium ions (alkylcarbocations). Also strong Brønsted acid sites can abstract hydrides and generate alkylcarbenium ions. After rearrangements and/or scissions these alkylcarbenium ions desorb from the acid sites as alkenes and are hydrogenated at the metal site to yield saturated reaction products [113]. Provided that hydrogenation-dehydrogenation and protonation-deprotonation are fast enough, the rearrangements of the alkylcarbenium ions become the rate-limiting steps of the reaction scheme.
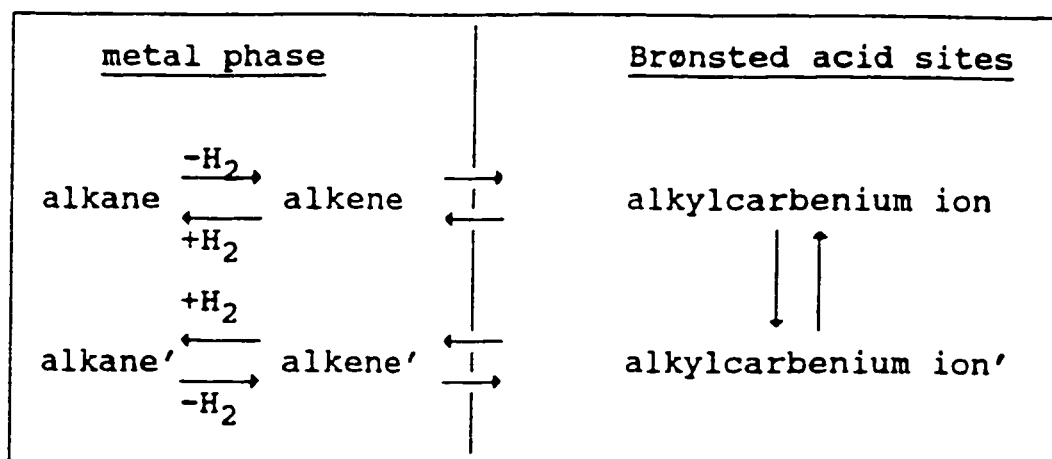
Figure 1.9. Classical bifunctional reaction scheme (ref. 115).

Generally, it is accepted that the reaction intermediates in the conversion of hydrocarbons over heterogeneous acid catalysts are carbocations [115], although direct evidence for the presence of carbocations has never been provided. Depending on the coordination number of the positively charged carbon atom two classes of carbocations, alkylcarbenium ions and alkylcarbonium ions, have been proposed to occur during hydrocarbon conversion over bifunctional catalysts [117].

Alkylcarbenium ions are tertiary coordinated carbocations in which a positively charged carbon atom is bonded to three alkyl groups and/or hydrogen atoms. These carbocations can be generally represented by the formula of CR_3^+, in which **R** stands for a hydrogen atom or an alkyl group.

Alkylcarbonium ions are pentacoordinated carbocations, which can be generally represented by the formula of CR_5^+, keeping in mind, that these five bonds only contain eight electrons. The stability of the alkylcarbenium or alkylcarbonium ion increases along the following cation sequence:

$$Primary < secondary < tertiary < quaternary \qquad (1.2)$$
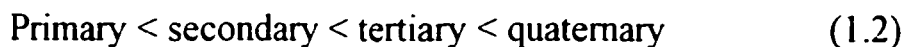
Alkylcarbonium ions are potential intermediates in the isomerization mechanism of acyclic alkylcarbenium ions as substituted protonated cycloalkanes. Substituted protonated cyclopropanes (**PCP**) contain the smallest possible rings among these structures and they exist in three different forms as shown in (Figure 1.10) [117].
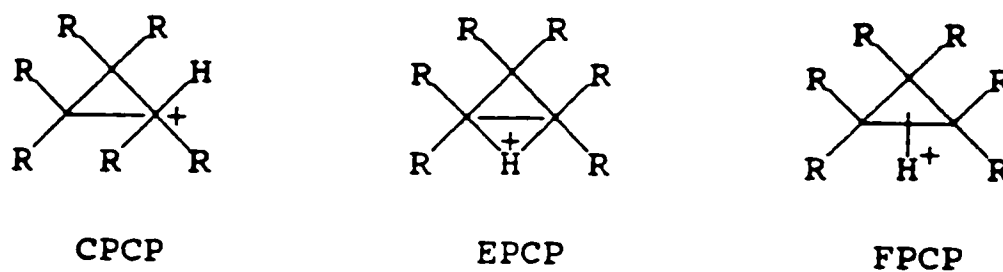
Figure 1.10. Representation of substituted corner (CPCP), edge (EPCP) and
face (FPCP) protonated cyclopropanes. R stands for a hydrogen
or an alkyl groups (ref. 117).

1.8.2 Skeletal Isomerization

The isomerization reactions of acyclic alkylcarbenium ions in superacids formally belong to one of the following two categories [117]:

(i) Isomerization reactions of type A, which change the position of a side chain, without changing the degree of branching. Isomerization of type A is illustrated as below, for the isomerization of 2-methyl-2-pentyl into a 3-methyl-3- pentyl cation.

$$(1.3)$$
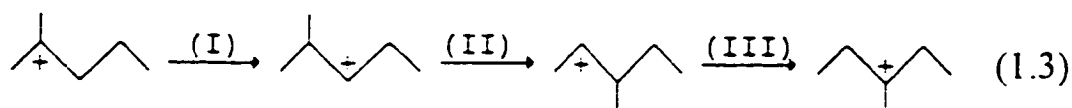
The 1,2-alkyl shift shown in step (II) is not necessarily an elementary step but, according to generally accepted principles in superacid chemistry, may proceed through cyclization of the alkylcarbenium ion into an intermediate corner protonated cyclopropane (CPCP) structure followed by reopening of the cyclopropane ring producing 3-methyl-2- pentyl cation, as below:

$$(1.4)$$
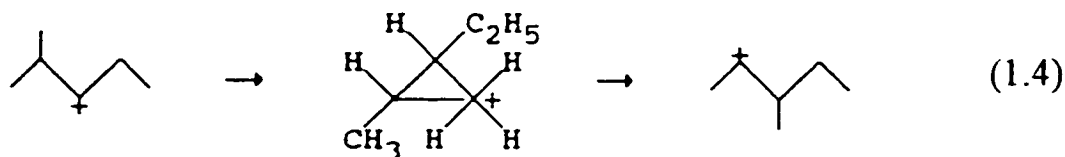
(ii) Isomerization reactions of type B, which increase or reduce the degree of branching. The isomerization mechanism take place via formation of CPCP intermediates followed by a corner-to-corner proton jump. Type **B** isomerization reactions are always slower than type **A** ones. The energy barriers of processes involving an overall change of the degree of branching in type **B** isomerization reactions are higher with about 12 kJ/mol than one of the type **A** isomerization reactions. The mechanism is illustrated in (Figure 1.11) [117].
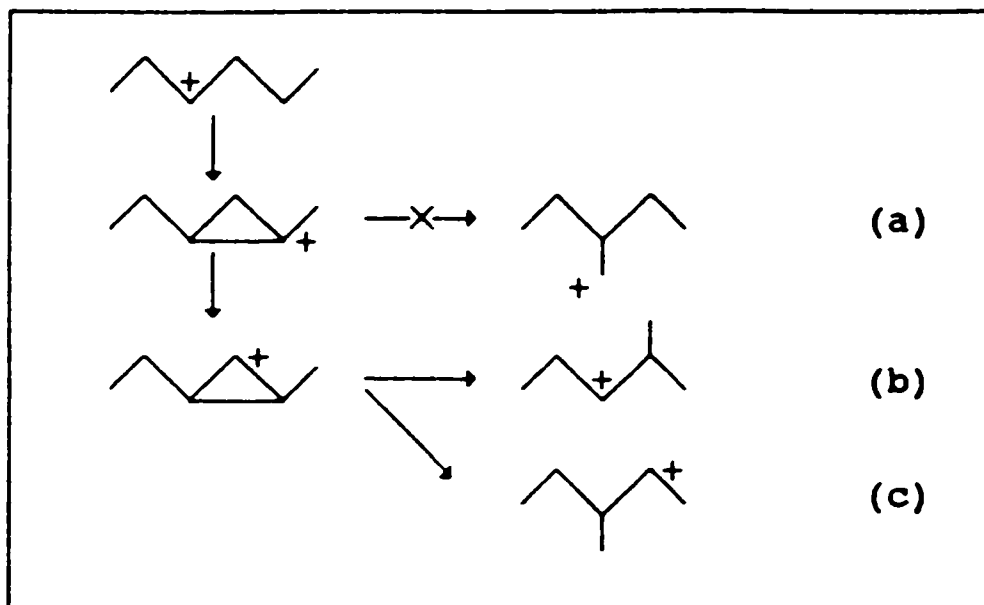
Figure 1.11. Possible type **B** isomerization of 3-hexyl cation (ref.117).

1.8.3 Cracking (β-scission)

Cracking of alkylcarbenium ions in superacids proceeds via β-scission [118]. β-scission involves the migration of two electrons of the C-C bond in the β position of the positively charged carbon atom toward the C-C bond in the α position and this αC-C bond becomes olefinic and the C atom in the γ position ends up as the positively charged carbon atom of a smaller alkylcarbenium ion. There are five modes of β-scission of secondary and tertiary alkylcarbenium ions possible, depending on the branching configuration of the original alkylcarbenium ion [119,117]. These modes are shown in (Figure 1.12) [117].
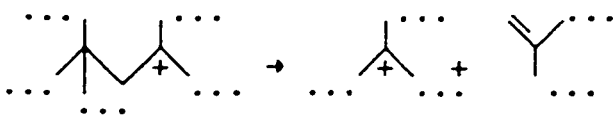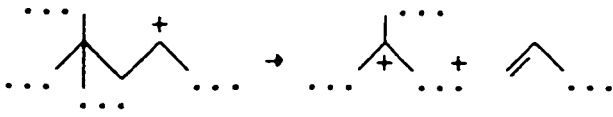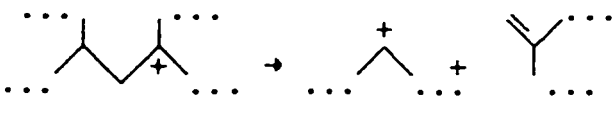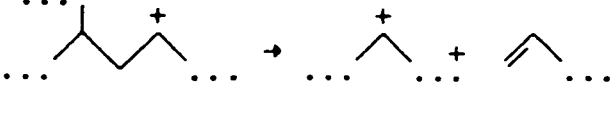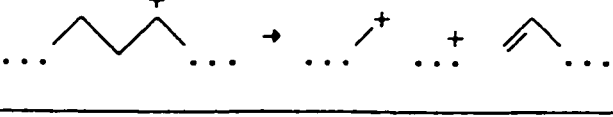
Scission reaction	Mode	Specific Configuration in feed
	A	α,γ,γ-tribranched
	B₁	γ,γ-dibranched
	B₂	α,γ-dibranched
	C	γ-monobranched
	D	unbranched

Figure 1.12. Specific branching configurations and β-scission modes of acyclic alkylcarbenium ions (ref. 117).

Cracking of alkylcarbenium ions via β-scission depends on the branching configuration of the original carbenium ions. Also by increasing the number of carbon atoms of carbenium ion and the reaction temperature the rate of cracking increases. Kinetic studies show that type A β-scission is not only faster than B_1, B_2 and C β-scission but also faster than isomerization via 1,2-methyl shift, (Table 1.5) [120,117].

As mentioned before, during isomerization of long chain hydrocarbons over bifunctional catalysts cracking reactions occur and lighter hydrocarbons are produced. For example, the conversion of octane over a Pt/USY zeolite catalyst at 469 K, produces propane, butane, isobutane, pentane and isopentane as cracked products. The conversion pathways of octyl cations on the Pt/USY zeolite catalyst at 469 K are shown in (Figure 1.13) [117].

	Temperature (K)			
	469	439	434	405
	Isooctanes	Isononanes	Isodecanes	
Cracking				
B_1	0.34	1.5	2.8	
B_2	1.0	1.0	1.0	
C	0.34	0.77	0.40	
A				1050
Type B isomerization				
Mono- →dibranched	0.34	0.85	0.80	0.80[a]
Di-→Tribranched	0.28	0.77	0.80	
Type A isomerization				
1,2-methyl shift				56

a) Taken as standard = 0.80.

Table 1.5. Relative apparent rate constants of types A, B_1, B_2 and C cracking, 1,2-methyl shift, and branching of isooctanes, isononanes and isodecanes with B_2 as standard over the Pt/USY catalyst (ref.120,117).

```
  ┌─────────────────┐
  │  n-octyl cation │
  └─────────────────┘
        B ↑↓ B
  ┌──────────────────────────┐                    C
  │ monobranched octyl cation │ ─────────────╲
  └──────────────────────────┘                  ╲
        B ↑↓ B                                    ↘
  ┌────────────────────────────────────┐
  │ γ,γ-dibranched octyl cation        │──B₁──→   ┌────────┐
  │                                    │          │  C₃    │
  │            A↑↓A                    │          │  i-C₄  │
  │                                    │          │  n-C₄  │
  │ α,γ-dibranched octyl cation        │──B₂──→   │  i-C₅  │
  │                                    │          │  n-C₅  │
  │            A↑↓A                    │          └────────┘
  │                                    │            ↗
  │ other dibranched octyl cations     │───C──→
  └────────────────────────────────────┘
        B ↑↓ B                              B₂ ╱   B₁
  ┌────────────────────────────────────┐     ╱  C
  │ other tribranched octyl cations    │────╱
  │                                    │
  │            A↑↓A                    │
  │                                    │          ┌──────┐
  │ 2,2,4-tribranched-4-pentyl cation  │───A──→   │ i-C₄ │
  └────────────────────────────────────┘          └──────┘
```
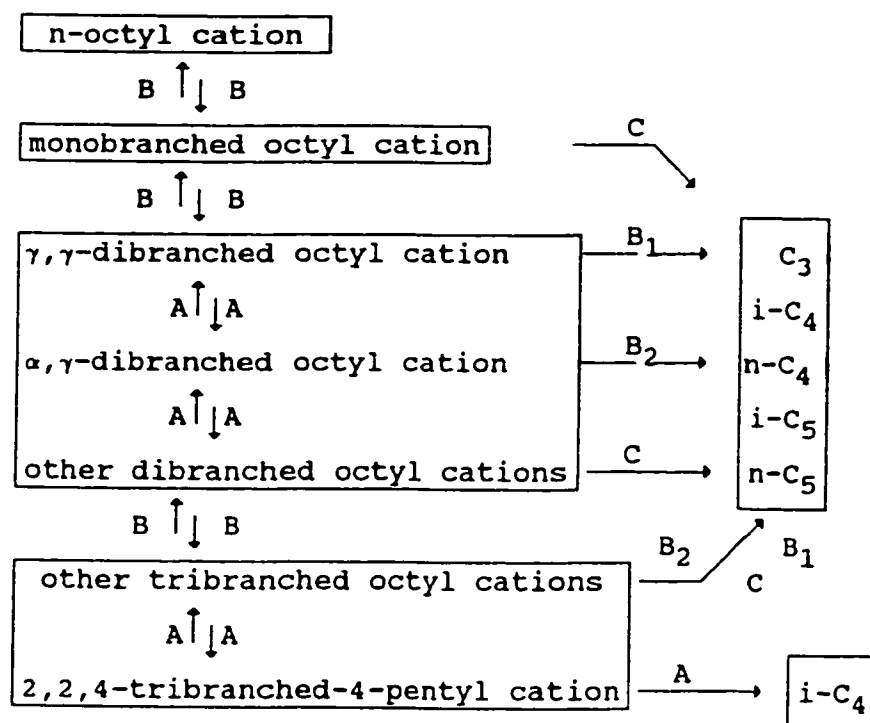
Figure 1.13. Conversion pathways of octyl cations at 469 K on Pt/USY zeolite catalyst (ref. 117).

1.9 Objectives of this research work and thesis presentation

In the complex sequence of isomerization of long chain n-paraffins the production of branched paraffins, particularly multi-branched paraffins is affected by the fierce competition between isomerization and cracking. The purpose of this research work was:

(i) To identify the condition to have predominance of isomerization over cracking in accordance with the bifunctional catalyst concept and the conventional sequential reaction mechanism

(ii) To modify the catalyst formulation by introducing species capable of shortening the residence time of the reaction intermediates (alkylcarbocations) on acid sites in order to favor the formation of branched paraffins

(iii) Finally, by using kinetic data obtained with the new catalysts to provide support for our trifunctional catalysis hypothesis

In this chapter, the general background and basic theories as well as the main features of zeolite materials associated with the hydroisomerization of n-heptane and related problems have been reviewed.

Chapter two will deal with the preparation and modification of HY zeolite catalysts by impregnation of different cations such as Al^{3+}, Zn^{2+}, Cd^{2+}, Ni^{2+}, Cr^{3+}, Ga^{3+}, Ru^{3+} and halogenated modified HY zeolite catalysts.

The characterization of these prepared catalysts through the use of different techniques such as: AAS, XRD, BET surface measurement, ammonia-TPD and FTIR is included in chapter two. In addition, the experimental set up, operation conditions, catalyst testing using n-heptane as a model molecule and the effect of reaction parameters including temperature, hydrogen partial pressure and contact time, are all reported in chapter two.

In chapter three, a comparison between the activity and selectivity of the parent zeolite and the modified ones will be made, and the results will be interpreted. Also the formation of new desorption-transfer promoting sites as a result of modification of HY zeolite catalyst and the hypothesis of a trifunctional 'zeolite acid/pt dehydro-hydrogenating/Al desorption-transfer promoting' site configuration will be discussed.

Conclusions for this thesis will be given in chapter four.

CHAPTER II

EXPERIMENTAL

In this chapter, the experimental methods used in this research work including preparation and characterization of the zeolite catalysts and the catalytic activity testing are described in detail.

2.1 Preparation of catalysts

2.1.1 Source of Chemicals

The chemicals and zeolite materials used in the preparation and characterization of catalysts used in this work were purchased from several suppliers as below:

Chemicals	Suppliers
Air (Compressed)	PraxAir
Aluminum Chloride	Anachemia
Aluminum Nitrate	Fisher Scientific company
Aluminum Sulfate	Anachemia
Ammonia	Air Products
Ammonium Bromide	Aldrich Chemical Co.
Ammonium Chloride	Aldrich Chemical Co.
Ammonium Fluoride	Aldrich Chemical Co.
Ammonium Iodide	Fisher Scientific company
Bentonite USP grade	Anachemia
Cadmium Nitrate	Aldrich Chemical Co.
Chromium Nitrate	Fisher Scientific company

Copper(II) Nitrate	Aldrich Chemical Co.
Gallium Nitrate	Aldrich Chemical Co.
n-Heptane	Aldrich Chemical Co.
Hydrochloric acid	Fisher Scientific company
Hydrogen UHP grade	PraxAir
2,2-Dimethylbutane	Aldrich Chemical Co.
NH_4-Y Zeolite (Lzy-84)	Universal Oil Product (UOP)
Nickel Nitrate	Aldrich Chemical Co.
Nitrogen	PraxAir
n-Octane	Aldrich Chemical Co.
Pyridine	Aldrich Chemical Co.
Ruthenium (III)Acetylacetonate	Aldrich Chemical Co.
Silica-Alumina	Aldrich Chemical Co.
Sodium Hydroxide	Anachemia
Tetraammineplatinum (II) Chloride	Alfa AESAR
Zinc Bromide	Aldrich Chemical Co.
Zinc Chloride	Aldrich Chemical Co.
Zinc Fluoride	Aldrich Chemical Co.
Zinc Iodide	Aldrich Chemical Co.
Zinc Nitrate	Aldrich Chemical Co.

2.1.2 HY zeolite catalysts

The acid form of Y zeolite was obtained by calcination of the ammonium form of Y zeolite [LZY-84 provided by U.O.P. in two forms: 1) 1/16 in., pellet form, containing ca. 80 wt% of NH_4Y and some non-defined large pore-sized binder, and 2) a fine powder of NH_4Y] in air at 550 °C overnight. At this temperature, NH_4Y is decomposed and HY and NH_3 are obtained.

2.1.3 "Internal" impregnation

Prepared by this technique, the hybrid catalysts obtained at the final step are assumed to have metallic Pt and other metal species (finally decomposed to metal oxide) incorporated directly into the micropores of the HY zeolite (non-hybrid configuration, $Pt-M_y-HY$).

Pt-HY (bifunctional) catalyst: A 15 ml solution 0.172 g of tetraammineplatinum (II) chloride hydrate $[Pt(NH_3)_4Cl_2.H_2O]$ in water was prepared.Then 10 g of HY zeolite pellets were immersed in the solution. The suspension was slowly evaporated to dryness at low temperature. The resulting material was dried at 120 °C overnight and then activated overnight in the air at 350 °C. The content of Pt of all the final catalysts was 1 wt.% (0.51×10^{-4} mol/g) [121].

Series of Pt-M-HY zeolite catalysts were prepared as follows:

(a) Pt-Al$_y$-HY (simultaneous incorporation of Pt and Al): A 15 ml solution of x g of [Al(NO$_3$)$_3$.9 H$_2$O] and 0.172 g of tetraammineplatinum (II) chloride hydrate [Pt(NH$_3$)$_4$Cl$_2$.H$_2$O] in water was prepared. The amount x was calculated so that the Al content of the final catalyst was equal to y with y varying from 1 to 7 wt % (0.37×10^{-3} to 2.59×10^{-3} mol/g). Then 10 g of HY zeolite pellets were immersed in the solution. The suspension was slowly evaporated to dryness at low temperature. The resulting material was dried at 120 °C overnight and then activated overnight in the air at 350 °C. The content of Pt of all the final catalysts was 1 wt.% (0.51×10^{-4} mol/g) [121]. In addition, in some tests Pt-Al$_y$-HY sample was prepared using a mixture of AlCl$_3$ and [Al(NO$_3$)$_3$.9 H$_2$O] in order to increase the strength of Brønsted acid site on zeolite surface because of electron withdrawing effect of Cl species.

(b) Al^y-Pt-HY (sequential incorporation of Pt and Al): These zeolite catalysts were prepared with the same contents of Pt and Al as in (a), but through separate incorporation of Al and Pt [122]. Pt was first incorporated into the HY zeolite in the same amount and in the same way as mentioned in (a). Then the resulting solids were dried at 120 °C overnight and activated overnight in the air at 350 °C. Al species were then incorporated into the resulting solids in the same way and in the same amounts as in (a). After drying at 120 °C overnight, the materials were activated in the air at 350 °C overnight.

(c) Pt-Zn$_y$-HY (simultaneous incorporation of Pt and Zn): The same procedure as in (a) was used for preparation of these zeolite catalysts, except instead of aluminum nitrate [Al(NO$_3$)$_3$.9 H$_2$O], zinc nitrate [Zn(NO$_3$)$_2$.6 H$_2$O]

was used. The content of Zn (y) in the final catalyst varied from 1 to 10 wt % $(0.15 \times 10^{-3}$ to 1.53×10^{-3} mol/g). In addition, in some tests Pt-Zn$_y$-HY sample was prepared using a mixture of $ZnCl_2$ and $[Zn(NO_3)_2.6\ H_2O]$ in order to increase the strength of Brønsted acid site on the surface of this type zeolite catalysts.

(d) Zn^y-Pt-HY (sequential incorporation of Pt and Zn): These zeolite catalysts were prepared with the same contents of Pt and Zn as in (c), with separate incorporation of Zn and Pt. The same procedure as in (b) was used for preparation of these zeolite catalysts except instead of aluminum nitrate $[Al(NO_3)_3.9\ H_2O]$, zinc nitrate $[Zn(NO_3)_2.6\ H_2O]$ was used. Again the content of Zn (y) in the final catalyst varied from 1 to 10 wt % $(0.15 \times 10^{-3}$ to 1.53×10^{-3} mol/g).

(e) Pt-Cd$_y$-HY (simultaneous incorporation of Pt and Cd): The same procedure as in (a) was used for preparation of these zeolite catalysts, except instead of aluminum nitrate $[Al(NO_3)_3.9\ H_2O]$, cadmium nitrate tetrahydrate $[Cd(NO_3)_2.4\ H_2O]$ was used. The content of Cd (y) in the final catalyst varied from 1 to 10 wt.% $(0.09 \times 10^{-3}$ to 0.89×10^{-3} mol/g).

(f) Cd^y-Pt-HY (sequential incorporation of Pt and Cd): These zeolite catalysts were prepared with the same contents of Pt and Cd as in (e), with separate incorporation of Cd and Pt. The same procedure as in (b) was used for preparation of these zeolite catalysts except instead of aluminum nitrate $[Al(NO_3)_3.9\ H_2O]$, zinc nitrate $[Cd(NO_3)_2.4\ H_2O]$ was used. The content of Cd

(y) in the final catalyst varied from 1 to 10 wt.% (0.09×10^{-3} to 0.89×10^{-3} mol/g).

(g) Ni^y-Pt-HY (sequential incorporation of Pt and Ni): The same procedure as in (b) was used for preparation of these zeolite catalysts, except instead of aluminum nitrate [$Al(NO_3)_3.9\,H_2O$], nickel nitrate [$Ni(NO_3)_2.6\,H_2O$] was used. The content of Ni (y) in the final catalyst varied from 1 to 10 wt % (0.17×10^{-3} to 1.70×10^{-3} mol/g).

(h) Cr^y-Pt-HY (sequential incorporation of Pt and Cr): The same procedure as in (b) was used for preparation of these zeolite catalysts, except instead of aluminum nitrate [$Al(NO_3)_3.9\,H_2O$], nickel nitrate [$Cr(NO_3)_3.9\,H_2O$] was used. The content of Cr (y) in the final catalyst varied from 1 to 10 wt % (0.19×10^{-3} to 1.92×10^{-3} mol/g).

(i) Pt-Ga_y-HY (simultaneous incorporation of Pt and Ga): The same procedure as in (a) was used for preparation of these zeolite catalysts, except instead of aluminum nitrate [$Al(NO_3)_3.\,9H_2O$], gallium nitrate [$Ga(NO_3)_2.\,7.5H_2O$] was used. The content of Ga (y) in the final catalyst varied from 0.3×10^{-3} to 2.5×10^{-3} mol/g.

(j) Pt-X-$Zn_{0.9}$-HY (halogenated zeolite catalysts, X= F, Cl, Br or I): A 15 ml solution of 5 mmol/g of NH_4F, NH_4Cl, NH_4Br or NH_4I in water was prepared. Then 10 g of HY zeolite pellets were immersed in the solution. The suspension was slowly evaporated to dryness at low temperature. The resulting material was dried at 120 °C overnight and then activated in the air first at 250

°C for 4 hours then at 450 °C for 5 hours (in the case of NH_4 Br the final temperature was 400 °C because of its lower sublimation temperature of 452 °C). Then the resulting solids were immersed in a 15 ml water solution of 2.678 g of $Zn(NO_3)_2.6 H_2 O$ and 0.172 g of $Pt(NH_3)_4Cl_2.H_2 O$. The resulting material was dried at 120 °C overnight and then activated overnight in the air at 350 °C. The content of Pt in all the final catalysts was 1 wt % (0.51×10^{-4} mol/g) and the content of Zn was 0.9×10^{-3} mol/g.

2.1.4 "External" impregnation (hybrid configuration)

Pt-HY/SA (SA = silica-alumina): HY powder was treated with a solution of tetraammineplatinum (II) chloride hydrate (the content of Pt in all the final catalysts was 0.5 wt % = 0.25×10^{-4} mol/g). The resulting materials was slowly evaporated to dryness at low temperature, and was dried at 120 °C overnight and then activated overnight in the air at 350 °C. A mixture of the resulting Pt-HY zeolite powder (80 wt.%) and silica-alumina (10 wt.%) and bentonite (10 wt.%) was prepared and mixed with distilled water to obtain malleable paste. The malleable paste was extruded from a syringe as a spaghetti-like piece by the procedure previously described elsewhere [123,124]. These extrusions were dried at 120 °C overnight and then activated overnight in the air at 350 °C.

Pt-Al$_{ex}$-HY (external configuration): in this technique, Al_2O_3 was obtained by calcination of $Al(NO_3)_3.9 H_2 O$ in the air at 350 °C. HY powder was treated with a solution of tetraammineplatinum (II) chloride hydrate (the content of Pt in all the final catalysts was 1 wt % = 0.51×10^{-4} mol/g).

The resulting materials was slowly evaporated to dryness at low temperature, and was dried at 120 °C overnight and then activated overnight in the air at 350 °C. A mixture of the resulting Pt-HY zeolite powder (80 wt.%), the alumina previously produced (y wt.%) and bentonite (binder, balance) was used for the preparation of the extrudates of the hybrid catalyst (external configuration Pt-Al_{ey}-HY). The resulting was mixed with distilled water to obtain malleable paste. The malleable paste was extruded from a syringe as a spaghetti-like piece by the procedure previously described elsewhere [123,124]. These extrusions were dried at 120 °C overnight and then activated overnight in the air at 350 °C. The $(Pt-HY)_c$ catalyst was prepared with the same procedure without adding Al_2O_3 powder.

2.2 Characterization of catalysts

For characterization of chemical and physical properties of zeolite catalysts following techniques were used: i) Atomic Absorption Spectroscopy (AAS), ii) X-Ray powder Diffraction (XRD), iii) determination of the BET surface area and pore size distribution, iv) ammonia Temperature Programmed Desorption (NH_3-TPD), and v) Fourier Transform Infrared Spectroscopy (FTIR).

2.2.1 Atomic Absorption Spectroscopy (AAS)

Atomic Absorption Spectroscopy was used to determine levels of Si, Al and Na. The zeolite sample (1.2 g) was weighed and placed in a platinum

crucible, calcined at 800 °C in the furnace for one hour, and weighed again to obtain the weight of the dried sample. Then 0.9 g of a fusion mixture (consisting of potassium carbonate and lithium tetraborate in a ratio of 2:1) was added to the calcined zeolite sample and after mixing, the resulting material was heated for another hour in the furnace at 800 °C. The resulting mixture was dissolved in a strong acid mixture of 4 ml concentrated HCl and 10 ml of 10 vol % H_2SO_4. Then the mixture was transferred to a beaker, the beaker was covered with watch glass and gently heated overnight to obtain a clear solution. Subsequently, 5 ml of hydrogen peroxide (30 %) was added to the solution and then heated until effervescence stopped. The solution was diluted to 100 ml in a volumetric flask and the dilute solution was used for atomic absorption analysis with a Perkin Elmer Model 503 instrument. The content of metal oxides was calculated by referring to external standards for the corresponding metals. From the atomic absorption results the Si/Al ratio of HY zeolite was calculated.

2.2.2 X-Ray powder Diffraction (XRD)

As zeolite materials are crystalline solids, they have a characteristic diffraction pattern which can be used to identify their particular structure and determine the degree of crystallinity. Modifications of the zeolite framework can be characterized using XRD. With this technique the aluminum content in the framework of the zeolite can be determined. This method is based on the decrease of the unit cell parameter with increasing Si/Al ratio (Si^{4+} is smaller than Al^{4+}) [125,126]. Powder diffraction diagrams are obtained by measuring

the angles at which an X-ray beam of wavelength λ is diffracted by the zeolite sample. The spacing d between two planes (hkl) is related to the diffraction angle 2θ by the Bragg law [127].

$$n\lambda = 2d \sin \theta \tag{2.1}$$

where n is an integer.

A sample of zeolite (0.6 g) was pressed in a plexiglass sample holder after fine grinding. The X-ray powder diffraction pattern was obtained and recorded on the Phillips PW 1050/25 diffractometer (automated with the SIE Ray 112 system from Sietronics) operating at 40 KV and 20 mA. At an angular velocity of 1° (2θ) /min $^{-1}$ with a step size of 0.02° (2θ), the data were collected using Kα radiation of copper (λ = 1.54178 Å). The diffraction pattern of modified HY zeolite sample obtained was compared to that of the parent HY zeolite. For determination of relative crystallinity (RC%) or the degree of crystallinity of samples, the intensity of the characteristic five most intense peaks in the range of 2θ (from 5° to 35°) was taken to account in accordance with the method of Scherzer et al. [127].

The percent of crystallinity was determined by dividing the sum of the peak area (or heights) of the modified HY zeolite sample by the sum of the peak area (or heights) of the parent zeolite which designated to be 100 % crystalline. The following formula was used to calculate the degree of crystallinity [129].

$$RC \% = \frac{\text{Peak area (or height) of sample between } 5° \text{ to } 35°(2\theta)}{\text{Peak area (or height) of reference sample between } 5° \text{ to } 35°(2\theta)} \quad\quad (2.2)$$

2.2.3 Determination of the BET surface area and pore size distribution

Although the catalytic activity may be related only indirectly to the total surface area, most catalysts of practical importance are highly porous and possess large specific surface areas. Therefore, determination of surface area is generally considered to be an important requirement in the characterization of catalysts [129]. These parameters are important in studying the relationship between pore structure, surface area and morphology with catalytic activity. The recorded values of porosity and pore volume are likely to depend on the experimental methods employed. However, no experimental method can be expected to provide absolute values of these parameters. Gas adsorption methods are most often used to determine the surface area and pore size distribution of catalysts. As mentioned before, the Brunauer-Emmett-Teller (BET) method is based on gas adsorption [81] which in spite of its theoretical limitations [79,80], continues to be widely used for the evaluation of the surface area from physisorption isotherm data. In the original form, the BET theory involved an extension of the kinetic model of Langmuir to multilayer adsorption [130].

The catalysts used in this research work are microporous materials, and it is necessary to measure their surface area and pore size in order to understand

the mechanism of diffusion of the reactants. The nitrogen adsorption/desorption isotherms at liquid nitrogen temperature (T= - 196 °C) were obtained with a Micromeritics 2000 V2.05 unit using a volumetric technique. Each sample was subjected to the following experimental procedure. About 0.4 g of zeolite was placed in a glass tube, and moisture was removed under vacuum at 220 °C overnight. Then the nitrogen adsorption/desorption isotherms were recorded. The BET surface area was calculated from nitrogen uptakes using these isotherms at relative pressures lower than 1. In the application of the BET procedure, first it is necessary to derive the monolayer capacity n^a_m (the amount of adsorbate required to form a complete monolayer on the surface of unit mass of the adsorbent). The specific surface area a_s (BET), is then obtained from n^a_m by taking a value for the average area a_m, occupied by the adsorbate molecule (i.e. the molecular cross-sectional area in the filled monolayer). Thus

$$a_s(\text{BET}) = n^a_m \times a_m \times \text{L} \tag{2.3}$$

where L is the Avogadro constant.

The amount of gas adsorbed, n^a, by unit mass of solid surface, m^s, depends on the relative pressure p/p_0, (where p is the equilibrium pressure and p_0 is the saturation vapor pressure of the adsorbant at given temperature), temperature and the nature of the gas-solid system. If the gas used is below its critical temperature and the temperature of the solid surface is held constant, n^a becomes a function of the equilibrium pressure. A plot of n^a/m^s against p/p_0 represents an adsorption isotherm which illustrates the relationship between the

amount of gas adsorbed by unit mass of solid surface and relative pressure at a known temperature. In order to obtain an equation for this isotherm curve, the BET model makes the following assumptions [77]:

i) Under the steady conditions of dynamic equilibrium the rate of adsorption in each layer is equal to the rate of evaporation from that layer

ii) The molecules in the first layer are located on a set of equivalent surface sites and that these molecules act as sites for the second layer, this arrangement is extended into multilayer

iii) There are no lateral adsorbate-adsorbate interaction

iv) in all layers after the first, the adsorption-desorption conditions are identical

v) In all layers except the first, the energy of adsorption is equal to the condensation energy

vi) When $p=p_0$, the multilayer has infinite thickness.

From these assumption the BET equation becomes:

$$(p/p_0)/(n^a(1-p/p_0)) = 1/ (n^a_m c) + ((c-1)/(n^a_m c))\times(p/p_0) \qquad (2.4)$$

where c is a constant.

The nitrogen adsorption/ desorption isotherms do not give information about micropore, while the Ar adsorption isotherms do. The argon adsorption

isotherms were recorded at the liquid argon temperature (T= -185.8 °C). The following experimental procedures were used. About 0.2 g of zeolite was placed in the glass tube, and kept under vacuum at 220 °C overnight to remove moisture. Then the micropore size distribution and the micropore volumes were interpreted by means of the Horvath and Kawazoe (HK) method. This method is based on potential function in the pore, which takes in account the adsorbate-adsorbent and adsorbate-adsorbate interactions [131]. The typical BET physisorption model is shown in (Figure 2.1) [132].

Figure 2.1. BET physisorption model (ref. 132)
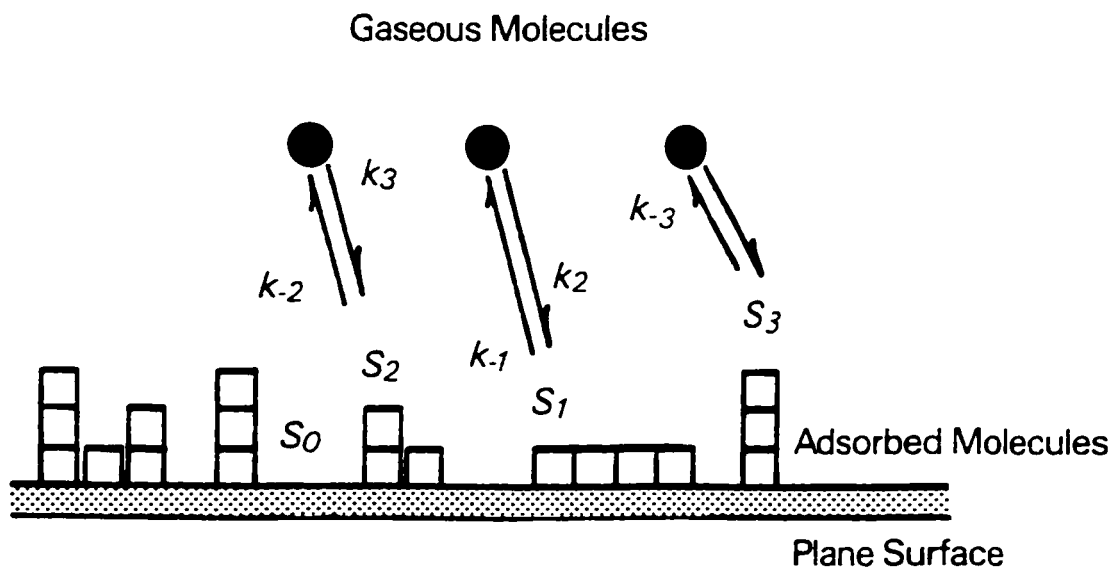
S_0 Fraction of surface not covered

S_1 Fraction of surface covered with one molecule

S_2 Fraction of surface covered with two molecules

S_3 Fraction of surface covered with three molecules

2.2.4 Ammonia adsorption and temperature programmed desorption (NH₃-TPD)

Temperature programmed desorption and micro-calorimetric studies employ probe molecules to investigate the interactions of surfaces with gas or liquid phase molecules. The probe molecules are chosen with respect to the nature of the adsorbed species believed to be important in the catalytic reaction or chosen to provide information on specific types of surface sites. Ammonia is a probe molecule which is widely used to study the surface acidity of zeolite catalysts [133]. The ammonia adsorption and temperature programmed desorption (NH₃-TPD) method was used to study the total acid density and the distribution of acid strength on the surface of acidic zeolite catalysts [69,134].

2.2.4.1 NH₃-TPD profile (acid sites strength distribution)

The NH₃-TPD experimental was identical to that described by R. Le Van Mao (Figure 2.2) [135,129]. During the experiment the temperature of the furnace was monitored using an Omega series CN - 2010 programmable temperature controller. 1 g (1.015±0.003 g) of catalyst was placed in a quartz tube reactor held in the middle of the reactor by ceramic disks. In order to remove the moisture from the catalyst and reduce the platinum to a metallic state, H_2 was passed through the catalyst at a flow rate of 15 ml/min at a temperature of 300 °C for 3 hours. The catalyst was then cooled down to 100 °C. At this temperature, pre-dried ammonia passed through the chamber at flow rate of 20 ml/min for 45 minutes. The zeolite sample saturated with ammonia

was flushed with helium at 20 ml/min at 100 °C for 20 hours in order to remove any remaining ammonia in the reactor system or any physisorbed ammonia in the zeolite sample. The chemisorbed ammonia in acid sites was desorbed gradually by heating the catalyst sample from 100 °C to 600 °C at a rate of 13.7 °C /min using helium at 20 ml/min as the carrier gas. The desorbed ammonia was measured using a HP 5890 gas chromatograph equipped with a thermal conductivity detector (TCD) set at 150 °C and the result was recorded by a HP 3392A integrator. The qualitatively obtained NH_3-TPD profile showed acid sites with different strength (weak, medium and strong) on the surface of zeolite catalysts. As a general rule, at lower temperature weak binding ammonia is released which correspond to weak acid sites, by increasing temperature medium and then strong binding ammonia are released which correspond to medium and strong acid sites, respectively.

2.2.4.2 Determination of total acid density

The same NH_3-TPD set up was used to measurement of total acid density using the following procedures. 1 g (1.015±0.003 g) of catalyst was placed in a quartz tube reactor. The sample was held in the middle of the reactor by ceramic disks. In order to remove the moisture from the catalyst and reduce the platinum to the metallic state, H_2 was passed through the catalyst at a flow rate of 15 ml/min at a temperature of 300 °C for 3 hours. Then, the temperature was decreased to 100 °C. At this temperature, pre-dried NH_3 was passed through the sample, at a flow rate of 20 ml/min for 45 min. Then pre-dried N_2 was passed through the sample at 100 °C for 20 hours in order to desorb

physisorbed NH_3. Then the TPD technique was used to desorb the chemisorbed NH_3. First the temperature was increased to 340 °C and the sample was kept at this temperature for 2 hours. Then, it was increased to 580 °C and was kept at this temperature for 4 hours. During the TPD experiment, nitrogen was passed through the sample at a rate of 20 ml/min and desorbed ammonia was trapped in 60 ml 0.038 M HCl. Then by using back titration, the amount of desorbed ammonia was measured, and the surface acid density was calculated as described below.

$$nNH_3 = V_A N_A /0.8 \text{ (80\% zeolite)} = Mol/g \text{ (acid density/g zeolite)} \qquad (2.5)$$

where V_A and N_A are acid volume and acid molarity respectively.

For the NH_3 -TPD experiment, again an Omega series CN - 2010 programmable temperature controller was used to control the temperature.
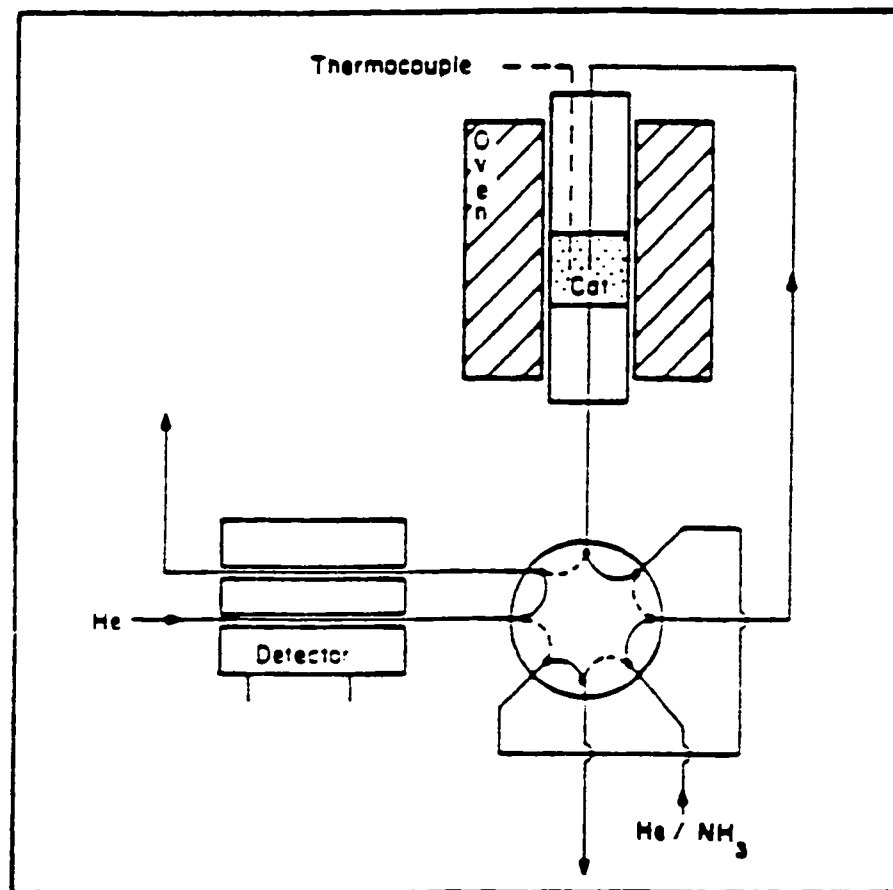
Figure 2.2. Ammonia temperature programmed desorption experimental set-up

2.2.5 Fourier Transform Infrared Spectroscopy (FTIR)

The application of infrared spectroscopy to the identification of unknown organic compounds is well established and extensively used. However, the infrared spectra derived from inorganic materials usually have broad absorption bands and overlapping, making the specific identification and assignments of a cation-anion pair difficult [136]. Since zeolites are widely used as solid acid catalysts in many industrial processes, characterization of acid sites in zeolites is an important subject [137]. In acid forms of high silica containing zeolites such as ZSM-5 and mordenite two different types of hydroxyl groups exist. These two OH groups in the fundamental stretching vibrations are characterized by narrow absorption bonds at 3740 and 3610 cm^{-1}, which correspond to silanol and bridged acidic OH groups, respectively [138]. A spectroscopic characterization of OH groups in zeolites is often carried out using probe molecules such as ammonia, pyridine, nitrogen and carbon monoxide [139].

2.2.5.1 FTIR study of chemisorbed pyridine on acid sites

Chemisorbed pyridine molecules on Bronsted and Lewis acid sites were studied by FTIR using a Nicolet Magna-IR spectrometer 550 equipped with the Omnic software. The transmission mode with resolution of 1 cm^{-1} was used. The FTIR spectra show peaks at 1545 cm^{-1}, 1453 cm^{-1} and 1489 cm^{-1} which are known to be due to the Brønsted acid site, the Lewis acid site and both types of site, respectively [140,141,142]. The procedure used for the FTIR experiments is as follows. i) About 22 mg of sample, were pressed in the center

of an O-ring. Then, the O-ring was placed in a glass tube and the moisture was removed from the sample under vacuum (10^{-2} mmHg) at 200 °C for 5 hours. ii) The sample was exposed to pyridine gas at 150 °C for 3 hours. iii) Physisorbed pyridine was removed under vacuum at 80 °C for 1 hour. iv) FTIR spectra were run.

2.2.5.2 IR diffuse reflectance (DRIFTS) study of adsorbed carbon monoxide on acid sites

Chemisorbed carbon monoxide molecules on Brønsted acid sites were studied by DRIFTS using a ABB Bomem spectrometer (Model MB 155S) equipped with the high temperature vacuum chamber (P/N 0030-103) and the Bomem Grams/32 software. The temperature was controlled using an Omega temperature controller (0019-022). The absorbance mode with resolution of 8 cm^{-1} and 128 scans were used. The DRIFTS spectra of HZSM-5 (Si/Al=50) before absorption of carbon monoxide show peaks at about 3740 cm^{-1} and 3608 cm^{-1}, corresponding to fundamental stretching vibrations of silanol and isolated bridged OH groups respectively (Figure 3.3). The DRIFTS spectra after absorption of carbon monoxide show extra peaks at about 2117 cm^{-1} and 2173 cm^{-1}, corresponding to stretching vibrations of chemisorbed carbon monoxide molecules on Brønsted acid sites. The procedure used for the DRIFTS experiments is as follows:

i) About 40 mg of quartz powder were placed in the sample cup and the moisture was removed from the quartz powder by passing nitrogen gas

through the vacuum chamber with a flow rate of 40 ml/min at 350 °C for 20 hours

ii) the temperature was reduced to 100 °C and the background spectra were taken

iii) the nitrogen flow was stopped and carbon monoxide was passed into the chamber with flow of 40 ml/min for 20 minutes and the background spectra were taken after absorbed carbon monoxide at 100 °C

iv) the temperature was reduced to 25 °C and again background spectra were taken

v) the quartz powder was taken out and 40 mg of sample (2% of zeolite diluted in 98% of quartz powder) was placed in the sample cup using the same procedures and related backgrounds, the DRIFTS spectra were run at 100 °C before chemisorbed carbon monoxide and after chemisorbed carbon monoxide at 100 °C and 25 °C.

2.3 Catalytic activity testing

2.3.1 Experimental set-up

The experimental set-up for n-heptane isomerization, shown in (Figure 2.3) was identical to that described elsewhere [123,124]. The final extrudate catalyst sample was loaded into a fixed bed tubular pyrex glass reactor with internal diameter of 1.2 cm and length of 40 cm. During the reaction period the reactor was heated using a digitally controlled furnace. The n-heptane reactant was fed into a heated (350 °C) vaporization flask using an injection syringe for

which the rate of reactant flow was regulated by an infusion pump. The flow of hydrogen as carrier gas was measured by a connected flow meter on line and entered into the flask to mix with n-heptane vapor before passing through the catalyst bed. A connected chromel-alumel thermocouple to a digital meter unit was positioned at the center of the catalyst bed to monitor the temperature of the catalyst. The hot vapor of reaction products was condensed in a liquid collector flask immersed in an ice-salt bath to obtain liquid sample. The separated gaseous products from the liquid phase were passed through a glass bulb from which the gas sampling was performed. Both the gas and liquid phases of the products were characterized using an HP 5790 Gas Chromatograph (GC) equipped with a 2.5 meter squalane column and a HP 3292 A integrator.
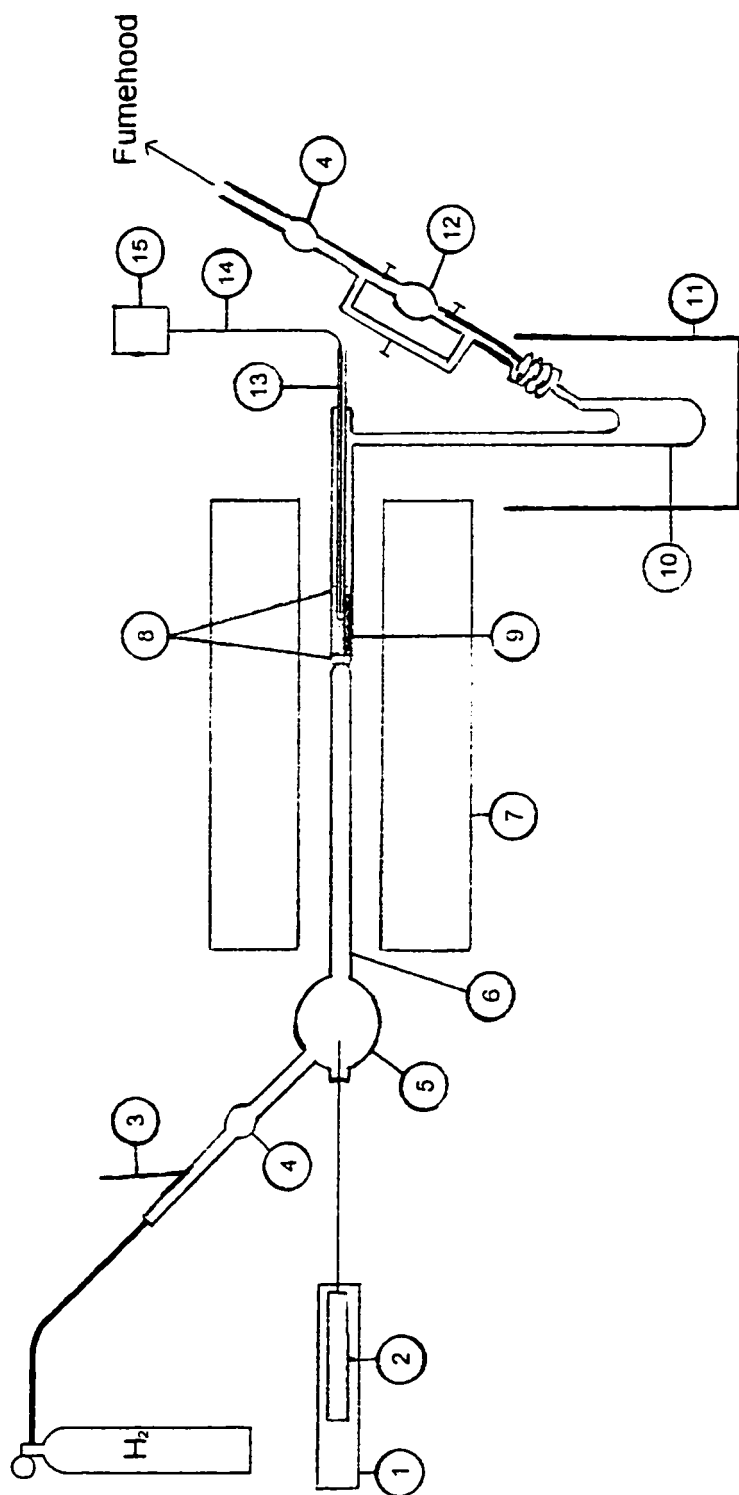
Figure 2.3. Experimental set-up for *n*-heptane isomerization

1. Infusion pump	6. Reactor tube
2. Syringe	7. Furnace
3. Flow meter	8. Porous disc
4. Soap bubble meter	9. Catalyst
5. Vaporization flask	10. Liquid sampling flask

11. Ice-salt bath
12. Gas sampling chamber
13. Thermowell
14. Thermocouple (chromel-alumel)
15. Digital thermometer unit

2.3.2 Operation conditions

Isomerization and cracking are competing reactions and the rates of isomerization and cracking depend on the reaction temperature. At high reaction temperature the level of n-heptane conversion is high, and a high conversion corresponds normally to a high cracking activity. After performing some experimental runs at different temperatures, the results show that at high reaction temperature n-heptane conversion is high but mostly cracking reactions occur while at low reaction temperature isomerization reactions are higher than cracking reactions but n-heptane conversion is low. As a result, the reaction temperature at normal operation conditions was chosen as 225 °C although some tests were done at 195 °C, 210 °C, 245 °C and 255 °C. The other reaction parameters were as follows:

i) At normal operation conditions 2.0 g (2.015 ± 0.003) of sample was used but in some tests the weight of catalyst decreased or increased in order to change contact time

ii) The flow rate of hydrogen (carrier gas) was about 15.4 ml/min except it was increased when the flow rate of reactant increased

iii) The contact time (gram of catalyst per g of n-heptane injected per hour) was 0.410 - 6.12 h

iv) The duration of a run was 2.5 hours. Prior to testing, the catalyst was reduced in-situ under hydrogen at 275 °C for 2 hours to obtain $Pt°$

The testing procedure and product analysis techniques used were identical to those described elsewhere [121,123,124]. After loading 2.0 g (2.015 ±0.003) of pre-dried zeolite catalyst into the reactor hydrogen gas at a flow rate of about 15.4 ml/min was passed through the catalyst at 275 °C for 2 hours in order to obtain Pt° and to remove any adsorbed moisture.

After this, the temperature of the catalyst in the reactor bed was reduced to the desired reaction temperature. Then n-heptane at a flow rate of 2.5 ml/min was fed into the heated vaporization flask and the mixture of n-heptane vapor and hydrogen gas allow to pass through the catalyst in the catalyst bed. The products vapor was trapped in the liquid sampling flask to obtain the liquid phase. The separated gaseous products from the liquid phase were passed through the glass bulb from which the gas sampling was injected into the GC to analyze. It is worth noting that all the Pt bearing zeolite catalysts showed a good on-stream stability through the run except for the first 15 min of reaction. Thus, the catalytic data reported herein were average values of the data collected from 30 min up to 2.5 hour of reaction. After finishing the reaction, the hydrogen gas passed through the catalyst in the catalyst bed for 30 min in order to remove all of products from catalyst. Finally, after collecting of liquid phase a sample of liquid phase was analyzed by GC.

2.3.3 Determination of the conversion and product selectivities

The number of carbon atom reactants and products were used to determine the conversion and product selectivities instead of normal molar

percent. This allows us to visualize the number of carbon atoms of n-heptane converted into the carbon containing products without being concerned about the molecular weight or molecular length and chemical composition of these products. Using 2,2-dimethylbutane as an internal standard and corresponding correction factors for products and n-heptane for the column and flame ionization detector (FID) detector used, the chromatographic peak areas were converted to the carbon atoms.

The total conversion of n-heptane is defined as follows [143]:

$$C\ (\ C\ atom\%\ ) = 100 \times [(NC)_f - (NC)_p] / (NC)_f \qquad (2.6)$$

where $(NC)_f$ and $(NC)_p$ are the number of C atoms of n-heptane in the feed and in the reactor out stream, respectively.

The selectivity (S_i) and yield (Y_{pi}) of product P_i are given by:

$$S_i = 100 \times (NC)_{pi} / [(NC)_f - (NC)_p] \qquad (2.7)$$

$$Y_{pi} = 100 \times (NC)_{pi} / (NC)_f \qquad (2.8)$$

where $(NC)_{pi}$ is the number of C atoms of product P_i .

The product selectivity (isomerization/cracking) R, is defined as:

R = sum of the selectivities for the branched C_7 paraffins / sum of the selectivities for the paraffins having C number lower than 7.

The composite selectivity ratio (Iso/Crk), is used to qualitatively assess the extent of the isomerization with respect to the cracking. This ratio relates to the selectivity ratio R as follows:

$$(Iso/Crk) = (Product\ selectivity\ ratio\ R) \times (Conversion/100) \qquad (2.9)$$

Thus, the composite selectivity ratio is the Product selectivity R multiplied by the mole fraction of converted n-heptane. The composite selectivity ratio (Iso/crk) is related to R and also to the conversion of n-heptane in order to use a parameter which can take into account the level of n-heptane conversion. In fact, the kinetic behavior of the β-scission (cracking) depends on the level of n-heptane conversion:

a) A high conversion corresponds normally to a high cracking activity [144] and thus to a low value of both product selectivity ratio R and composite selectivity ratio (Iso/Crk). At the level of the acid sites, the higher the total conversion, the higher the degree of branching of the carbocations, the faster the rates of β-scission [117]. This is an ideal situation for the study of the action of the Zn, Al, Cd and other species incorporated into the bifunctional catalyst because if these species could decrease the effect of cracking, thus increasing the selectivity to the isomerization product, the composite selectivity ratio and the product selectivity ratio R would account correctly for any change in the

competition between the isomerization and cracking.

.

b) At low conversion levels, the selectivity to branched C_7 may be high and the selectivity to cracked products may be low, and the value of the resulting R ratio maybe high. However, this situation is of little interest for us since the branched paraffins, being mainly mono-branched, have a much slower cracking rate and the effect of the Zn, Al, Cd and other species incorporated cannot be significant. Fortunately, because of the correction due to the (lower value of the) conversion, the value of the composite selectivity ratio is much lower than that of the R ratio, thus reflecting correctly our lack of interest. For this reason, the use of the composite selectivity ratio appears to be more advantageous in our study than that of the product selectivity ratio R.

The branching degree ratio (mu/mo) is defined as the ratio of the selectivity of product tri- and di-branched heptanes (mu) to the selectivity of product mono-branched heptanes (mo). A value of the branching degree ratio indicate a high yield of multi-branched heptanes.

The reactant contact time τ and the weight hourly space velocity (WHSV) used in this research work were defined as follows:

τ (expressed in hours) = W_{cat} / F_{reac} (2.10)

WHSV (expressed in hr^{-1}) = F_{reac} / W_{cat} (2.11)

where W_{cat} and F_{reac} are the weight of the catalyst (in gram) and the total flow rate of the reactants (in g/hr), respectively. Satisfactory reproducibilities with respect to different reaction runs preformed using the same catalyst and same conditions were within 5%.

2.3.4 Kinetic studies

Zeolite based catalysts are extensively used in many acid-catalyzed reactions such as hydroisomerization and hydrocracking due to their high activity, selectivity, stability and resistance to catalytic poisoning [145]. The theoretical basis for zeolitic diffusion i.e., diffusion in pores where the dimensions of the molecules are nearly the same as those of the pores, is complex and not well defined [146]. An extensive effort has been invested in the understanding of the zeolitic diffusion and reaction networks leading to the formation of isomers as well as cracked products from normal and branched paraffins. Hydroisomerization and hydrocracking of normal paraffins have been shown to proceed in consecutive steps and the competition between these two reactions is effected by the nature of catalyst used and reaction conditions, and the values of activation energies may be different over different catalysts.

The objective of kinetic studies in this work include:

i) The determination of the initial rates of the isomerization and cracking in the conversion process of n-heptane

ii) Calculation of the apparent activation energies and the pre-exponential

factors using the Arrhenius equation:

$$k = A \exp(-E_a / RT) \tag{2.12}$$

where k is the rate constant, which in our case, k is proportional to the initial reaction rate r_0, E_a is the apparent activation energy, A is the pre-exponential factor, R and T (in K) have their usual meaning.

> iii) Kinetic data will be used as an experimental support to the mechanistic hypothesis of (trifunctional catalyst concept)

CHAPTER III

RESULTS AND DISCUSSION

3.1 Zeolite catalysts for hydrocracking and hydroisomerization

In typical bifunctional zeolite catalyst formulations, the noble metal catalyzes hydrogenation-dehydrogenation reactions, and the zeolite hydroxyl groups catalyze the carbocation rearrangements. Such catalysts are particularly useful for the branching isomerization of n-alkanes. In contrast to monofunctional catalysis, in bifunctional catalysis a synergism exists between the two sets of sites leading to an enhanced catalytic activity, suppressed deactivation, and higher yields of tertiary and quaternary C atoms products [147]. Classic hydrocracking takes place when branched secondary and tertiary alkylcarbenium ions are derived from feed molecule. These carbenium ions are cleaved by a single β-scission into smaller alkylcarbenium ions and alkanes, in which the formation of primary alkylcarbenium ions is unlikely and the carbon number of cracked products from a C_nH_{2n+2} alkane are within the 3 and n-3 [119,148]. On strong acid sites, olefinic reaction intermediates may dimerize and by rapid cracking generate cracked products which cannot be formed via classic hydrocracking, such as C_5 and C_6 from a C_7 feed [149,150,151].

3.2 Study of the n-octane hydrocracking using hybrid catalysts

The objectives of this study were as follows:

i) To perform the hydrocracking/isomerization of n-octane over wide temperature range by making use of the parent Pt-HY zeolite and the hybrid Pt-HY/SA (SA= silica-alumina used as co-catalyst). The resulting

Arrhenius plot from these kinetic studies could allow us to determine at which reaction temperature the co-catalyst start having some effects on the diffusion of the products

ii) By using the information from the n-octane reaction, to prepare hybrid catalysts for the isomerization of the n-heptane. These hybrid catalysts would contain Al species incorporated as "diffusion accelerators" in two different ways: impregnation into the zeolite crystallites resulting in the "internal", or extrusion (embedment) with these crystallites, generating in the "external" hybrid configurations.

The Pt-HY and Pt-HY/SA both contained 80 wt % of HY zeolite and 0.5 wt % of Pt. The Pt-HY/SA sample contained in addition 10 wt % of SA, being a hybrid catalyst with "external" configuration, i.e. the micro-sized HY zeolite crystallites being embedded in the larger-sized particles of silica-alumina. The Pt-SA (Pt = 0.5 wt %, SA = 80 wt % and balance = bentonite) as reference sample was also prepared. The preparation procedure was described in section 2.1.3. Some of the physico-chemical properties of the HY zeolite and the SA are reported in (Table 3.1).

	Particle size[*] (μm)	BET surface area (m^2/g)	Pore diameter (10^{-9} m)	Surface acidity[&] (mmol/g) (mmol/m^2)	
HY	1-2	610	0.74	0.92	1.5
SA	50-100	641	4.6	0.32[☆]	0.5

(*) determined by scanning electron microscopy;

(&) measured by the NH$_3$ TPD technique

(☆) weak acid sites when compared with those of the HY zeolite.

Table 3.1. Some physico-chemical properties of the HY zeolite and the co-catalyst used in the *n*-octane conversion.

The experimental set-up for the conversion of n-octane was identical to that described in section 2.3.1. The reaction parameter were as follow:

i) temperature = 172 °C - 297 °C (445.15 K - 570.15 K)

ii) contact time = 0.13 to 2.5 h

iii) partial pressure of n-octane=0.02 atm

iv) ratio of flow-rate of nitrogen (used as carrier gas) to flow-rate of hydrogen = 4/3

v) weight of catalyst = 0.625 gr

vi) duration of a run = 4 h

The testing procedure and product analysis techniques used were identical to those described in section 2.3.1. The total conversion of n-octane were calculated using equations 2.6. As mentioned before, for each catalyst at each reaction temperature, the experimental data for total conversion were fit to a function $f(\tau)$, of contact time τ (equations 3.10).

Arrhenius plots of the Pt-HY parent zeolite (a) and the Pt-HY/SA hybrid catalyst (b) is shown in (Figure 3.1). From this figure it is clear that the slope of the curve 3.1a (parent zeolite) is the same for all the points corresponding to the temperature range investigated, there is a clear slope change for curve 3.1b hybrid catalyst starting at a temperature of 250 °C (523.15 K). This is indicative of the occurrence of a diffusional phenomenon leading to a lower value of the apparent activation energy. Since under the same reaction condition the reference sample Pt/SA (silica-alumina alone) did not give any significant

n-octane conversion, the effect of the co-catalyst could not be attributed to any cooperation of the co-catalyst surface to the total conversion. The large surface area and mesoporosity of the co-catalyst used, led to the same interpretation as in hypothesis where the formation of a pore continuum within the hybrid catalyst was proposed by Le Van Mao [152]. The newly formed funnel-shaped pore system effected the outward-diffusion of the reaction products only with reactions occurring at high temperature. Co-catalyst can speed up the removal of the reaction products at large distance, but at low reaction temperature it does not show any significant effect of co-catalyst (Table 3.2 and Figure 3.1). Thus, it is the reason, why "internal" impregnation was used instead of "external" impregnation for the hydroisomerization of *n*-heptane. In addition, in the conversion of *n*-octane the catalyst with an external hybrid configuration behaved like the parent zeolite when the reaction temperature was lower than 250 °C (523.15 K).

Catalyst	$k_t^{(*)}$	$\ln k_t$	T (K)	$1/T \ (\times 10^{-3})$
Pt-HY	339.3	5.8269	548.15	1.8243
	207.8	5.3366	523.15	1.9115
	123.6	4.8171	503.15	1.9875
	16.4	2.7972	463.15	2.1591
	13.4	2.5953	445.15	2.2464
Pt-HY/SA	113.4	4.7309	570.15	1.7539
	101.0	4.6151	548.15	1.8243
	98.2	4.5870	523.15	1.9115
	58.4	4.0673	498.15	2.0074
	20.1	3.0007	473.15	2.1135
	8.7	2.1633	448.15	2.2316

(*): $k_t = k_{total}$

Table 3.2. Arrhenius plots for the Pt-HY and Pt-HY/SA zeolite catalysts.
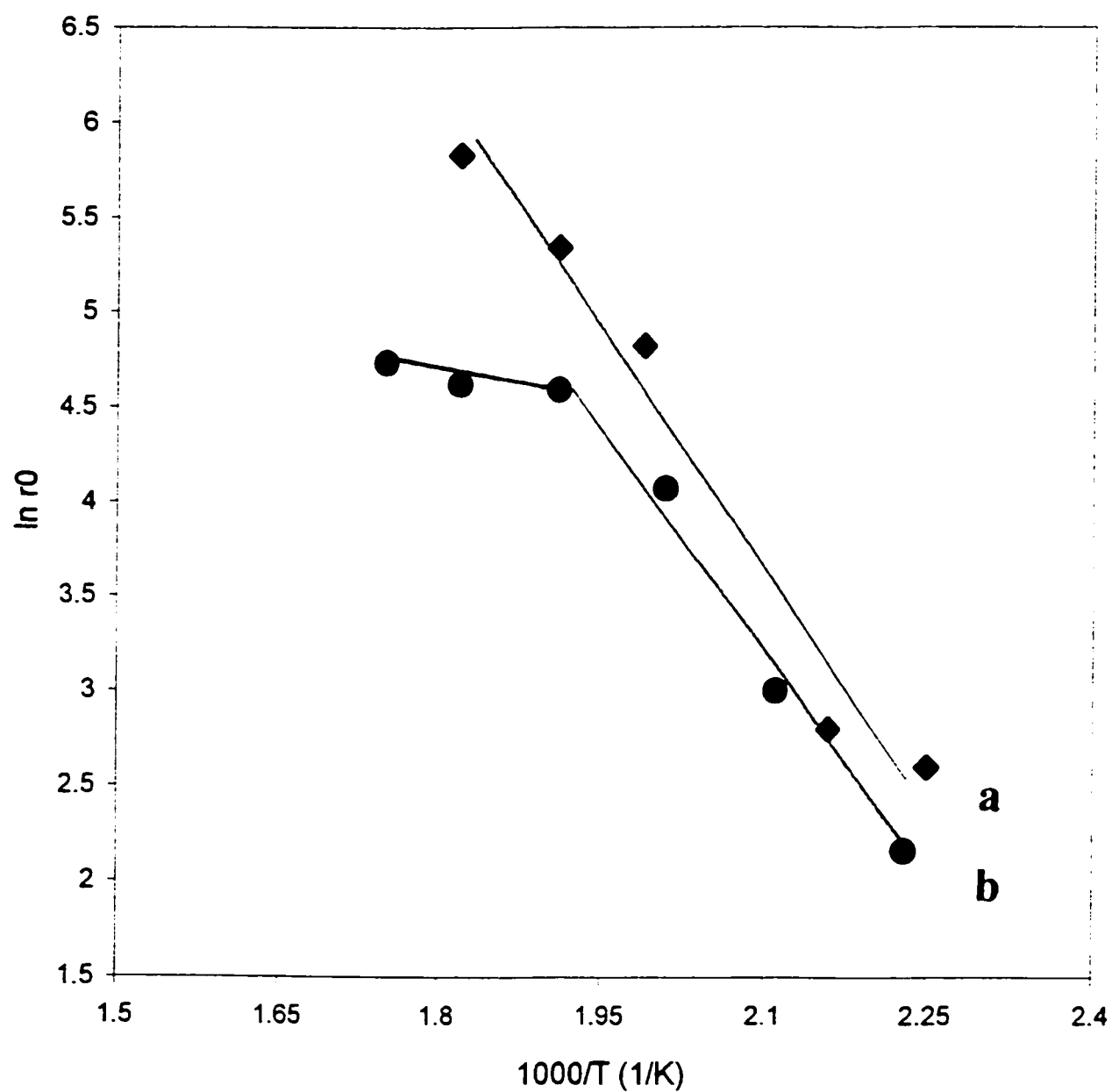
Figure 3.1. Arrhenius plots of the *n*-octane conversion obtained with the Pt-HY

(a) and Pt-HY/SA zeolite catalysts (b).

3.3 Study of *n*-heptane hydroisomerization using modified Pt-HY zeolite catalysts

In the hydroisomerization processes of long-chain *n*-paraffins, branched paraffins are the desired products. Production of a large proportion of mono-branched paraffins is adequate for most lubricant dewaxing processes, this is not the case for motor fuels upgrading which aims at production of more multi-branched paraffins. The later paraffins exhibit higher octane rating properties, so that considerable efforts have been made to avoid the devastating effect of cracking on the final production of these multi-branched paraffins. The traditional approach is to search catalysts with stronger surface acidity [145,153]. These catalysts include zeolites and superacidic solid materials. The isomerization reaction is carried out at lower temperature using these very acidic catalysts. Under such mild condition the isomerization reaction is increased and cracking reaction is much reduced, because of difference in reaction kinetics favoring the isomerization products. In addition, it is found the use of molecular hydride transfer agents such as adamantyl compounds significantly decreased the cracking [145], or affected by zeolite-type catalysts with different pore size [154,106], and/or structure/surface composition [119,111]. Even large pore mouths promoted cracking [104].

3.3.1 Al, Zn and Cd loaded Pt-HY zeolite catalysts

3.3.1.1 Catalyst preparation

The HY zeolite was obtained by calcination of ammonium-Y zeolite in air at 550 °C overnight (as described in section 2.1.2). The Pt-Al$_y$-HY (simultaneous incorporation of Pt and Al), Pt-Al^y-HY (sequential incorporation of Pt and Al) and Pt-HY zeolite catalysts (all internal configuration) were prepared using HY zeolite, [Al(NO$_3$)$_3$.9 H$_2$O] and tetraammineplatinum (II) chloride hydrate [Pt(NH$_3$)$_4$Cl$_2$.H$_2$ O]. The techniques used for the preparation were identical to those described in section 2.1.3 with the same content of Al and pt. Also Pt-Al$_{ey}$-HY and (Pt-HY)$_e$ (both external configuration) using the same technique and materials as described in section 2.1.4 with the same content of Al and pt. The Pt-Zn$_y$-HY (simultaneous incorporation of Pt and Zn) and Pt-Zn^y-HY (sequential incorporation of Pt and Zn), also Pt-Cd$_y$-HY (simultaneous incorporation of Pt and Cd) and Pt-Cd^y-HY (sequential incorporation of Pt and Cd) were prepared and tested using the same procedure and instead of aluminum nitrate (Al(NO$_3$)$_3$.9H$_2$O), zinc nitrate (Zn(NO$_3$)$_2$.6H$_2$O) and cadmium nitrate tetrahydrate (Cd(NO$_3$)$_2$ .4 H$_2$O) were used.

3.3.1.2 Catalyst characterization

Characterization techniques, which have already been introduced in chapter 2, include the determination of :

i) Chemical composition by atomic absorption spectroscopy

ii) Total surface area, micropore area and pore size by the **BET** method

iii) Total acid density and the distribution of acid strength on the surface by ammonia adsorption and temperature programmed desorption (NH_3-TPD) method

iv) The nature of acid sites (Brønsted and Lewis) by diffuse reflectance IR spectroscopy and FTIR study of chemisorbed pyridine on these sites

3.3.1.2.1 Determination of BET surface area and pore size distribution

The total **BET** surface areas, micropore area and average pore diameters of HY, Pt-HY (bifunctional catalyst) and Pt-Al$_x$-HY zeolite catalysts are reported in (Table 3.3). It is clear that, the pore size (0.74 nm) almost stays unchanged upon Al loading at low concentration (< 2%). This pore size is large enough that molecule of n-heptane and its isomers able to pass through in it (Figure 3.2). However, at lower Al loading (< 2%) there are minor decrease on total **BET** surface area and micropore area. By increasing the Al loading there was large decrease of total **BET** surface area, and the micropore area. This is maybe due to pore blockage phenomena.

Catalyst	Al loading (wt.%)	Total (BET) surface area (m²/g)	Micropore area (m²/g)	Pore size (nm)
HY	0	562	406	0.74
Pt-HY	0	518	381	0.74
Pt-Al$_1$-HY	1	505	367	0.74
Pt-Al$_2$-HY	2	487	363	0.74
Pt-Al$_3$-HY	3	439	319	0.73
Pt-Al$_5$-HY	5	395	280	0.73
Pt-Al$_7$-HY	7	364	265	0.72
(Pt-HY)$_e$[a]	0	514	425	0.74
(Pt-Al$_{e2}$-HY)[a]	2	517	431	0.74

a) external impregnation

Table 3.3. Some physico-chemical properties of the parent and modified HY zeolite catalysts used in this work.
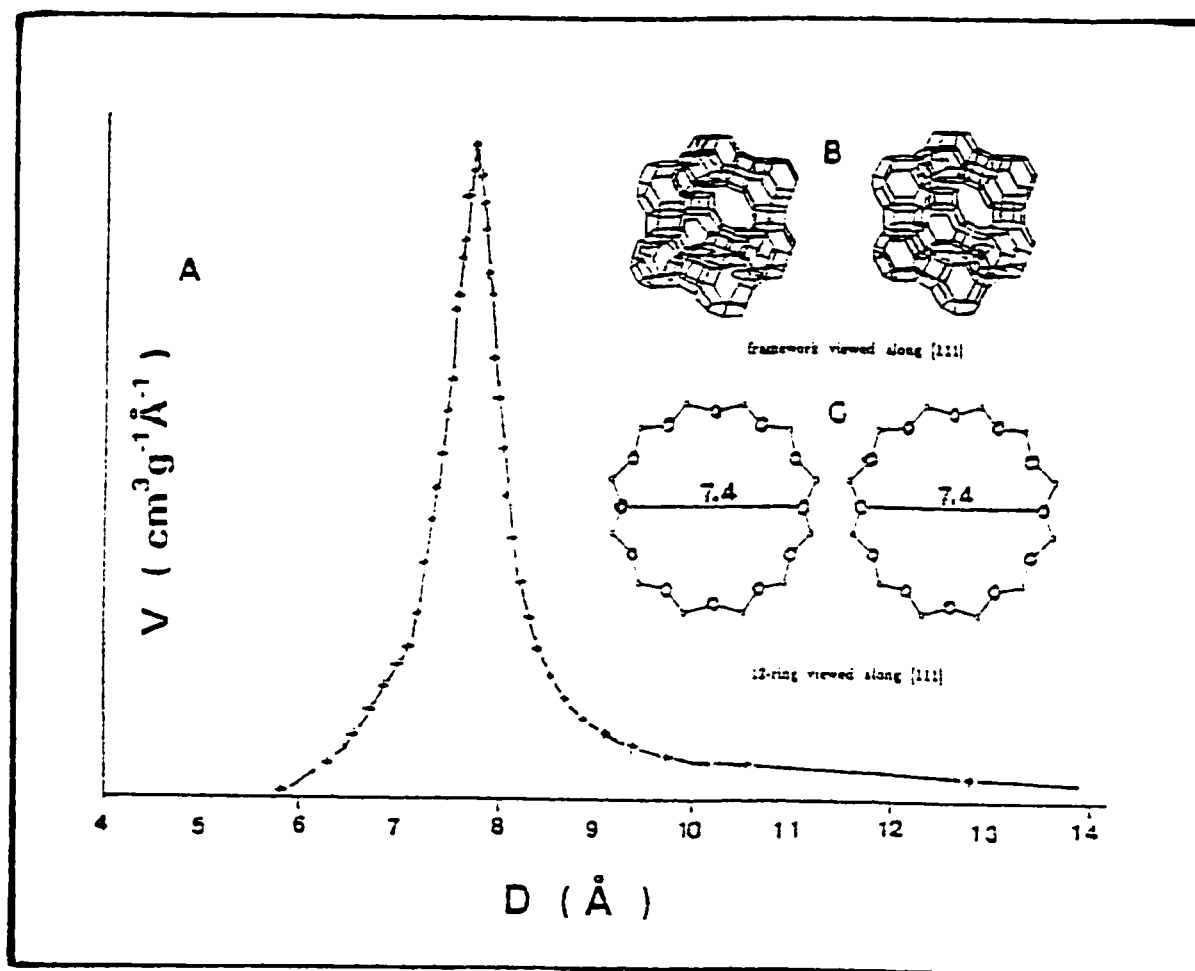
Figure 3.2. Micropore size distribution of HY zeolite (A), its theoretical
structure (B) and pore system (C).

V: volume of N_2 adsorbate physisorbed, D: Pore diameter

3.3.1.2.2 Determination of the acid density and strength

Diffuse reflectance IR spectroscopy show that, in hydrogen forms of high-silica containing zeolites such as ZSM-5, and in mordenite, two different types of hydroxyl group exist. Two fundamental stretching vibrations are characterized by narrow absorption bands at 3740 and 3605 cm^{-1} in the region of the OH-bond stretch, which correspond to silanol and bridged acidic OH groups (silanol associated with Al tetrahedra), respectively [138]. These adsorption bands of hydroxyl group in the HZSM-5 network with ratio of (Si/Al = 50) were found at 3740 and 3608 cm^{-1} using diffuse reflectance FTIR spectroscopy (Figure 3.3), and in HZSM-5 network with ratio of (Si/Al = 20) were found at 3741 and 3611 cm^{-1} (Figure 3.4). However, these adsorption bands of hydroxyl group in HY network with ratio of (Si/Al = 2.5) were found at 3745 and 3614 cm^{-1} using diffuse reflectance FTIR spectroscopy (Figure 3.5). Acid sites could be classified as weak, medium and strong acid sites. The profiles of acid strength provided by ammonia-TPD technique were plotted in (Figure 3.6). From this profile it is clear that the density of weak acid sites are higher than that of strong or medium acid sites. The profiles obtained for Pt-Al$_{0.7}$-HY and Pt-Al$_{0.9}$-HY are similar to that of the Pt-HY zeolite catalyst. However, from these profiles it is clear that, by loading of Al species, the Lewis acid sites increase, and by loading of Zn species, the Lewis acid sites increase even more than in the case of Al loading. In order to quantitatively estimate the distribution of acid strengths in each catalyst, these profiles were deconvoluted according to a previous classification of acid strength, the results of this estimation are recorded in (Table 3.4).
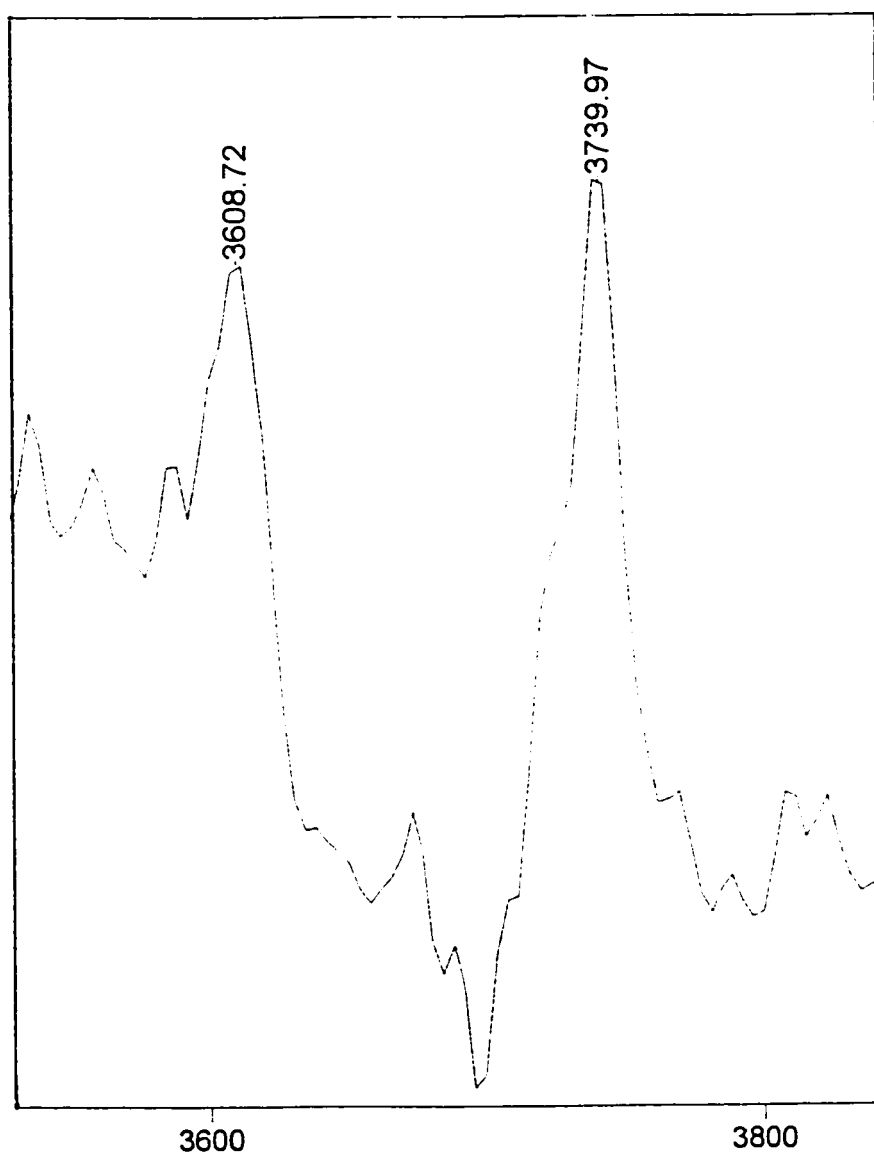
Figure 3.3. Diffuse reflectance FTIR spectroscopy of HZSM-5 (Si/Al = 50).
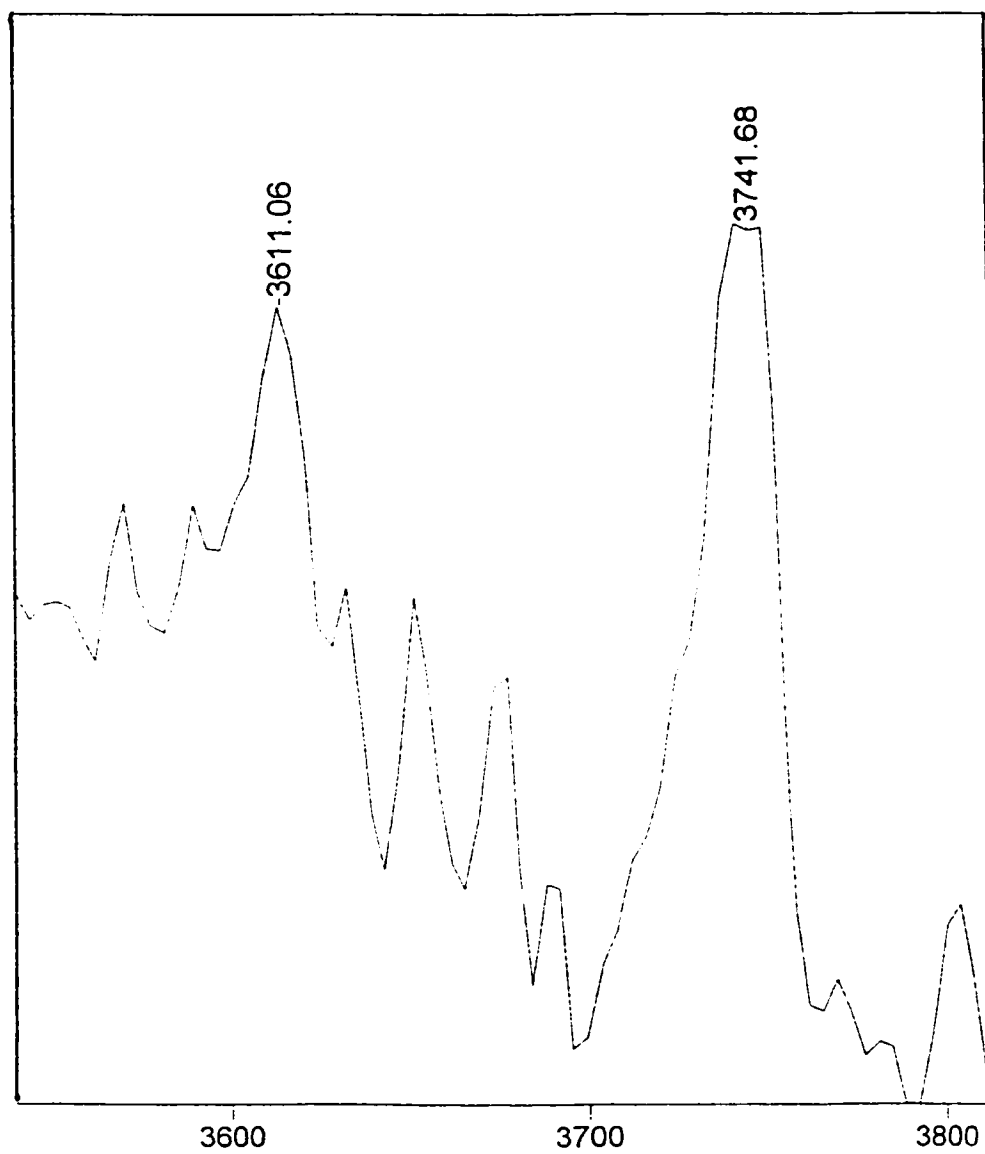
Figure 3.4. Diffuse reflectance FTIR spectroscopy of HZSM-5 (Si/Al = 20).
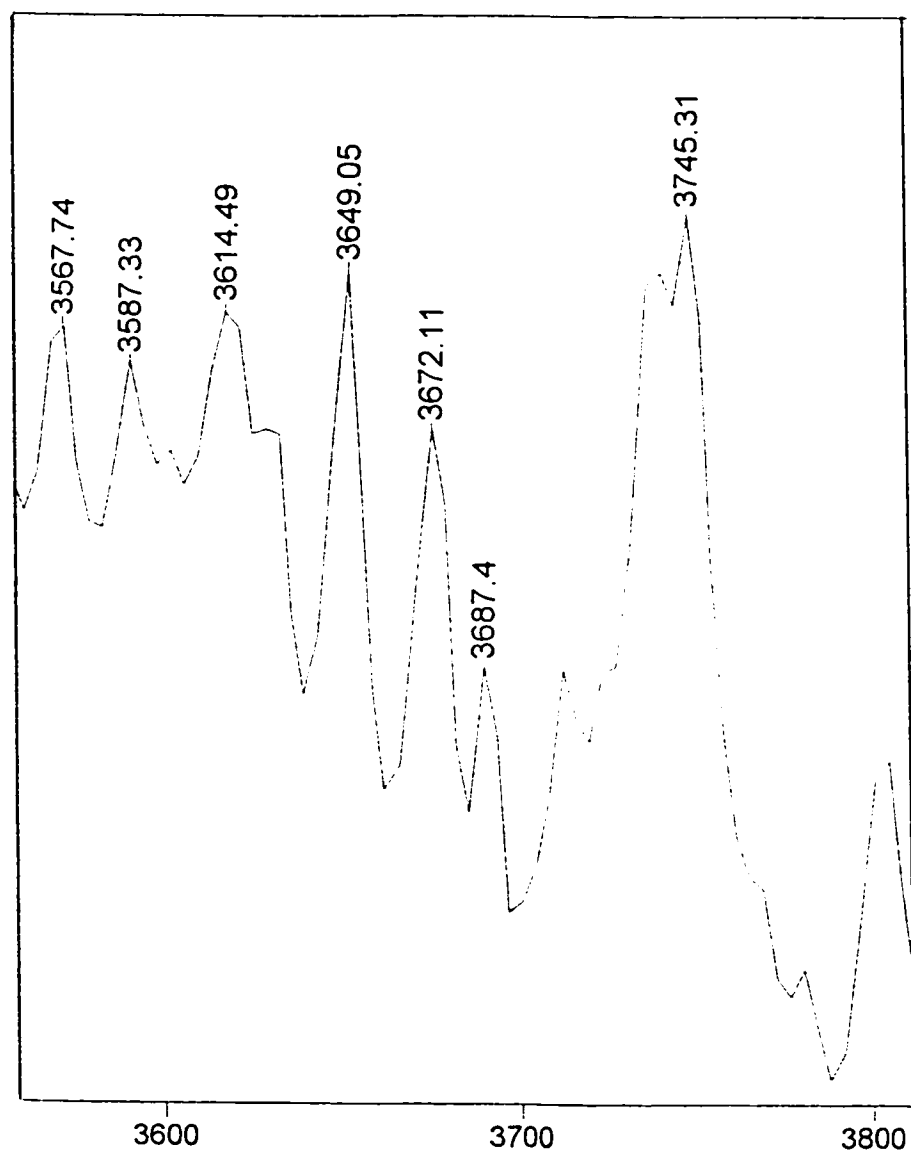
Figure 3.5. Diffuse reflectance FTIR spectroscopy of HY (Si/Al = 2.5).
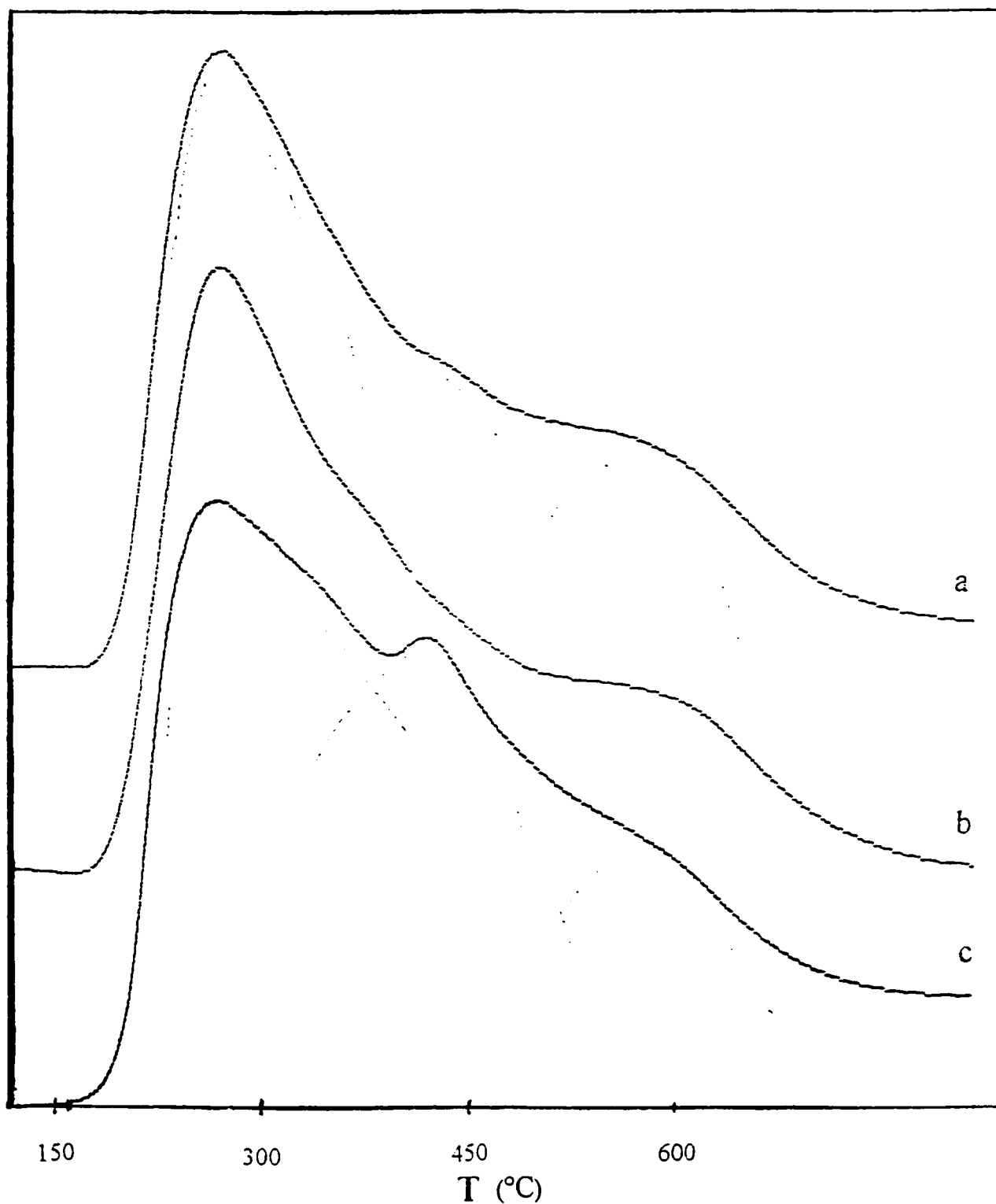
Figure 3.6. TPD curves of ammonia adsorbed at 100 °C, for a) Pt-HY, b)

Pt-Al$_{o.7}$-HY and c) Pt-Zn$_{o.9}$-HY zeolite (Al = 0.7 and

Zn = 0.9 mmol/g of zeolite).

Sample	Weak acid site density %	Medium acid site density %	Strong acid site density %
HY	50	17	33
Pt-HY	48	27	25
Pt-Al$_{0.7}$-HY	47	27	26
Pt-Zn$_{0.9}$-HY	48	32	20

Table 3.4. Influence of the incorporated Al and Zn species(Al = 0.7 and Zn = 0.9 mmol/g of zeolite) on the strength of different acid sites of HY zeolite (estimated distribution of acid strength)

Chemisorbed pyridine molecules on Brønsted and Lewis acid sites were studied by FTIR to investigate the nature of acid sites and the effect of incorporated species such as Al on these sites. It is worth noting that pyridine is classified as a weaker base than ammonia and pyridine is more stable than ammonia.

The pyridine molecule can undergo coordination to aprotic sites, it can be protonated to form the pyridinium ion PyH^+ on acidic OH group and it can undergo H-bonding with less acidic groups. The infrared spectra of pyridine coordination compounds [155] are clearly distinct from those of PyH^+ and of H-bonded pyridine [141, 156].

However, upon pyridine adsorption on the acid sites, three IR bands at 1545 cm $^{-1}$, 1453 cm $^{-1}$ and 1489 cm $^{-1}$ were observed, which are assigned to Brønsted , Lewis and both (Brønsted and Lewis) sites respectively (Figure 3.7, 3.8 and 3.9). The density of acid sites and some calculation of acid density ratio for Brønsted and Lewis acid site using peak area is recorded in (Table 3.5). From these results it is clear that there was no significant change of the total surface acid density, and the density of Brønsted and Lewis acid sites when the results of the Pt-HY are compared to that of the Pt-Al$_y$-HY zeolite catalysts.
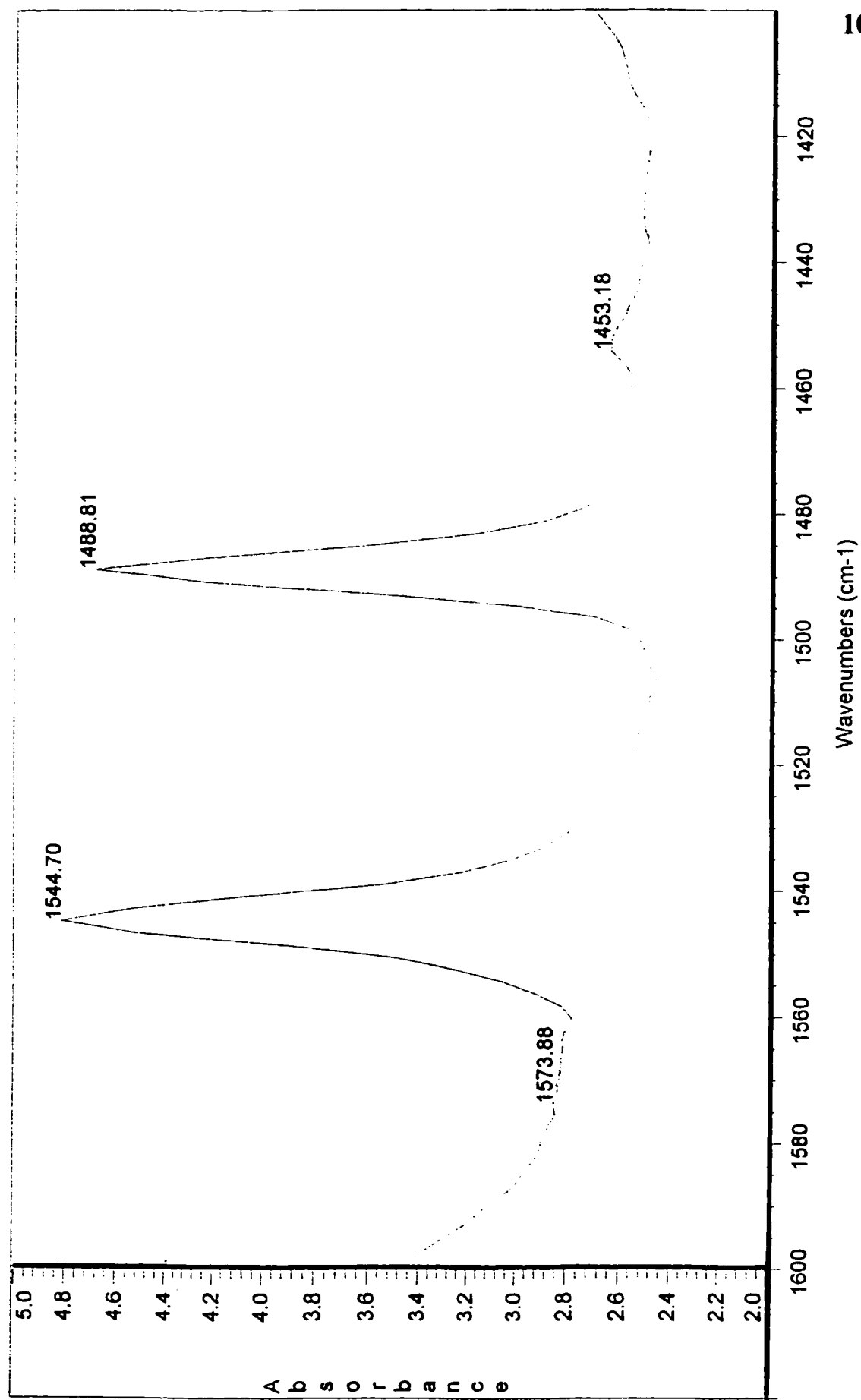
Figure 3.7. The FTIR spectroscopy of chemisorbed pyridine on HY zeolite.

102
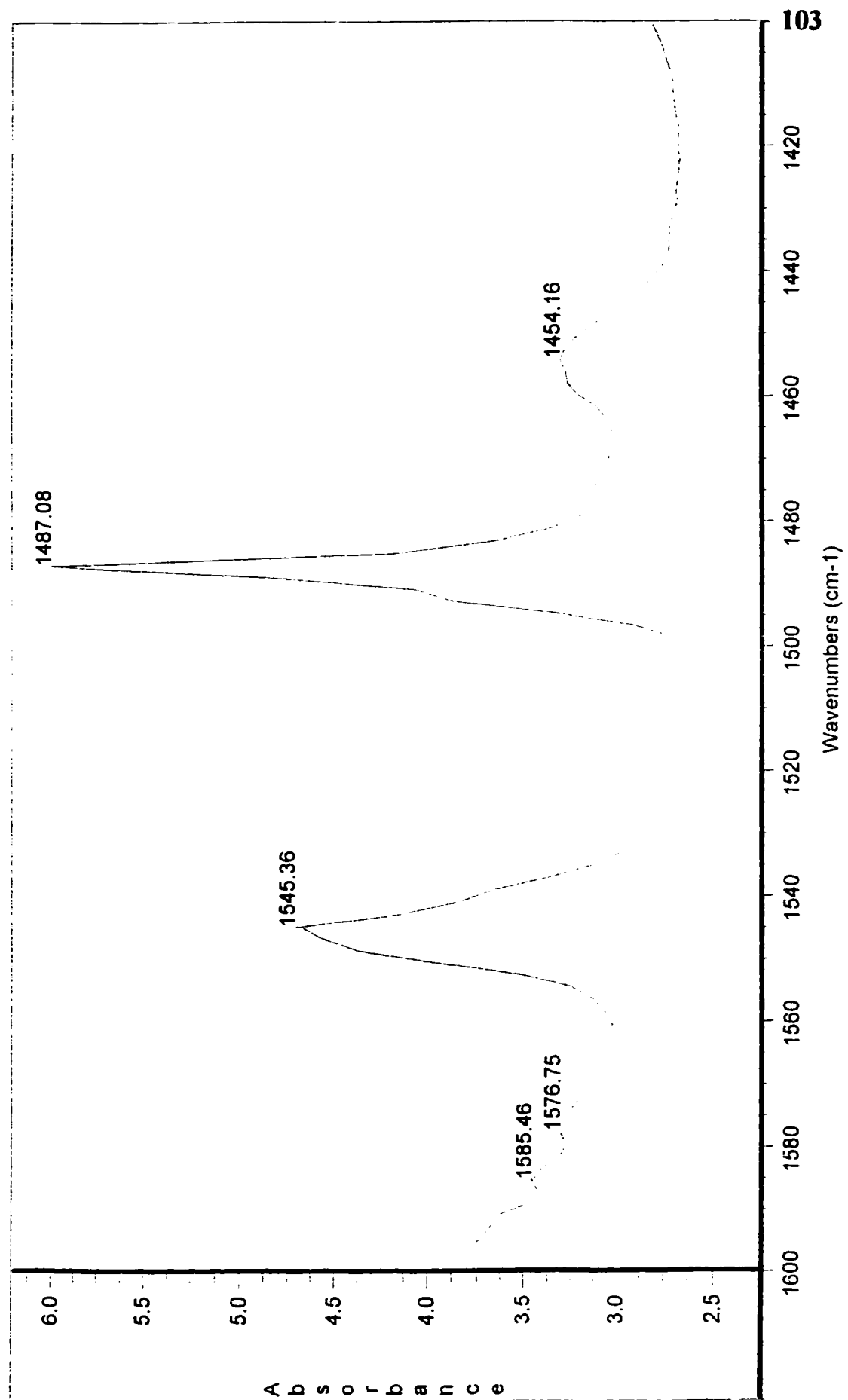
Figure 3.8. The FTIR spectroscopy of chemisorbed pyridine on Pt-HY zeolite.
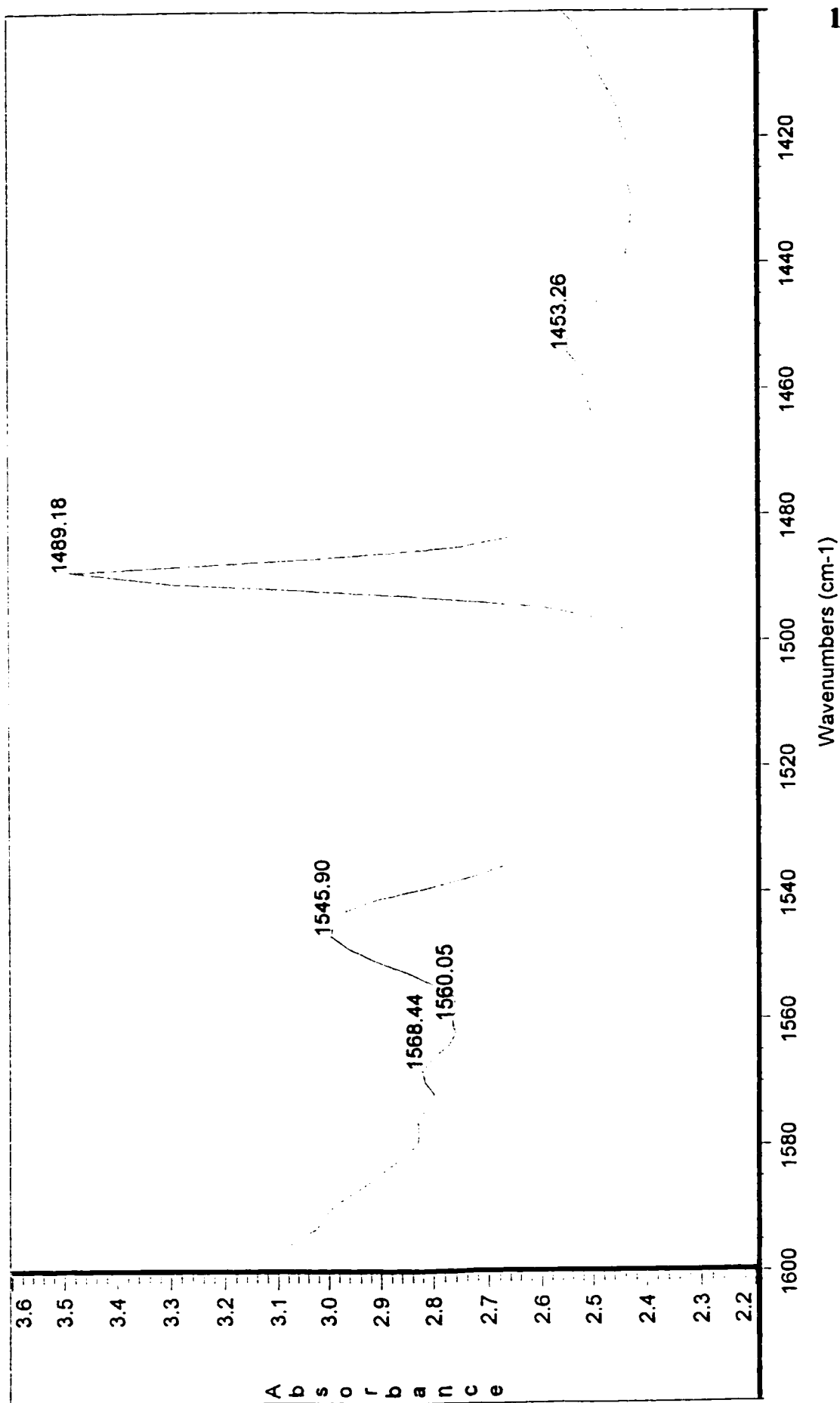
Figure 3.9. The FTIR spectroscopy of chemisorbed pyridine on Pt-Al$_l$-HY zeolite (Al = 1 wt.% of zeolite catalyst).

104

Catalyst	Al loading (wt.%)	acid site density (10^{-3} mol/g)	(Ac/tet. Al)^a	B/M^b	L/M
HY	0	2.3	1.0	1.2	0.1
Pt-HY	0	2.5	1.1	0.9	0.2
Pt-Al$_1$-HY	0	2.5	1.1	0.8	0.2
Pt-Al$_2$-HY	0	2.6	1.1	0.8	0.2

a) Number of acid sites/number of the zeolite tetrahedra Al sites.

b) B (1545 cm^{-1}) and (1453 cm^{-1}) are IR bands assigned to Brønsted and Lewis acid sites, respectively, Band M (1489 cm^{-1}) assigned to both sites. B/M and L/M: ratios of band areas.

Table 3.5. Density of surface acid sites and some results of the FTIR analysis of adsorbed pyridine.

3.3.1.3 Catalytic performance of the modified Pt-HY zeolites

The isomerizing properties of the bifunctional Pt-HY catalyst significantly increased when Al species in small amounts were incorporated into this catalyst.

Figure 3.10a illustrates the variations of the yield of (C_5-C_7) branched paraffins, Y_{liso}, with the weight % of aluminum incorporated into the zeolite material which already contains Pt species (Pt-Al^y-HY samples obtained by sequential incorporation of Pt and Al). The isomerizing properties of the bifunctional Pt-HY catalyst significantly increases by incorporation of small amounts of Al species. From this figure it is clear that, the curve of the yield versus the Al loading goes through a maximum at quite low concentration of Al: ca. 1-1.5 wt.% of Al (ca. 0.5×10^{-3} mol of Al/g of zeolite), then decreases with higher Al loading.

Figure 3.10b illustrates the variations of the yield of (C_5-C_7) branched paraffins, Y_{liso}, with the weight % of aluminum incorporated at same time with Pt species into the zeolite material (Pt-Al$_y$-HY samples obtained by simultaneous incorporation of Pt and Al). The variations of the isomerization products resulted from simultaneous incorporation of Pt and Al catalysts are similar to those of the sequential incorporation of Pt and Al catalysts, i.e. same initial enhancement and same curve shape with maximum at almost the same Al loading. It is clear that, Al loading in small amount has positive effect on the production of (C_5-C_7) branched paraffins (Table 3.6). However, higher yield of (C_5-C_7) products were obtained with the simultaneous loading of Pt and Al.

Al loading		Conversion (C atom %)	Y_{iso} (C_5-C_7)	Product selectivity		mu/mo	Selectivity ratio	
(wt%)	(10^{-3} mol/g)			S_{iso}	S_{Crk}		R	(Iso/Crk)
Pt-Al$_y$-HY catalysts (method of simultaneous incorporation)								
0.0	0.00	82.9	40.8	46.2	53.8	0.48	0.9	0.7
0.5	0.18	83.4	65.2	75.6	24.4	0.40	3.1	2.3
1.0	0.37	81.4	68.1	79.6	20.4	0.39	3.9	3.2
1.5	0.56	82.1	65.8	79.2	20.8	0.33	3.8	3.1
2.0	0.74	71.7	54.9	84.1	15.9	0.32	5.3	3.8
3.0	1.11	50.7	45.7	87.5	12.5	0.28	7.0	3.6
5.0	1.85	38.4	34.1	86.4	13.6	0.28	6.4	2.4
Pt-Al^y-HY catalysts (method of sequential incorporation)								
0.5	0.18	77.0	48.8	53.5	46.5	0.32	1.2	0.9
1.0	0.37	79.4	53.6	52.4	47.6	0.33	1.1	0.9
1.5	0.56	74.5	44.0	54.5	45.5	0.34	1.2	0.9
2.0	0.74	75.1	45.1	56.2	43.8	0.33	1.3	1.0
3.0	1.11	64.3	36.9	50.1	49.9	0.29	1.0	0.6
5.0	1.85	58.4	36.6	54.5	45.5	0.30	1.2	0.7

Table 3.6. Activity and selectivity versus the Al loading (contact time=1.042 h and T = 225 °C).
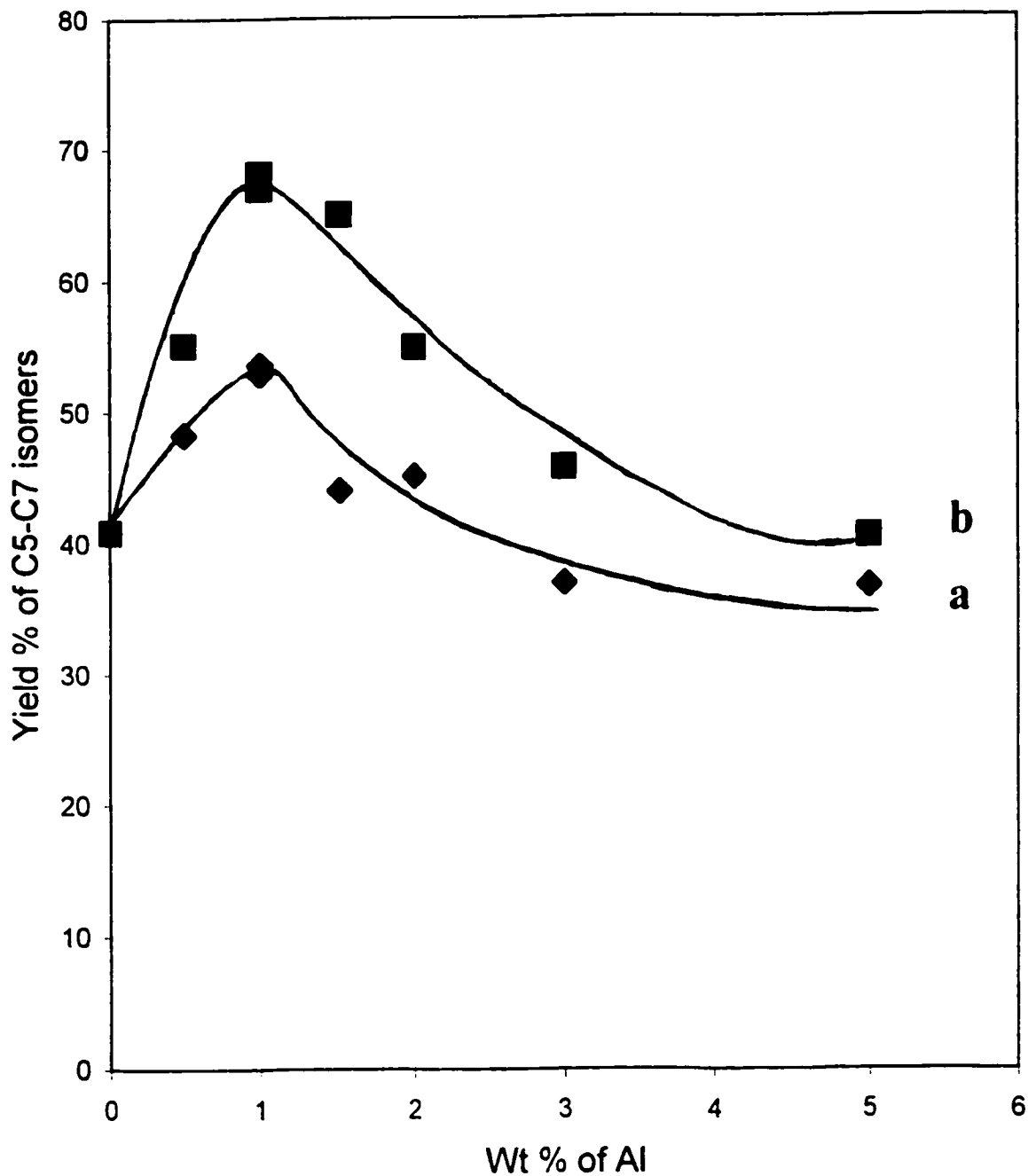
Figure 3.10. Variation of the yield of (C_5-C_7) branched paraffins with the weight

% of Al species incorporated into the zeolite structure:

(a)sequential incorporation of Pt and Al (Pt-Al^y-HY samples).

(b)simultaneous incorporation of Pt and Al (Pt-Al$_y$-HY samples).

The same tests were done using Zn and Cd loaded Pt-HY zeolite catalysts. The same trends were observed using these catalysts (Figure 3.11 and 3.12), (Table 3.7 and 3.8). Other species, such as Ni and Cr showed the same catalytic behavior with lower selectivities for isomerization.

Figures 3.11 and 3.12 illustrate the variations of the yield of (C_5-C_7) branched paraffins, Y_{liso}, with the weight % of Zn and Cd incorporated into the zeolite material with simultaneous loading of Pt $(Pt-Zn_y-HY$ and $Pt-Cd_y-HY$ samples) respectively. From these figures it is clear that, the curve of the yield versus the Zn loading goes through a maximum at the low concentration of Zn: ca 5 wt.% Zn $(ca.0.8×10^{-3}$ mol of Zn/g of zeolite) and of the Cd loading the curve pass through a maximum at the concentration of Cd: ca. 3.0 wt% $(ca.0.3×10^{-3}$ mol of Ca/g of zeolite).

In addition, sequential loading of Zn or Cd species with Pt $(Pt-Zn^y-HY$ and $Pt-Cd^y-HY$ samples) gave similar results to the simultaneously loaded samples with lower yield of (C_5-C_7) branched paraffins, Y_{liso}.

However, as with the Al loading, simultaneous loading of these species with Pt increases the activity and selectivity of zeolite catalysts toward higher isomer products better than that of the sequentially loaded samples, in particular Zn loaded catalysts increases the yield of mono-branched and multi-branched C_7 isomers better than that of the other species (Figure 3.13).

Figure 3.13 illustrates the variation of the composite selectivity ratio (Iso/Crk) with the molar concentration of Al, Zn and Cd species incorporated into the zeolite material, which Zn gave better results than Al and Cd. It is clear that the maximum isomerizing properties are obtained at almost the same molar concentration of the species incorporated, i.e. 0.5×10^{-3}- 0.7×10^{-3} mol/g of zeolite. By using composite selectivity ratio (Iso/Crk), it is possible to justify this properties. However, the difference in catalytic activity of these three catalysts and parent bifunctional Pt-HY zeolite catalyst in terms of maximum composite selectivity ratio Iso/Crk, corresponded to the following sequence.

$$Pt\text{-}Zn_y\text{-}HY > Pt\text{-}Al_y\text{-}HY > Pt\text{-}Cd_y\text{-}HY > Pt\text{-}HY$$

Zn loading		Conversion (C atom %)	Y_{Iso} (C_5-C_7)	Product selectivity		mu/mo	Selectivity ratio	
(wt%)	(10^{-3} mol/g)			S_{Iso}	S_{Crk}		R	(Iso/Crk)
Pt-Zn$_y$-HY catalysts (method of simultaneous incorporation)								
0.0	0.00	82.9	40.8	46.2	53.8	0.48	0.9	0.7
1.0	0.15	92.8	39.4	40.8	59.2	0.37	0.7	0.6
1.5	0.23	93.1	39.2	38.8	61.2	0.25	0.6	0.6
2.0	0.31	94.5	40.2	40.1	59.9	0.29	0.7	0.6
3.0	0.46	82.6	48.4	51.2	49.8	0.31	1.1	0.9
5.0	0.77	59.7	55.4	91.1	9.9	0.11	10.2	6.1
5.9	0.90	52.5	50.2	94.7	5.3	0.17	17.8	9.4
7.0	1.07	41.5	39.2	93.5	6.5	0.12	14.4	6.0
8.0	1.22	40.3	37.9	92.7	7.3	0.13	12.7	5.1
10.0	1.53	29.7	28.1	93.6	6.4	0.07	14.5	4.3

Table 3.7. Activity and selectivity versus the Zn loading (contact time = 1.042 h and T = 225 °C).
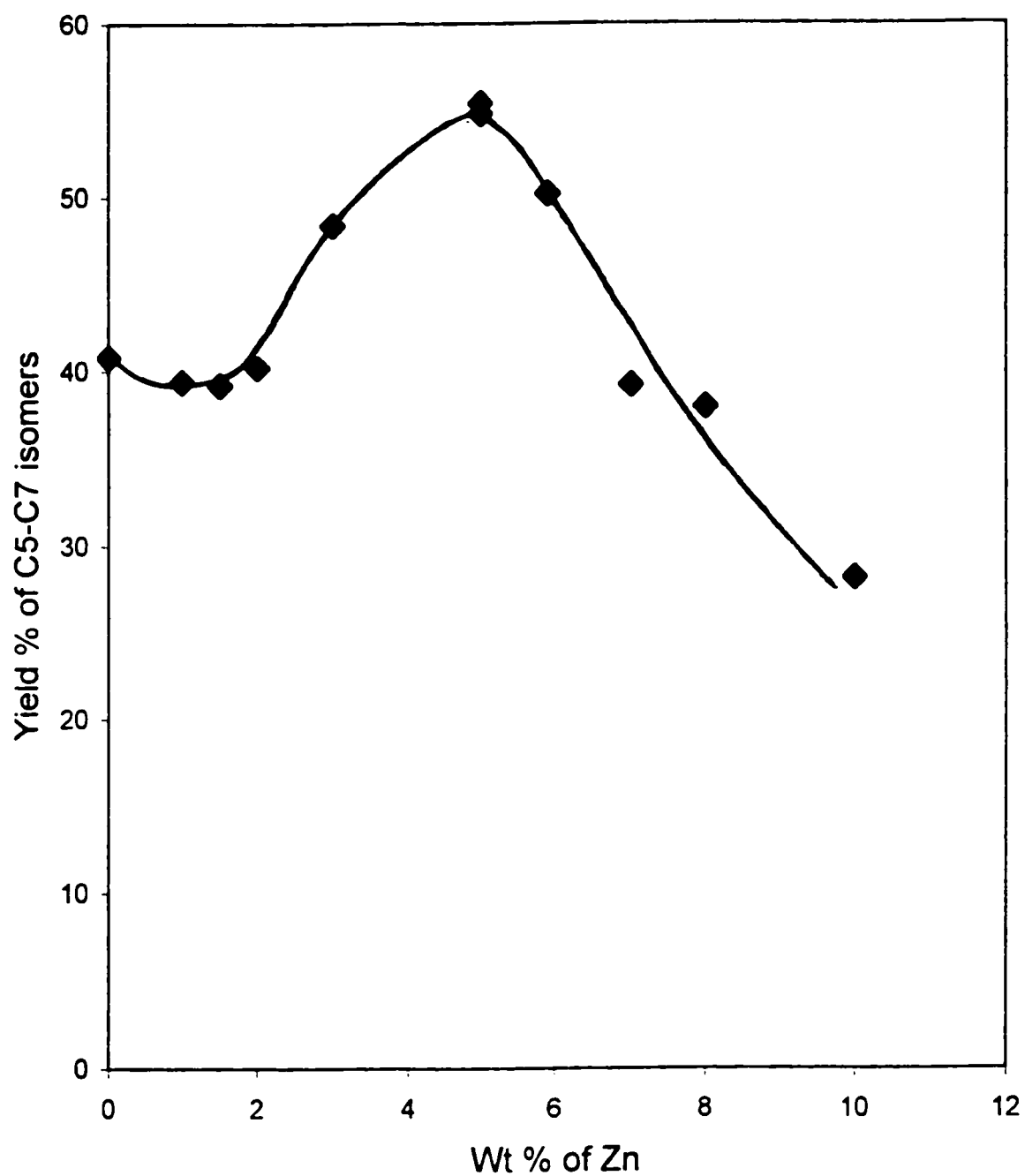
Figure 3.11. Variation of the yield of (C₅-C₇) branched paraffins with the weight % of Zn species incorporated into the zeolite structure, simultaneous incorporation of Pt and Zn (Pt-Zn_y-HY samples).

Cd loading		Conversion (C atom %)	Y_{Iiso} (C_5-C_7)	Product selectivity		mu/mo	Selectivity ratio	
(wt%)	(10^{-3} mol/g)			S_{iso}	S_{Crk}		R	(Iso/Crk)
Pt-Cd_y-HY catalysts (method of simultaneous incorporation)								
0.0	0.00	82.9	40.8	46.2	53.8	0.48	0.9	0.7
1.0	0.09	86.3	42.7	38.4	61.6	0.28	0.6	0.5
1.5	0.13	94.6	43.3	38.7	61.3	0.24	0.6	0.6
2.0	0.18	89.4	44.9	42.2	57.8	0.22	0.7	0.7
3.0	0.27	81.0	53.1	58.6	41.4	0.20	1.4	1.1
5.0	0.45	54.2	43.8	75.6	24.4	0.25	3.1	1.7
7.0	0.62	31.8	24.1	69.6	30.4	0.20	2.3	0.7
8.0	0.71	12.9	10.1	69.7	30.3	0.18	2.3	0.3

Table 3.8. Activity and selectivity versus the Cd loading (contact time=1.042 h and T = 225 °C).
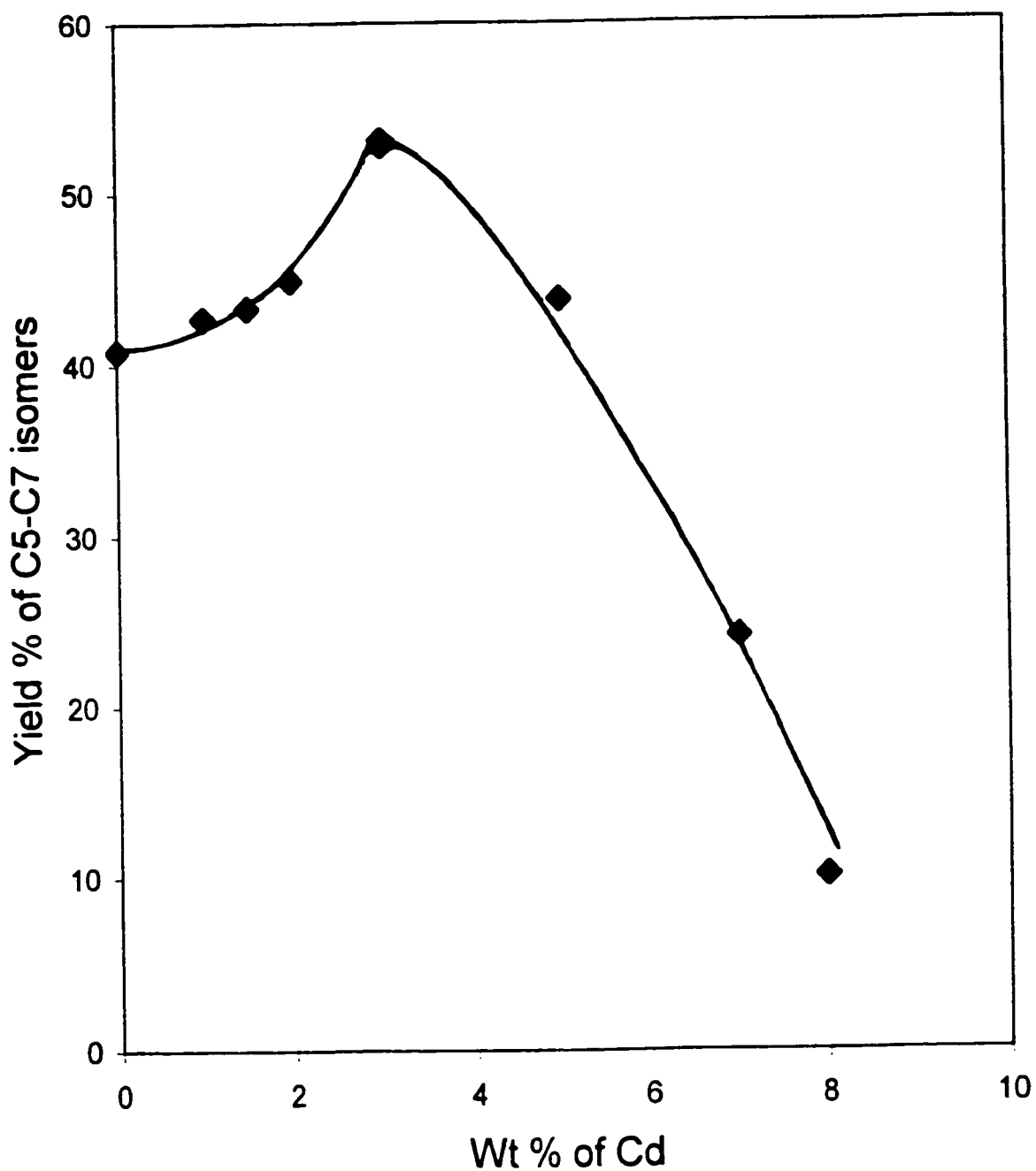
Figure 3.12. Variation of the yield of (C_5-C_7) branched paraffins with the weight % of Cd species incorporated into the zeolite structure, simultaneous incorporation of Pt and Cd $(Pt-Cd_y-HY$ samples).
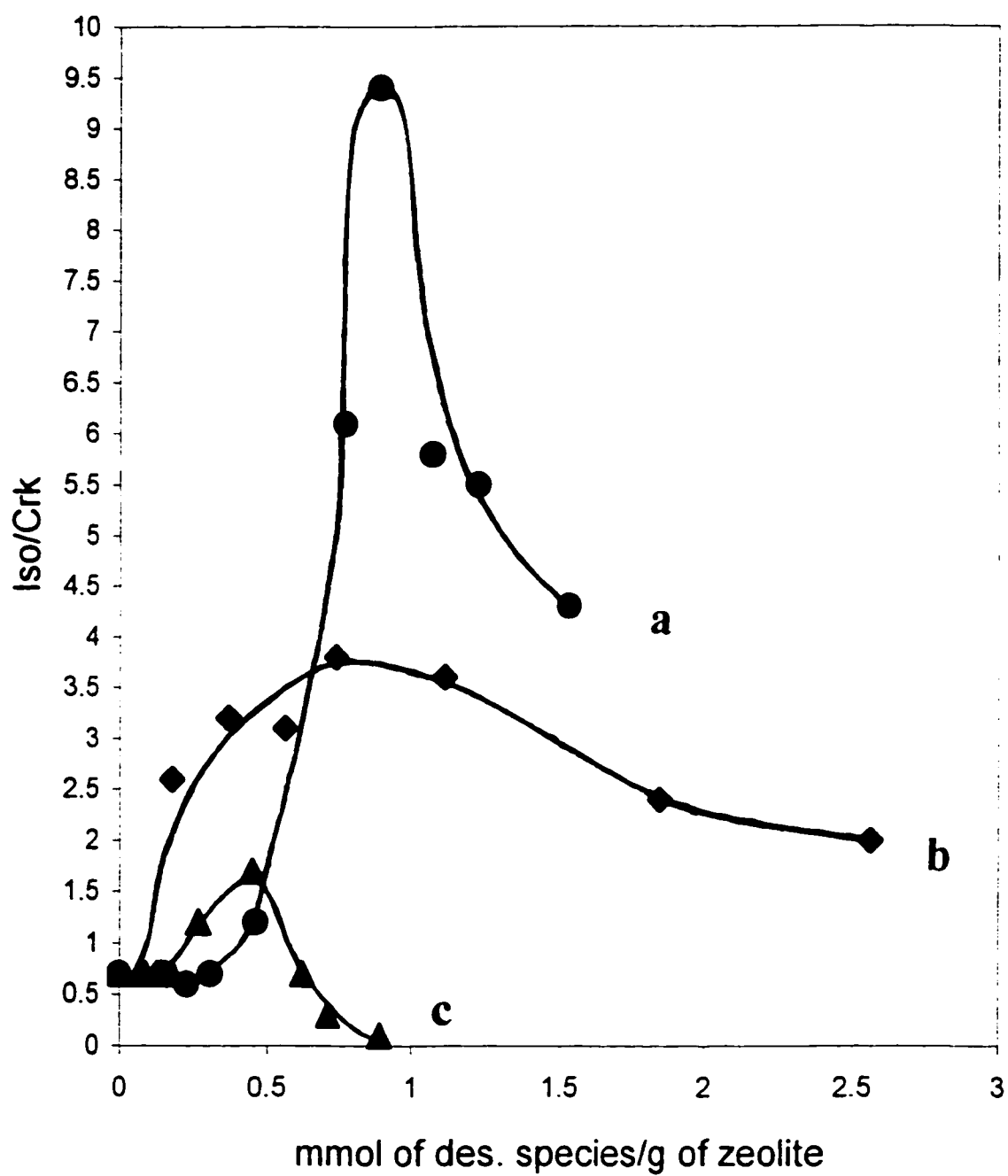
Figure 3.13. Composite selectivity ratio (Iso/Crk) versus loading (10^{-3} mol/g of zeolite) of: (a) Zn; (b) Al and (c) Cd.

3.3.1.4 Possible role of incorporated species on isomerization

(i) Several researchers reported that, the zeolite pore size and structure may have some effect on the product selectivity [104, 119, 157, 106]. However, our data reported in Table 3.3 show that the zeolite pore size remains almost unchanged at lower Al loading where the maximum in the catalytic performance for the isomerization is observed (Figs. 3.10 and 3.13 and Table 3.6) although the total surface area show some decrease. As a result, the significant variations of the yield of (C_5-C_7) branched paraffins cannot be ascribed to any modification of the zeolite pore size.

(ii) In another series of test of catalysts where first Al was incorporated into the HY zeolite and then Pt was incorporated into the resulting Al-HY catalyst, the data in terms of the yield of (C_5-C_7) branched paraffins was similar to that of the Al^y-Pt-HY (obtained by incorporation of first Pt then Al species to HY zeolite), i.e. no effect of sequence of incorporation of Al.

(iii) Simultaneous incorporation of Pt and Al $(Pt-Al_y-HY$ samples) resulted in maxima of the yield of (C_5-C_7) branched paraffins much higher than that of sequential incorporation of Pt and Al $(Pt-Al^y-HY$ samples) (Figure 3.10). Other species such as Zn and Cd gave similar results (Figure 3.11 and 3.12).

(iv) in considering the higher isomerizing properties of the $Pt-Al_y-HY$ over the Al^y-Pt-HY, it should be noted that the probability for competitive and selective adsorption of such small amount of Pt and Al species on the zeolite

surface is low. Such competitive adsorption would modify the spatial configuration of the Pt sites and/or alter the distance between the zeolite acid sites and the Pt sites of the bifunctional catalyst surface. Instead, our interpretation of this phenomena is that, when Al species are incorporated simultaneously with Pt species, Al merely deposits onto the zeolite surface next to the Pt sites.

v) The incorporated species such as Al, Zn, and the others investigated in this research work, are in the cationic form, and their effects at low loadings (< 2 wt %) are as follows:

a) Al species do not enter the network of the zeolite; the ^{27}Al-NMR data of the modified samples do not show any significant difference from the unmodified one, (20 wt % H-ZSM5 pellets is bentonite as binder which, unfortunately contain a high proportion of Al) [158].

b) Comparison of acid densities of Pt-HY and Pt-Al$_1$-HY zeolite catalysts show that there is no variation of the total acid density of the acid sites as measured by the technique of back-titration of desorbed ammonia with HCl (Table 3.5).

c) The dramatic change in the catalytic performance cannot be ascribed to an extended exchange of Al^{-3} (or its hydroxylated forms) with zeolite protons, otherwise how can the difference between the sequential incorporation procedure and the simultaneous one be explained, since all of these procedures

preparation used the same impregnation technique? In addition, at low incorporation of Al (in both simultaneous (Pt-Al$_s$-HY) and sequential (Pt-Al^y-HY) loading) the total conversion almost stays unchanged with increasing the Al loading (Table 3.6), suggesting that there is no significant replacement of the acidic protons of zeolite surface by Al^{3+} cations. These results suggest again that when Al is incorporated simultaneously with Pt species, Al species locate next to Pt on the zeolite surface and cause such dramatic changes of the catalyst activity and selectivity. On the other hand, at Al loading higher than 2 %, the total conversion decreased. This is due to coverage of the zeolite surface with Al to cause a decrease of the surface area, and a significant loss of surface acid sites (Table 3.6).

v) The ammonia adsorption/TPD technique using a Thermoconductivity Detector TCD/GC as detection means shows that the ammonia desorption profiles of the Pt-HY is not exactly the same as of the Pt-Al$_f$-HY (0.7×10^{-3} mole of Al/gr of zeolite) and of the Pt-Zn$_f$-HY (0.9×10^{-3} mole of Zn/gr of zeolite). The incorporated Al and Zn species may create some Lewis acid sites where the effect of Zn is higher than Al species (Table 3.5 and Figure 3.5). In addition, the use of the "strong base" such as ammonia and pyridine (their interactions with acid sites are stronger than those of CO and H$_2$), in the FTIR spectroscopy, to study the strength of the acid sites of oxide surfaces would not be very appropriate for detecting small variations of the acid site strength, which might be induced by weak interactions with the incorporated ions [159,160]. Instead very weak basic molecule such CO and H$_2$ must be used [161,162].

3.3.1.5 Our hypothesis of the formation of new desorption-transfer promoting site

As mentioned before, in accordance with the bifunctional catalysts concept, n-paraffins dehydrogenate on a metal site (Pt) producing thus olefins. These olefinic species are then transferred onto the acid site where they are converted into carbocations by absorbing of H^+. Rearrangement of these carbocations occurs on acid sites. The resulting species are desorbed from acid site as olefinic species and are then adsorbed on the Pt site where they are subsequently hydrogenated. These isoparaffin products are finally desorbed from Pt site. Therefore, this step, which includes a desorption from the acid site and a transfer to the metal site (Figure 3.14), is of the utmost importance in the isomerization of long-chain n-paraffins. Iglesia et al [145] state that "cracking steps are inhibited by the concurrent decrease in the residence time of isomeric carbocations, which desorb before β-scission reaction occur".

| alcarbon |

(DHY)   Pt ⇇ ══════════ H⁺ (ACI)

a

b

Al³⁺

(DES)
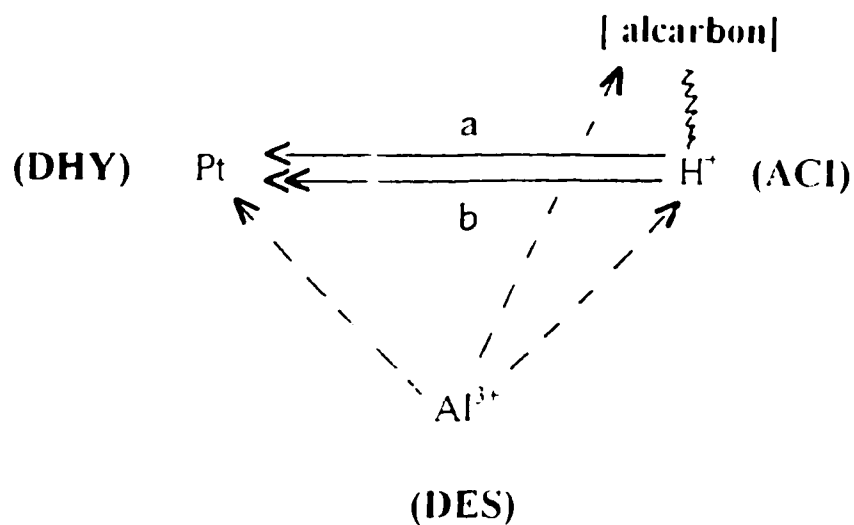
Figure 3.14. Schematic representation of the action of the incorporated, on the

desorption and transfer of branched olefinic species : a = normal mode (←);

b = assisted mode (< ←); < ------ = possible interaction with;

[alcarbon] = adsorbed alkylcarbocation.

(ACI) = acid site

(DHY) = dehydro-hydrogenation site

(DES) = desorption-transfer promoting site

To better understand the effect of the incorporated Al and other species on the isomerization of long chain paraffins, the data obtained at high level of n-heptane conversion and low level of conversion using Al loaded zeolite catalysts will be discussed.

(i) At high levels of n-heptane conversion (>70%), the intermediate carbocations are highly branched because of reaction conditions (high reaction temperature or longer contact time) and thus the β-scission reactions are the most rapid, so that the effect of the Al species can be greatly amplified and easier to identify and to study. At these high levels of conversion, the data obtained using bifunctional Pt-HY zeolite catalysts show that the composite selectivity ratio (Iso/Crk) has a value equal to or lower than 0.9 (Table 3.9). When Al species are incorporated in quite limited amounts (Al loading ranging from 0.5 wt % to 2.0 wt %) into the bifunctional Pt-HY zeolite structure, the value of (Iso/Crk) is increased and multiplied by 3 or more, and the selectivity to cracking products decreases dramatically (Table 3.6). Particularly interesting when Al species are present on the zeolite surface: the values of the branching degree ratio (mu/mo) are lower (Table 3.6). These latter results are in line with the hypothesized role of the Al species which reduce the residence time of the carbocations on the acid sites: "these shorter turnover times also decrease the probability of additional methyl shifts and the concentration of dimethyl isomers among isoheptane products" Iglesia et al [145].

(ii) At low n-heptane conversions (< 50 %) the intermediate carbocations are not highly branched and mostly mono-branched because of the reaction

conditions and thus the β-scission reactions are not rapid, so that the effect of the Al species is not significant, and the values of the composite selectivity ratio (Iso/Crk) with Pt-Al$_y$-HY zeolite catalyst are relatively low (Table 3.6), thus justifying our low interest in these catalysts. This demonstrates the usefulness of the (Iso/Crk) ratio for illustrating the effect of incorporated species such as Al and Zn in zeolite catalyst for the isomerization of long chain n-paraffins.

Finally, the catalytic data reported in Table 3.10 which are obtained with the Pt-Al$_{2.0}$-HY constitute strong evidence of the intervention of the Al species on the catalyst activity/selectivity. This catalyst was tested under reaction conditions which resulted in higher conversions at constant temperature and for longer contact time. At almost the same conversion levels (92.6 % and 72.6 % for the bifunctional catalyst, Pt-HY, in Table 3.9; 91.9 % and 71.7 % for the modified catalyst in Table 3.10), the composite selectivity ratio (Iso/Crk) is significantly higher for the modified catalyst (0.8 and 3.8 for the modified zeolite in Table 3.10, against 0.3 and 0.9 for the Pt-HY zeolite in Table 3.9, respectively), showing that the Al species are effectively playing their role as expected. On the other hand, the shorter residence time of the carbocations on the acid sites results in lower value of the branching degree mu/mo = 0.46 and 0.32 for the modified catalyst (Table 3.10) against 0.73 and 0.5 for the parent Pt-HY zeolite (Table 3.9), in agreement with the results obtained by Iglesia et al [145].

Contact time (h)	Conversion (C atom %)	Product selectivity		mu/mo	Selectivity ratios	
		S_{Iso}	S_{crk}		R	(Iso/Crk)
1.563	92.6	21.6	78.4	0.73	0.3	0.3
1.064	86.4	35.4	64.6	0.49	0.6	0.5
0.658	72.6	53.8	46.2	0.50	1.2	0.9
0.410	62.6	75.2	24.8	0.31	3.0	1.9

Table 3.9. Influence of the total conversion versus contact time on the selectivity ratios (R and Iso/Crk) using the Pt-HY zeolite catalyst at a constant hydrogen/n-heptane molar ratio ($\approx$ 2.11) and T = 225 °C.

Contact time (h)	Conversion (C atom %)	Product selectivity		mu/mo	Selectivity ratios	
		S_{Iso}	S_{crk}		R	(Iso/Crk)
3.266	96.3	28.6	71.4	0.48	0.4	0.4
2.273	94.7	39.4	60.6	0.45	0.7	0.6
1.563	91.9	46.7	53.3	0.46	0.9	0.8
1.042	71.7	84.1	15.9	0.32	5.3	3.8

Table 3.10. Influence of the total conversion versus contact time on the selectivity ratios (R and Iso/Crk) and the branching degree ratio (mu/mo) using the $Pt-Al_{2.0}$-HY zeolite catalyst at a constant hydrogen/n-heptane molar ratio ($\approx$ 2.11) and T = 225 °C.

3.3.1.6 Effect of desorption sites on residence time of intermediate carbocations

Desorption sites can decreases the residence time of intermediate carbocations on acid site as follows:

(i) The incorporated species may weaken the strength of acid sites. This effect decreases the strength of the bond between acid site and carbocation. As a result the intermediate carbocations are easily removed as olefin from the acid site. The desorption sites maybe partially changed from cation M^{n+} to metal hydroxide $M(OH)_i^{(n-i)+}$ during the various preparation or reduction phases. The hydrogen of the acid site silanol group of the zeolite may establish some hydrogen bonding the metal hydroxide or/and metal oxide. As a result, the acid strength will be lowered. The adsorbed intermediate carbocation on such a weakened acid site will desorb more easily. However, as mentioned before, ammonia and pyridine can not be used as probe molecules for these investigation, thus, as suggested by Zecchina et al. [163], a weak base such as CO and H_2 must be used. Carbon monoxide CO is a soft base with small molecular size and heats of adsorption are typically low. In a carbon monoxide molecule 14 electrons are divided equally between carbon and oxygen atoms. As a result, the carbon end of the molecule carries a partial negative charge and oxygen end of molecule carries a partial positive charge, although oxygen is more electronegative than carbon. Carbon monoxide makes a weak bond with the cationic center via carbon end, which leads to a decrease of the C-O bond order.

The carbonyl stretching frequency responds very sensitively to coordination onto cationic sites, leading to positive frequency shifts of up to 90 cm^{-1} relative to the gas phase frequency of 2143 cm^{-1}. But the carbonyl stretching mode is also sensitive relative to H-bonding to protonic sites. The high extinction coefficient of the C-O stretching mode provides good spectral sensitivity. Carbon monoxide is an almost ideal probe molecule that can discriminate between aprotic (Lewis) [164,165] and protic (Brønsted) [166,167] acid sites with high specificity for sites with different acid strength.

In the Brønsted adducts (AH---CO), not only the v(CO) mode is affected by the electrostatic interaction with the positively charged hydrogen atom, but the v(AH) stretching also undergoes a shift to lower frequency [162,64]. Therefore, the shift of the stretching the v(CO) and/or v(AH) modes can be used to detect changes in the acid strength. The diffuse reflectance FTIR spectroscopy of absorbed carbon monoxide on acid site of Pt-HY zeolite surface was obtained. The spectra show peaks at about 2117 cm^{-1} and 2172 cm^{-1} which correspond to absorbed CO stretching (Figure 3.15). The same spectrum was obtained using modified Pt-Zn$_{0.9}$-HY (Zn = 0.9 mmol/g of zeolite) zeolite catalyst where these two peaks appeared at about 2117 cm^{-1} and 2175 cm^{-1} (Figure 3.16). From these results it is clear that the incorporated species such as Zn and Al do not change the strength of acid sites on the surface of zeolite materials.
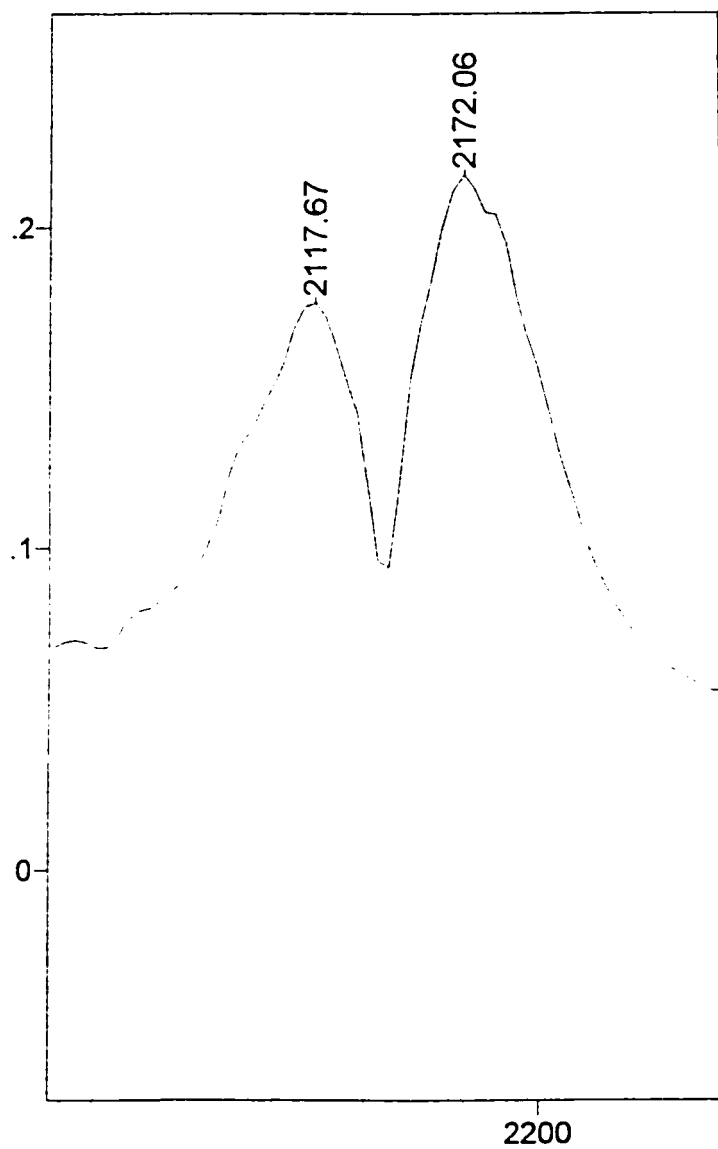
Figure 3.15. The diffuse reflectance FTIR spectra of absorbed CO on acid sites of 2 % Pt-HY zeolite catalyst diluted in quartz powder at 100 °C .
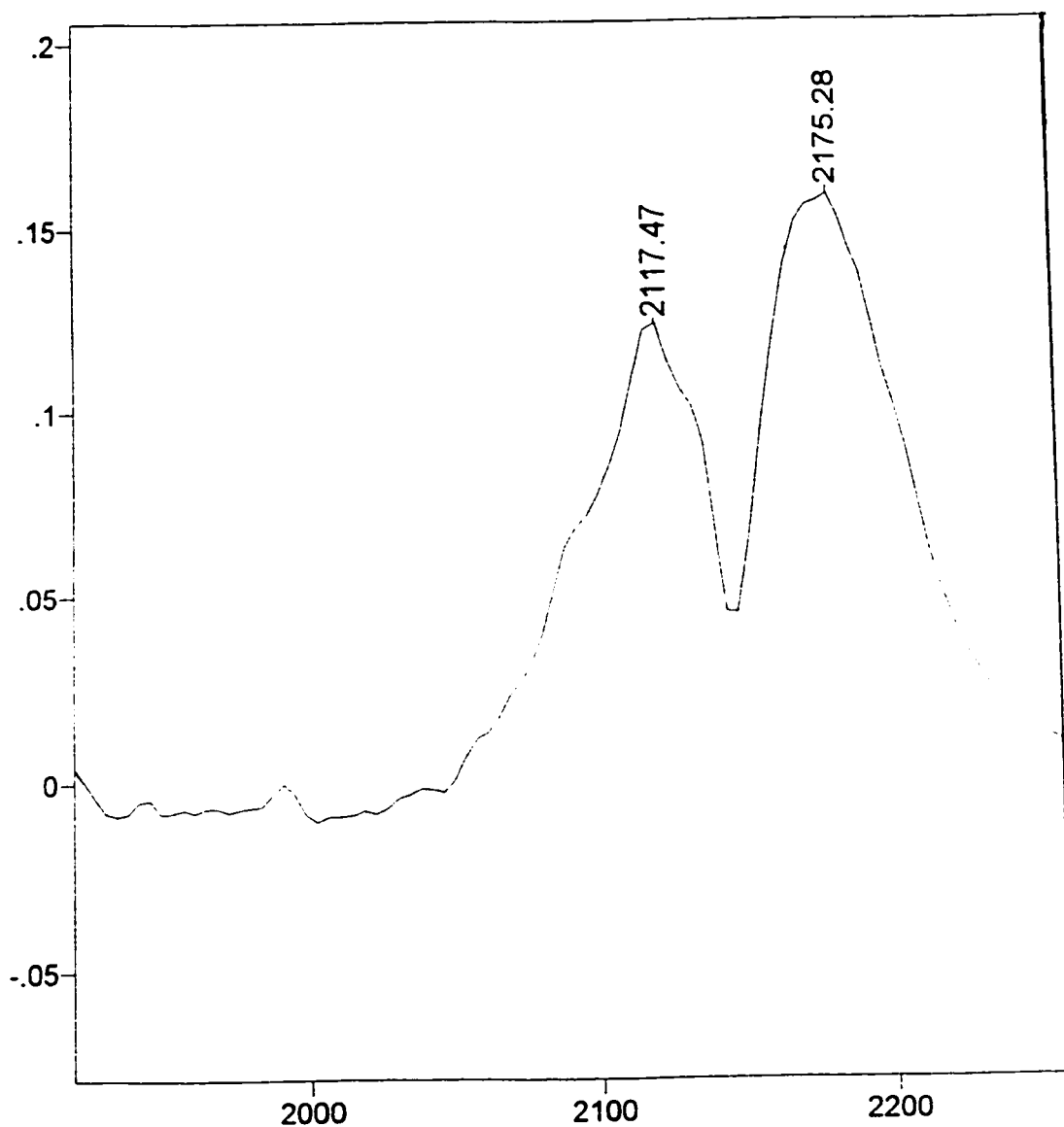
Figure 3.16. The diffuse reflectance FTIR spectra of absorbed CO on acid sites of 2 % PtZn$_{0.9}$-HY (Zn = 0.9 mmol/g of zeolite) zeolite catalyst diluted in quartz powder at 100 °C .

(ii) The obtained results show that the incorporated cationic species such as Al and Zn do not apparently change the strength of the zeolite acid sites. However, these species create some Lewis acid sites on the zeolite surface. These new sites act as "desorption-transfer promoting" sites [121,143] between the acid site and the Pt site which the molecular conformation of the alkylcarbocation would be a key factor because desorption-transfer promoting sites act as a 'receiver' for the olefinic species desorbing from the acid site. On the other hand, the cationic species incorporated would alter the electrostatic interactions between the branched carbocations and the zeolite surface [168], thus, changing the normal figure of the competition between isomerization and cracking (β-scission). In fact, the desorption kinetics of the olefinic species could be changed upon even slight modification of the 'alkylcarbocation-acid site' transition complex. In addition, maybe the incorporated species make a weak bond with the π-bond of olefinic species and decrease the absorption of these species on the other acid sites, whereby the further cracking of these species is decreased.

By considering the results obtained, the concept of a "trifunctional catalyst" (triangular configuration of acid/dehydro-hydrogenation/desorption-transfer sites) has been proposed to explain the results obtained (Figure 3.17). It is worth noting that, the trifunctional zeolite catalysts have higher isomerizing properties for long chain n-parafins than bifunctional catalysts.

(ACI)

H⁺

b

a   carbocation

olefin   Al³⁺(DES)

b

olefin

Pt

(DHY)
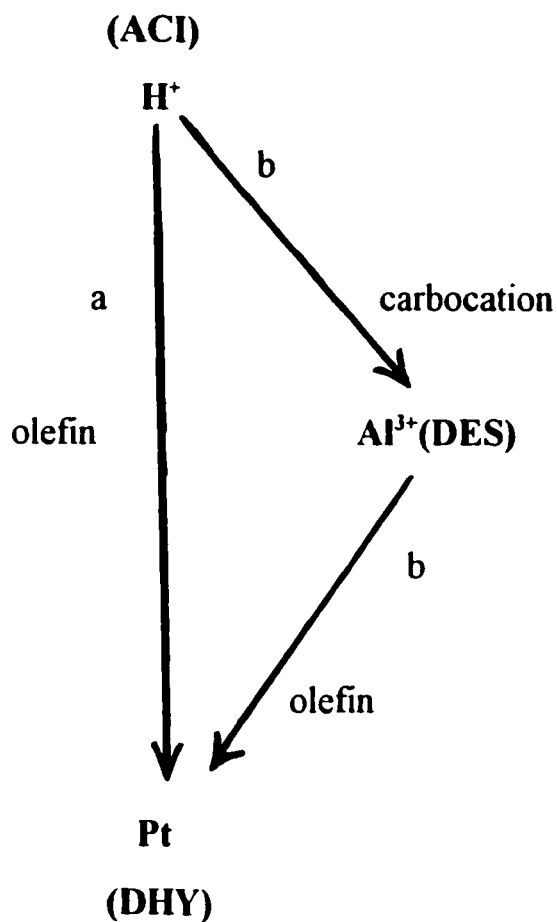
Figure 3.17. Desorption of carbocation species from the acid site (H⁺) and transfer as olefins to the hydrogenation-dehydrogenation site (Pt).

(a) Direct transfer of an olefin from the H⁺ site to the Pt site in the bifunctional catalyst.

(b) Transfer of the carbocation from H⁺ site to the DES site and transfer of the olefin from the DES site to the Pt site in the trifunctional catalyst.

3.3.2 Conclusion

The incorporation of cationic species such as Al and Zn in small amounts into the HY zeolite structure resulted in an enhanced yield of branched paraffins and a significantly decreased formation of cracked products. If the Al and Zn species were incorporated simultaneously with the Pt species, the isomerization properties of zeolite catalyst increased even more than that of the catalyst prepared by separate loading. There was no modification of the metal sites. Also, there was no variation of the strength of the acid site upon Al and Zn loading, and the pore size remained unchanged at low Al loading. In fact, these species created some Lewis acid sites, which are involved as desorption-transfer promoting site between acid and Pt site on the surface of the zeolite catalyst. The reaction intermediates were rapidly evacuated by the newly formed adsorption sites.

A triangular configuration of « acid/dehydro-hydrogenation/desorption-transfer » (ACI/DHY/DES) sites, has been proposed to explain the results obtained.

3.3.3 Effect of Pt loading on *n*-heptane isomerization

In order to maximize the product yield using a catalyst, it is usually desirable that the catalytically active phase should expose as large a fraction as possible of its atoms or ions to the reactant molecules. This implies decreasing particle size and increasing the surface area. The fraction exposed, more often called the degree of dispersion, a metal such as platinum, attains a value of about one-half when the particle size is 1.5 nm; such a particle contains about 200 atoms [169]. In addition, the reactivity of metal surfaces is distinct from that of complexes and clusters of the same metal and not easily predicted. Many metals have catalytic activity for many reactions and in practice, the catalytically important metals include most of the transition metals, especially the platinum group metals which find wide use, even though they are expensive [170].

In this research a solution of tetraammineplatinum (II) chloride hydrate [$Pt(NH_3)_4Cl_2.H_2O$] was used and activated at low temperature (350 °C) in order to obtain the metallic platinum particle with possible smallest size. A series of experimental runs were done with Pt loading of 0.5, 1, 1.5 and 2 wt.% (2.6×10^{-5} -1.03×10^{-5} mole/g) into the parent HY zeolite and HY zeolite with Al content of 1 wt.% (0.37 mmol/g) in order to obtain the maximum isomerization performance with the minimum amount of Pt incorporated into the zeolite. The results obtained show that 1 wt.% of Pt was enough to obtain the maximum isomerization (Table 3.11).

Pt loading		Conversion	Y_{iso}	Product selectivity		mu/mo	Selectivity ratio	
(wt%)	(10^{-3} mol/g)	(C atom %)	(C_5-C_7)	S_{iso}	S_{Crk}		R	(Iso/Crk)

Pt_y-HY catalysts

0.5	0.03	75.4	50.8	60.4	39.6	0.23	1.5	1.2
1.0	0.05	82.9	40.8	46.2	53.8	0.48	0.9	0.7
2.0	0.10	88.8	44.6	42.1	57.9	0.29	0.7	0.7
2.5	0.13	89.1	44.3	42.4	57.6	0.29	0.7	0.7
3.0	0.15	92.4	41.2	37.7	62.3	0.31	0.6	0.6

Pt_y-Al_1-HY catalysts (method of simultaneous incorporation)[*]

0.5	0.03	73.4	59.1	75.6	24.4	0.23	3.1	2.3
1.0	0.05	81.4	68.1	79.6	20.4	0.28	3.9	3.2
1.5	0.08	89.5	67.3	70.0	30.0	0.31	2.3	2.1
2.0	0.10	80.4	63.3	74.3	25.7	0.24	2.9	2.3

[*]) Al = 1 Wt. % of catalyst

3.11. Activity and selectivity versus the Pt loading (contact time = 1.042 h and T = 225 °C).

3.3.4 Effect of Zn loading of the Pt-Zn-HY trifunctional zeolite catalysts on *n*-heptane isomerization

As already seen , the incorporation of cations such as zinc, nickel, cadmium and aluminum, simultaneously with Pt into HY zeolite resulted in significant enhancement of *n*-heptane isomerization compared to cracking. To explain these results, a triangular zeolite acid/Pt dehydro-hydrogenation/ desorption-transfer promoting site configuration was hypothesized [121]. The main role of new site (desorption-transfer promoting) is to speed up the desorption of olefinic species from the acid site and its transfer to the metallic Pt site. As a result, the residence time of intermediate branched carbocations on acid sites are shorter, thus avoiding undesired cracking reactions. Among these species Zn was found to be the most effective, thus it was decided to focus on the effect of this species. Zinc nitrate was used as Zn incorporating agent. The following aspects were studied:

i) Zn loading at various reaction temperatures

ii) the effect of Zn loading on product selectivity at higher conversion level

iii) the Lewis character of the incorporated Zn species and specially designed catalytic tests.

The reference samples without Pt species showed rapid activity decay, and for comparison purpose their catalytic data were reported herein. Once again, the composite selectivity (Iso/Crk) ratio was used in order to have a

proper idea of the isomerization versus cracking competition.

The variation of the composite selectivity (Iso/Crk) ratio versus the Zn loading, obtained at four reaction temperatures in the range of 210 °C-255 °C is shown in (Figure 3.18). The composite selectivity (Iso/Crk) ratio always goes through a maximum in this temperatures range (Table 3.12). However, the corresponding Zn loadings are different, and with increasing the reaction temperature, the Zn concentration need for the maximum isomerization activity increases (Figure 3.18 and Table 3.12). On the other hand, the values of composite selectivity Iso/Crk and R ratios of the Zn loaded zeolite catalyst (Pt-Zn-HY) are higher than those of the reference zeolite catalyst (Pt-HY) (Table 3.12).

Catalyst	Zn loading $(10^{-3}$ mol/g)	(N_{Zn}/N_{H+}) Ratio	Reaction Temp. °C	Conversion (C atom %)	C_7 isomers (C atom %)	mu/mo	R	(Iso/Crk)
Pt-HY	0.0	0.0	210	72.4	81.8	0.23	4.5	3.3
Pt-HY	0.0	0.0	225	82.9	46.2	0.48	0.9	0.7
Pt-HY	0.0	0.0	240	92.9	36.0	0.31	0.7	0.5
Pt-HY	0.0	0.0	255	93.5	36.8	0.37	0.6	0.5
PtZn$_{0.7}$-HY	0.7	0.24	210	51.2	96.6	0.16	28.4	14.5
PtZn$_{0.9}$-HY	0.9	0.31	225	52.5	94.7	0.17	17.8	9.4
PtZn$_{1.2}$-HY	1.2	0.42	240	64.6	89.1	0.19	8.1	5.3
PtZn$_{1.8}$-HY	1.8	0.63	255	59.9	90.0	0.17	9.0	5.4

Table 3.12. Performance of the parent Pt-HY zeolite and the Zn modified zeolite catalysts giving the highest isomerization activity at the temperature studied (equal contact time = 1.04 h).
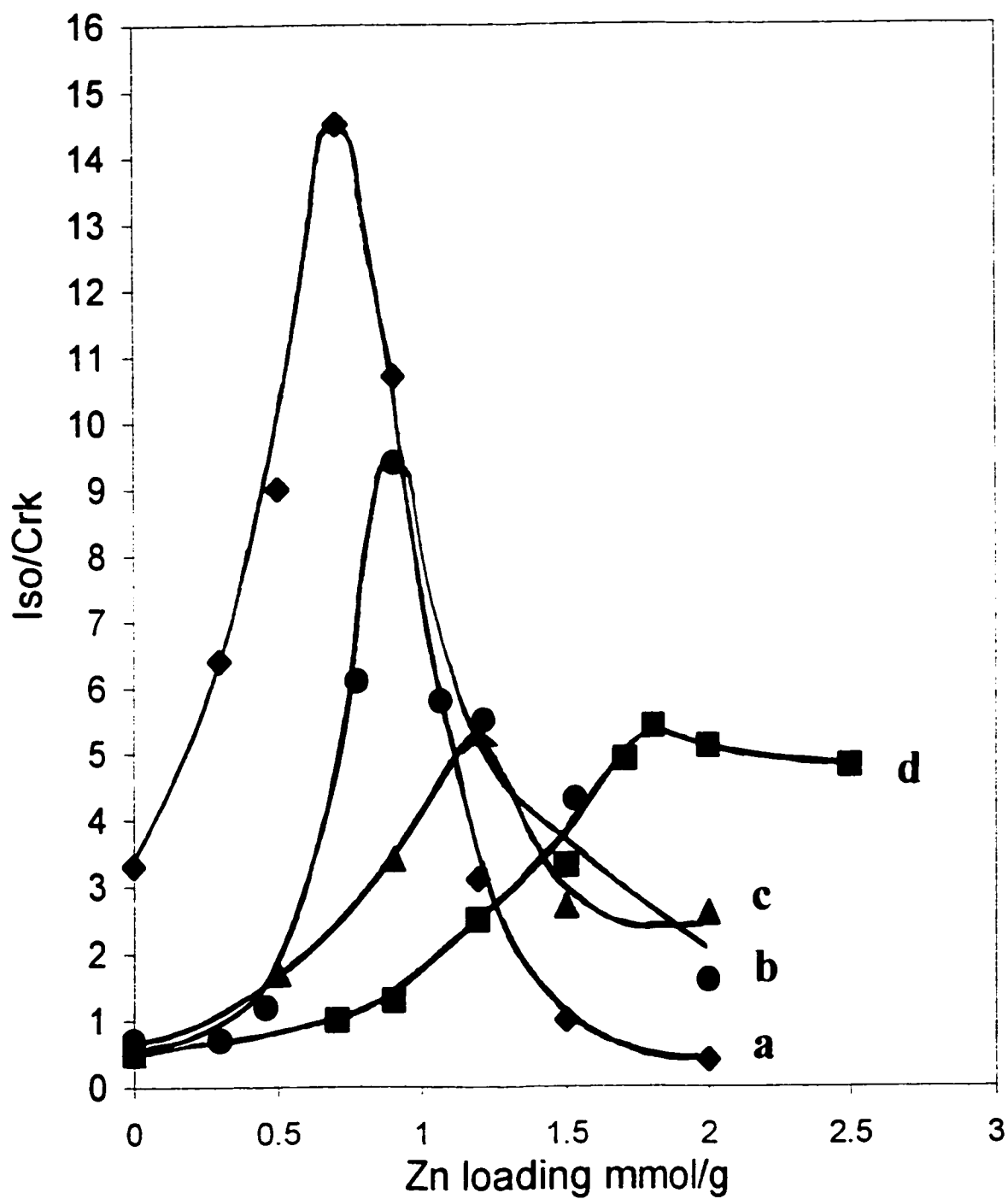
Figure 3.18. The (Iso/Crk) ratio versus the Zn loading at various reaction temperatures: (a) 210 °C; (b) 225 °C; (c) 240 °C; (d) 255 °C.

From data reported in Table 3.12 and Figure 3.18 the following conclusions are drawn:

(i) By increasing of reaction temperature more acid sites are activated and involved in the reactions. As a result, the conversion of n-heptane increases by increasing of reaction temperature. More interesting, data obtained using bifunctional Pt-HY (parent) zeolite catalysts show 21 % increase from 210 °C to 255 °C which is higher than that of the trifunctional Pt-Zn-HY zeolite catalysts (8.7 %). This is due to desorption-transfer promoting effect of Zn which decrease the residence time of intermediate carbocations on acid sites.

(ii) The production of C_7 isomers is high using trifunctional Pt-Zn-HY zeolite catalysts compared to that of the bifunctional Pt-HY zeolite catalysts. By increasing the reaction temperature the production of C_7 isomers decreases rapidly (45 % from 210 °C to 255 °C) using the bifunctional Pt-HY zeolite catalyst, compared to that of the trifunctional Pt-Zn-HY zeolite catalysts where the production of C_7 isomers does not decrease rapidly (6.6 % from 210 °C to 255 °C) (Table 3.12). Again this is due to shortening of the residence time of the intermediate carbocation on acid site by desorption-transfer promoting sites (Zn) of the trifunctional Pt-Zn-HY catalysts.

(iii) The mu/mo (multi-branched/mono-branched) ratio is higher using bifunctional Pt-HY zeolite catalysts than using trifunctional Pt-Zn-HY zeolite catalysts. By decreasing the residence time the intermediate carbocation on acid site not only the cracking reactions of intermediate multi-branched C_7

carbocations decrease, but also the conversion of intermediate mono-branched C_7 to intermediate multi-branched C_7 decreases.

(iv) Both the selectivity ratio R, and composite selectivity ratio (Iso/Crk) are higher using trifunctional Pt-Zn-HY zeolite catalysts than using bifunctional Pt-HY zeolite catalysts.

(v) Finally, the incorporation of zinc needed to have the maximum activity of isomerization, increases with increasing reaction temperature, i.e. a stronger cracking activity requires higher amount of zinc species.

All of these results tentatively can be explained by means of the hypothesis of triangular configuration of active sites (acid/Pt dehydro-hydrogenation/ desorption-transfer promoting) as follows:

The composite selectivity Iso/Crk ratio, as well as R ratio, are closely related to the k_{iso}/k_{crk} ratio where k_{iso} is the rate constant of the isomerization reaction (step) and k_{crk} is the rate constant of the cracking reaction. In accordance with the Arrhenius equation, the mentioned rate constant can be expressed as follows:

$$k_{iso} = A_{iso} \exp(-\Delta E_{iso}/RT) \tag{3.1}$$

$$k_{crk} = A_{crk} \exp(-\Delta E_{crk}/RT) \tag{3.2}$$

where ΔE_{iso} is the apparent activation energy of isomerization and ΔE_{crk} is the apparent activation energy of cracking. The preexponential factors A_{iso} and A_{crk}, which are associated with the isomerization and the cracking respectively, depend on the properties of the active surface of the bifunctional catalyst (Pt-HY), i.e. on the density of and strength of the acid sites of the zeolite, the dehydro-hydrogenation properties of the Pt sites, and their respective locations on the zeolite surface.

Data obtained using the reference zeolite (Pt-HY, bifunctional catalyst) for the isomerization of n-heptane show that by increasing of the reaction temperature the value of the k_{iso}/k_{crk} ratio is decreases this is due to the more favored kinetics for the cracking at higher temperature. This is expressed by an increase of the conversion to cracking products and as a results, a decrease of the composite selectivity ratio Iso/Crk as well as the value of the R ratio (Table 3.12).

It is important to understand the nature of zinc species on the surface of Zn loaded zeolite catalysts (Pt-Zn-HY), before studying the catalytic effect of the Zn incorporated, where the Zn species can exist as a cationic form or/and metallic form (after reduction using hydrogen gas) on the surface. We believe that the Zn species incorporated are predominantly in the cationic form (Zn^{2+}) after reduction to obtain metallic Pt on the surface of zeolite. Thus, a series of runs was done for the isomerization of n-heptane using the Zn-HY zeolite catalyst (after reduction using the same condition as used for the Pt-Zn-HY and Pt-HY zeolite catalysts). The data obtained show that the various Zn-HY

zeolite catalysts do exhibit some isomerization activity which is, however, extremely low (Table 3.13) when compared to that of the Pt-HY zeolite catalyst (Table 3.14), thus excluding any strong dehydrogenation/hydrogenation activity of the Zn species as one can normally expect for metallic Zn.

Catalyst	acid density (mmol/g)	Conversion (C atom %)	C₇ isomers (C atom %)	Selectivity ratios	
				R	(Iso/Crk)
Zn-HY (0.7)	3.3ᵃ	9.5ᵇ	57.2	1.3	0.13
Zn-HY (0.9)	3.2	7.6	59.2	1.5	0.11
Zn-HY (1.2)	3.2	6.3	61.7	1.6	0.10
Zn-HY (1.8)	3.2	5.4	62.8	1.7	0.09
Pt-NaY	≤0.4	1.3	0.0	0.0	0.00
Pt-Zn₀.₉-NaY	0.9	0.9	0.0	0.0	0.00

a) Acid density of: HY = 2.3 mmol/g, Pt-HY = 2.5 mmol/g, Pt-Zn₀.₇-HY (0.7) = 2.3 mmol/g, Pt-Zn₀.₉-HY (0.9) = 3.3 mmol/g.

b) Rapid on-stream activity decay.

Table 3.13. Catalytic properties of the Zn-HY samples studied (temperature = 225 °C, equal contact time = 1.04 h).

Catalyst	Reaction Temp. °C	Contact time (h)	Conversion (C atom %)	C$_7$ isomers (C atom %)	mu/mo	Selectivity ratio R	(Iso/Crk)
Pt-HY	210	1.04	72.4	81.8	0.23	4.5	3.3
		1.59	83.1	69.6	0.32	2.3	1.9
		2.13	88.4	51.1	0.34	1.1	1.0
		2.63	84.0	47 1	0.35	0.9	0.8
Pt-HY	225	0.41	62.6	75 2	0 31	3.0	1.9
		0.66	72.6	53 8	0 40	1.2	0.9
		1.04	82.9	46.2	0 48	0.9	0.7
		1.56	92.6	21.6	0.43	0.3	0.3
Pt-HY	240	1.05	92.9	36.0	0.31	0.7	0.5
		1.56	93.6	26.4	0.41	0.4	0.3
		2.08	96.2	19.4	0.39	0.2	0.2
		2.63	96.9	15 5	0 44	0.2	0.2
Pt-HY	255	1.05	93.5	36.8	0.37	0.6	0.5
		1.30	95.8	23.3	0.31	0.3	0.3
		1.54	96.8	17.4	0.40	0.2	0.2
		2.13	99.9	0.4	0.52	0.0	0.0

Table 3.14. Performances of the bifunctional Pt-HY (parent) zeolite catalyst at high conversion of n-heptane.

Catalyst	Zn loading (10^{-3} mol/g)	Reaction Temp. °C	Contact time (h)	Conversion (C atom%)	C_7 isomers (C atom%)	mu/mo	R (Iso/Crk)
PtZn$_{0.7}$-HY	0.7	210	1.05	51.2	96.6	0.16 28.4	14.5
			1.56	67.3	89.3	0.23 8.4	5.6
			2.63	78.6	83.9	0.27 5.2	4.1
			3.13	85.1	80.1	0.36 4.0	3.4
PtZn$_{0.9}$-HY	0.9	225	1.06	52.5	94.7	0.17 17.8	9.4
			1.84	74.3	84.6	0.28 5.5	4.1
			2.17	76.9	80.0	0.29 4.0	3.1
			3.13	82.1	76.9	0.27 3.3	2.7
PtZn$_{1.2}$-HY	1.2	240	1.04	64.6	89.1	0.19 8.1	5.3
			2.08	77.1	83.2	0.22 5.0	3.8
			2.63	79.9	74.1	0.25 2.9	2.3
			3.13	87.6	69.4	0.28 2.3	2.0
PtZn$_{1.8}$-HY	1.8	255	1.05	59.9	90.0	0.17 9.0	5.4
			2.05	80.2	80.4	0.28 4.1	3.3
			2.56	81.8	75.4	0.24 3.1	2.5
			3.13	87.3	71.5	0.33 2.5	2.2

Table 3.15. Performances of the modified trifunctional Pt-Zn$_y$-HY (y_{max}) zeolite catalysts at high conversion of n-heptane.

In addition, data reported in Table 3.13 clearly show that the total acid density of the various Zn-HY zeolite is significantly higher than that of the parent HY zeolite suggesting that the incorporated Zn^{2+} ions behave as Lewis acid species. This is also conformed by the following observations:

(i) A sample of $Pt-Zn_{0.9}-NaY$ zeolite catalyst was prepared using low-Brønsted acidity Na-Y zeolite and some catalytic runs were done using this catalyst. These catalysts show absolutely no isomerization activity (Table 3.13), because such a catalyst does not provide any strong Brønsted (protonic) acid sites although its acid density is higher than that of the reference Pt-NaY zeolite catalyst (Table 3.13), confirming thus the Lewis acid nature of the Zn^{2+} incorporated into the Pt-NaY Zeolite.

(ii) The results obtained of our recent diffuse reflectance IR study (DRIFTS) of the pyridine-treated $Pt-Zn_{0.9}-NaY$ sample, show a strong Lewis band at 1453 cm^{-1} and an extremely weak Brønsted band at 1545 cm^{-1} [171].

(iii) Finally, data reported for acid sites of the Pt-HY and the $Pt-Zn_{0.7}-HY$ in Table 3.13, suggest that the Zn loading procedure does not result, to any significant extent, in ion-exchange or blockage of the surface acid site by the Zn^{2+} ions.

By considering the chemical nature and the catalytic behavior of the incorporated Zn which was previously observed, and in accordance with the hypothesis of trifunctional catalyst, the ways Zn species can affect the system are as follows:

i) they can affect the zeolite surface acid sites (change the acid density or/and strength)

ii) they affect the Pt sites

iii) by absorption of intermediate alkylcarbocations they can decrease their residence time on acid sites.

In the eventuality of action (i) or/and action (ii) the respective preexponential factors of equations 3.1 and 3.2 (or the A_{iso}/A_{crk} ratio) of the Zn modified (namely Pt-Zn-HY) zeolite catalysts would remained constant, because in principle, the Zn loading required for the highest isomerization activity would be the same (the surface configuration active sites remain unchanged) for all reaction conditions, i.e. in the case of this research work, for all of the reaction temperatures used. In fact, the optimum configuration of the active surface of the zeolite obtained by important and exclusive interaction of incorporated Zn species with Pt sites or surface Brønsted acid sites, is assumed not to undergo any significant change with variation of such quite mild temperatures. In other words, if the effect of the incorporated Zn species were on the Pt sites and the Brønsted acid sites it would be only one configuration of Pt-Zn-H$^+$ which provided the maximum isomerization activity for all of the investigated reaction temperatures. In fact, it seems this is not the case here

because the data reported in Table 3.12 clearly show that the N_{Zn}/N_{H^+} ratio increases by increasing of the reaction temperature, confirming that the configuration of Pt-Zn-H^+ on the zeolite surface changes from one reaction temperature to another, i.e. when a higher reaction temperature is used the Zn loading has to be increased in order to maintain the maximum isomerization activity.

Moreover, the corresponding values of Iso/Crk and R ratios decrease significantly with increasing of the reaction temperature, suggesting that the overall reaction kinetics are closely dependent on the amount of the Zn species while the location and numbers of the Pt and the Bronsted acid sites were kept unchanged. It is worth noting that the incorporated Zn wt.% is so small when compared to the whole mass of the zeolite, that it does not significantly affect the density of the surface Brønsted acid sites.

Therefore, the variation of the ratio of rate constant for both competitive isomerization and cracking reactions upon Zn loading can be explained only by the variation of activation energies (ΔE_{iso} and ΔE_{crk}) of these reactions. Thus, the only action can be imagined for the Zn species is that they promote the removal of intermediate carbocation from surface acid site, liberating olefinic species and slowing down of further reactions of these species.

This tentative explanation coincides with results of (Table 3.14 and 3.15 and Figures 3.19 and 3.20). In fact, these results show that by increasing of the contact time the conversion of n-heptane increases for all of the catalyst at used

reaction temperatures.

When the total conversion of n-heptane exceeds 70% the percentage of branched heptanes (selectivity to branched C_7 isomers) produced by the reference to the Pt-HY (bifunctional) zeolite catalyst drops dramatically (Table 3.14 and Figure 3.19), whereas by using the Zn loaded zeolite catalyst (trifunctional Pt-Zn-HY samples) the selectivity to the branched C_7 isomers can be maintained at quite a high value (Table 3.15 and Figure 3.20).

It is possible to have higher total conversion of n-heptane, while keeping the isomerization selectivity of C_7 isomers at quite high level, using trifunctional Pt-Zn-HY zeolite catalysts (Table 3.15). This is indicative of a higher turnover frequency for the formation of an isomeric product, i.e rapid removal of the reaction intermediate carbocation from the acid sites. As mentioned before, this more rapid desorption of the olefinic species from the acid sites is also reflected in general decrease of the (mu/mo) upon Zn loading, again in accord with the observation of Iglesia et al [145].

In addition, it is obvious that by using a trifunctional catalyst, more contact time is needed to obtain the same conversion as that of the (parent) bifunctional catalyst (Table 3.14 and 3.15). This is due to the difference between the rates of isomerization reactions (slow) and rates of cracking reactions (fast), where the rate of cracking is predominant with the bifunctional catalyst, particularly at higher reaction temperatures.
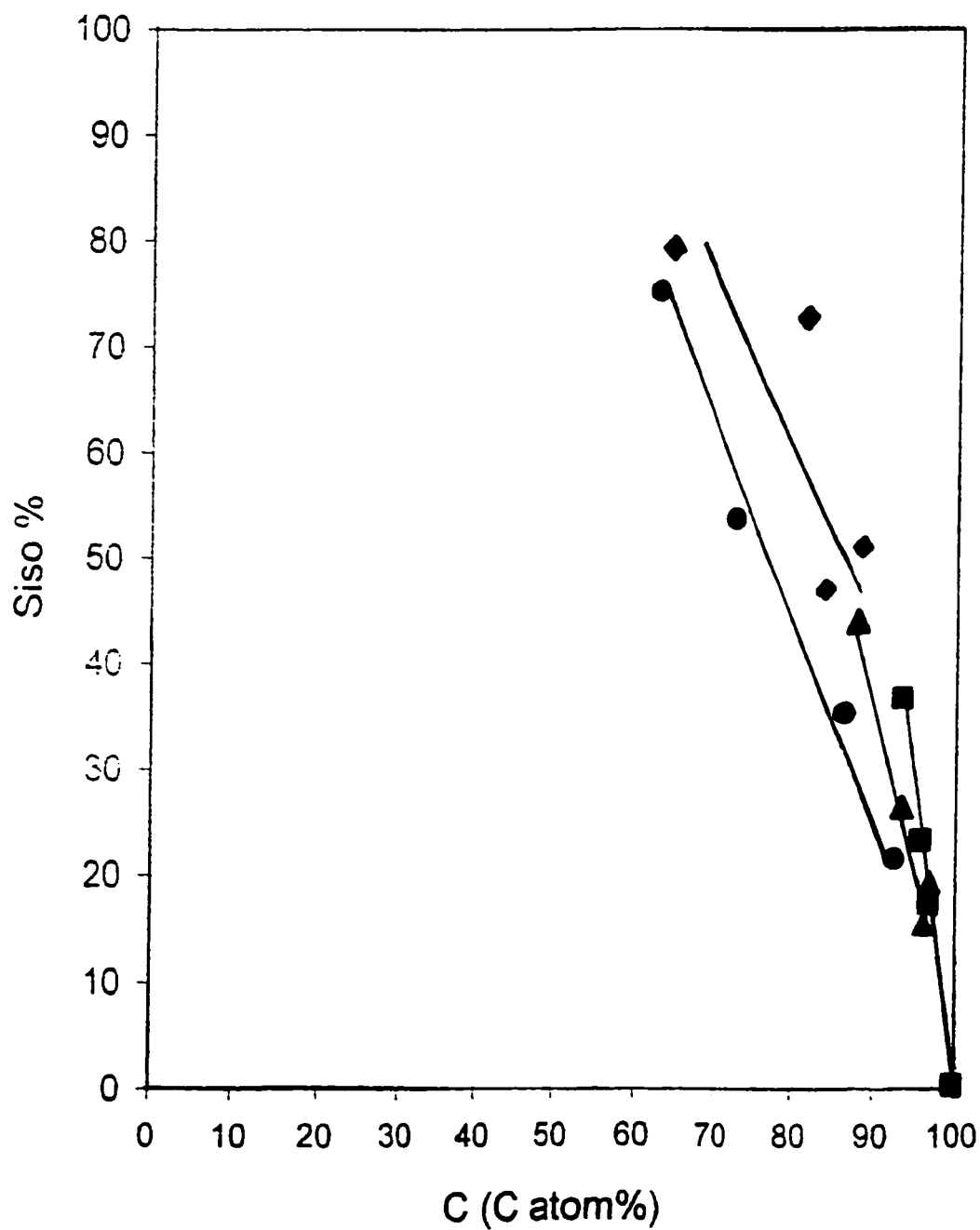
Figure 3.19. Selectivity to branched heptanes (S_{iso}) versus total conversion (C), obtained with the bifunctional catalyst Pt-HY: (◆) 210 °C; (●) 225 °C; (▲) 240 °C; (■) 255 °C.
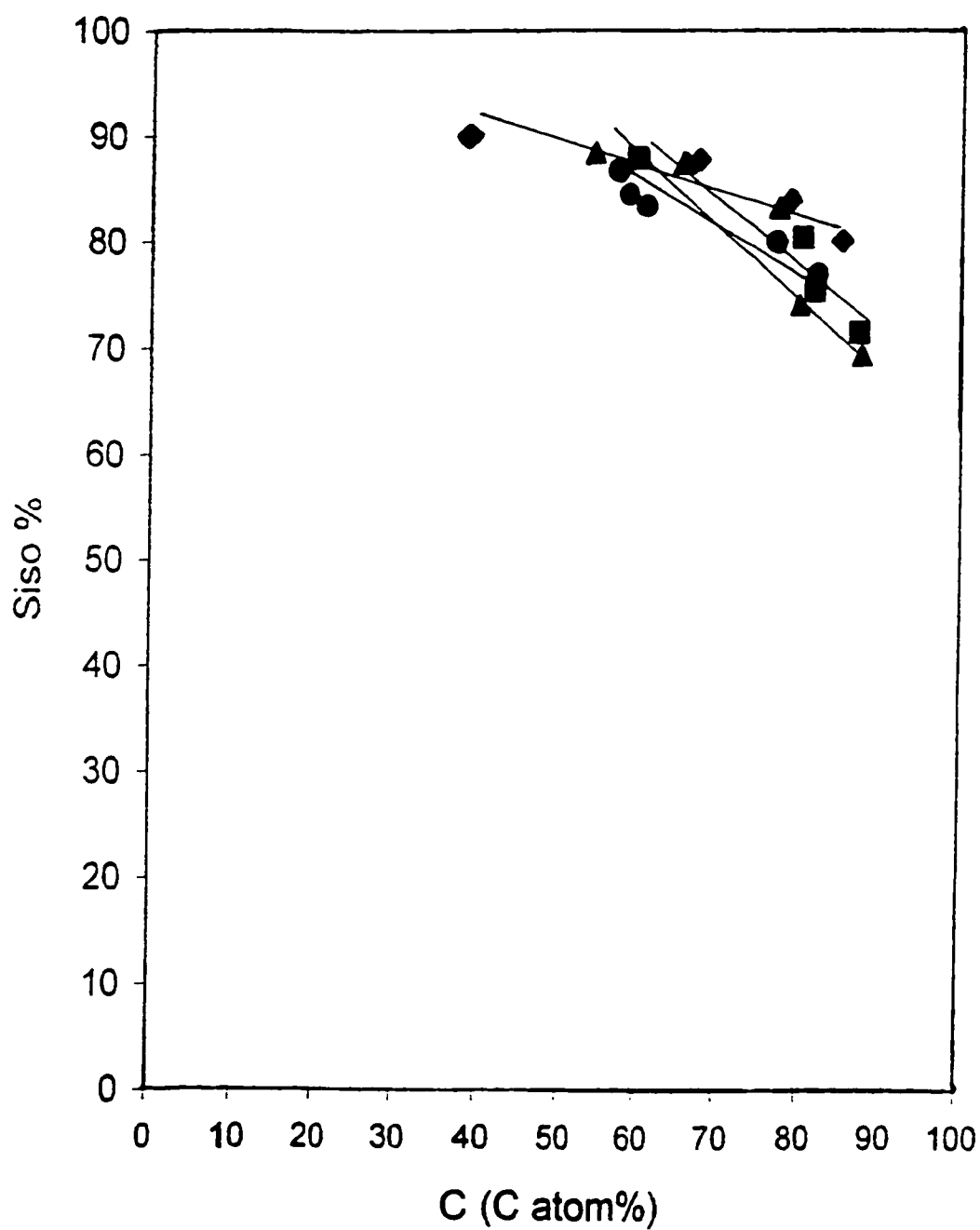
Figure 3.20. Selectivity to branched heptanes (S_{iso}) versus total conversion (C), obtained with the trifunctional catalyst Pt-Zn_y-HY (y_{max}): (◆) 210 °C; (●) 225 °C; (▲) 240 °C; (■) 255 °C.

The results obtained show that the difference in catalytic activity of the cations in terms of maximum isomerization performance, corresponds to the following sequence [121].

$$Zn^{2+}, Ni^{2+} > Al^{3+} > Cd^{2+}$$
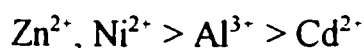
And the hardness and softness of Lewis acidity corresponds to the following sequence [172,173]:

$$Al^{3+} (hard) > Zn^{2+}, Ni^{2+} > Cd^{2+} (soft)$$
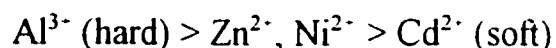
How can the desorption properties of the incorporated cations using hardness and softness of their Lewis acidity be explained? Does the capability to desorb intermediate alkylcarbocations from the protonic sites depend on the balanced Lewis character of the promoting ions? It seems that, with respect to proton (H^+) one of the hardest Lewis acid [172], a good desorption-transfer promoting species should have sufficiently hard acid character to accept π electrons of the reaction intermediate (desorbed olefinic species). However, this species should not be as hard an acid as the proton itself in order to avoid the induction of other detrimental secondary reactions. As mentioned by Pearson [174], the propensity of transition metal ions such as Zn^{2+} to establish π bonding with π electron bearing compounds like olefins, represents the third type of interaction. In addition, the principle of hard and soft acids and bases proposed the ionic and covalent interactions.

The straight lines of Figures 3.19 and 3.20 were interpolated using the curve fitting function as follow:

$$y = ax + b \tag{3.3}$$

where y is the selectivity to branched heptanes and x is total conversion.

At equal conversions it is possible to compare the selectivity of branched heptanes obtained with bifunctional Pt-HY zeolite catalyst (reference sample) to that of the trifunctional Pt-Zn-HY catalyst. Computed data are reported in (Table 3.16). These data show that:

(i) For all of the tested catalysts at constant conversion, lower reaction temperature results in a higher selectivity to the branched heptanes.

(ii) By use of a trifunctional (Pt-Zn-HY) catalyst the yield of branched heptanes higher than that for the bifunctional (Pt-HY) zeolite catalyst at all reaction temperatures.

In particular, at 210 °C (the lowest investigated reaction temperature) the results obtained show that the selectivity for the branched heptanes is higher than that a higher temperatures, and at a conversion of 85 wt.% the selectivity to branched heptanes is 80 wt.% and the multi-branched/mono-branched ratio is 0.36 (Table 3.14 and 3.15).

| Catalyst | Reaction Coefficient of the fitting curve | | | Sele. to bra. heptanes at conv. (Cat.%)[a] | |
	Temp.°C	a	b	r	75%	85%
Pt-HY	210	-1.195	157.4	0.82	68	56
	225	-1.709	180.8	0.99	53	36
	240	-3.116	298.2	0.96	65	33
	255	-0.568	56.8	0.99	14	9
PtZn$_{0.7}$-HY	210	-0.193	98.5	0.92	84	82
PtZn$_{0.9}$-HY	225	-0.327	104.3	0.97	80	77
PtZn$_{1.2}$-HY	240	-0.577	122.6	0.91	79	74
PtZn$_{1.8}$-HY	255	-0.558	121.9	0.95	80	74

a) Selectivity to branched heptanes at conversion (C atom %)

Table 3.16. Selectivity to branched heptanes at 75 and 85% conversion and different reaction temperatures, which are obtained by interpolating of data. (a) and (b) are coefficients of the fitting curve y = ax + b, r is the correlation coefficient.

If the (N_{Zn} / N_{H^+}) ratio (where N_{H^+} and N_{zn} are the number of zeolite protonic sites and Zn^{2+} ionic sites respectively) of the trifunctional zeolite catalysts which give the best isomerization activity at the investigated reaction temperature is considered (Table 3.12), the followings are observed:

(i) At the reaction temperatures investigated all of these ratios are lower than 1, so that each protonic acid site does not need more than one Zn^{2+} ionic sites.

(ii) By increasing the reaction temperature the value of this ratio increases. This behavior can be explained tentatively such that, at higher reaction temperature some weaker zeolite acid sites are activated and accessible for reactions. Thus, more Zn^{2+} sites are required to drive the reaction into the isomerization path.

(iii) This question always arises, why with incorporation of Pt and cationic species such as Zn simultaneously in the HY zeolite, the isomerization is improved more than with sequential loading (stepwise procedure of incorporation as reported in [121]) of Pt and Zn. It is thought that, when Pt and Zn species are incorporated separately into the HY zeolite, the zeolite surface cannot ensure a surface distribution of these two components in the same way as in the case of the simultaneous incorporation method. Thus, with the latter incorporation method, the zeolite surface configuration appears more favorable to the desorption-transfer action of the Zn species. By simultaneous loading of Pt and Zn species, followed by thermal activation and reduction using hydrogen

which involves mostly the mobile Pt species, clearly a surface restructuring is induced. This phenomena changes the properties of active sites on the zeolite surface toward more isomerization reactions with less cracking. This phenomena of surface restructuring which is induced by adsorbates was suggested by Somorjai [175].

3.3.5 Conclusion

The data obtained show that Zn loading needs to vary in order to provide the best isomerization activity at each reaction temperature. In addition, the results obtained show that higher isomerization performance can be achieved at lower reaction temperature by using a trifunctional catalyst and longer contact time. These observations are elements of experimental evidence for the desorption-transfer promoting action of the zinc species of the trifunctional (Pt-Zn-HY) zeolite catalyst, which their Lewis character play important role in the enhancement of the isomerization. In the near future, we aim at addressing this issue with more in-depth investigations on adsorbed reaction intermediate carbocations using the "in situ" FT-IR (DRIFTS) technique, and on the Lewis acid character of the desorbing sites using the microcalorimetry method with specific probe molecules [176,177].

3.3.6 Modification of the strength of the zeolite acid sites by incorporation of halogen containing species

3.3.6.1 Effect of AlCl₃ loading of the Pt-Al-HY trifunctional zeolite catalysts on *n*-heptane isomerization

As mentioned before, the traditional approach to obtaining higher multi-branch paraffins by isomerization of *n*-paraffins is to search for and use of a catalyst with stronger surface acidity such as zeolite and superacidic solid materials. These very acidic catalysts allow the reaction to be carried out at lower temperature. As a result, under such mild condition the isomerization reactions increase and cracking reactions decrease. In this section, it is proposed to investigate the incorporation of chlorine as electron withdrawing species into the HY zeolite for the promising perspective of this method in increasing the strength of acid sites on the surface of zeolite catalysts. For this purpose a mixture of $AlCl_3$ and $Al(NO_3)_3$ was used with simultaneous incorporation of Zn and Pt species into the HY zeolite in order to increase the acidity strength of the zeolite surface at the same time as Al loading (section 2.1.3). During incorporation, $AlCl_3$ was increased with decreasing of $Al(NO_3)_3$ in such a way that the Al species remained unchanged at 1 Wt.%. The results obtained show that incorporation of $AlCl_3$ has a negative effect on production of branched paraffins, and increases the cracking reactions (Table 3.17 and Figure 3.21). This is probably due to replacement of some of the OH groups with the Cl species on the surface of zeolite, whereby the strength of remaining OH groups increase because of electron withdrawing effect of Cl species.

Al_{Cl} loading* (wt%)	(10⁻³ mol/g)	Conversion (C atom %)	Y_{iso} (C₅-C₇)	Product selectivity S_{iso}	S_{Crk}	mu/mo	Selectivity ratio R	(Iso/Crk)
Pt-Al₁-HY catalysts (method of simultaneous incorporation)&								
0.00	0.00	81.4	68.1	79.6	20.4	0.39	3.9	3.2
0.29	0.11	81.2	53.6	60.8	39.2	0.42	1.6	1.3
0.55	0.20	91.5	52.0	51.2	48.8	0.23	1.1	1.0
0.79	0.29	90.2	41.9	42.0	58.0	0.22	0.7	0.7
1.00	0.37	93.0	38.3	34.7	65.3	0.18	0.5	0.5

*) (Al_{Cl}) Al loaded from $AlCl_3$ = x g and (Al_N) Al loaded from $Al(NO_3)_3$ = (1-x) g

&) Al = 1 Wt. % (0.37×10⁻³ mole/g) of catalyst

Table 3.17. Activity and selectivity versus $AlCl_3$ loading (contact time = 1.042 h and T = 225 °C).
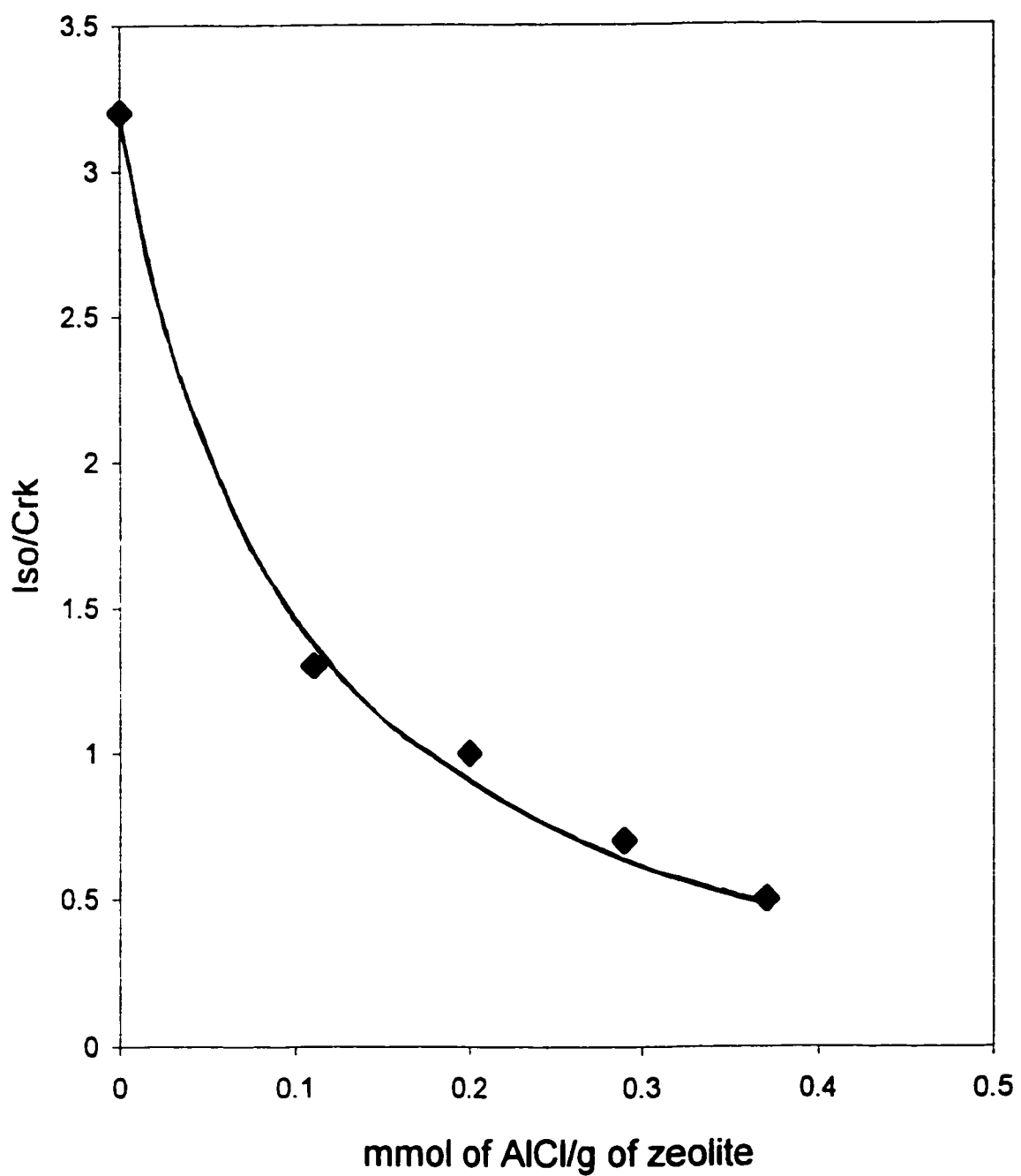
Figure 3.21. Composite selectivity ratio (Iso/Crk) versus AlCl$_3$ loading at
T = 225 °C.

3.3.6.2 Effect of the counter-anion (Cl⁻) used for the loading of Zn on the trifunctional zeolite catalysts on *n*-heptane isomerization

The purpose for incorporation of $ZnCl_2$ into the Pt-HY bifunctional zeolite catalysts was to increase the strength and the density of the surface acidity of the trifunctional Pt-$Zn_{0.9}$-HY zeolite catalysts. As mentioned before, chlorine is electronegative species and has electron withdrawing effect. The idea was, by using the obtained trifunctional Pt-$Zn_{0.9}$-HY zeolite catalysts at lower reaction temperature to increase the isomerization reactions and decrease the cracking reactions.

A mixture of $ZnCl_2$ and $Zn(NO_3)_2$ was used for simultaneous incorporation of Zn and Pt species into the HY zeolite. During incorporation, $ZnCl_2$ was increased with decreasing of $Zn(NO_3)_2$ so that Zn species remained unchanged at 0.9 mmol/gr of zeolite (section 3.12). The results obtained show that incorporation of $ZnCl_2$ has a negative effect on the production of branched paraffins and increase the cracked products (Table 3.18 and Figure 3.22). Some tests were also done using other halogens (F, Br and I) treated trifunctional (Pt-$Zn_{0.9}$-HY) catalysts. A mixture of each material of the ZnF_2, $ZnBr_2$, and ZnI_2 with $Zn(NO_3)_2$ was used for simultaneous incorporation of Zn and Pt species. These catalysts was prepared using the same procedure as for Cl treated Pt-$Zn_{0.9}$-HY zeolite catalyst, so that Zn species remained unchanged at 0.9 mmol/gr of zeolite ($Zn_{halogen}$ = 50% $Zn_{nitrate}$ = 50%). Again the results obtained show that the incorporation of ZnX_2 (X = F, Br and I) decrease the isomerization activity of trifunctional Pt-$Zn_{0.9}$-HY zeolite catalyst (Table 3.19).

Zn_{Cl} loading*	Contact time (h)	Conversion (C atom %)	Product selectivity		mu/mo	Selectivity ratio	
$(10^{-3}$ mol/g)			S_{iso}	S_{Crk}		R	(Iso/Crk)

Pt-$Zn_{0.9}$-HY catalysts (method of simultaneous incorporation)[&]

0.00	1.06	52.5	94.7	5.3	0.17	17.8	9.4
0.23	1.05	56.4	82.4	17.6	0.13	4.7	2.6
0.45	1.04	63.1	65.2	34.8	0.14	1.9	1.2
0.68	1.05	59.9	56.7	43.3	0.14	1.3	0.8
0.90	1.02	61.1	57.6	42.4	0.14	1.4	0.8

*) (Zn_{Cl}) Zn loaded from $ZnCl_2$ = x mmol/g of zeolite and (Zn_N) Zn loaded from $Zn(NO_3)_2$ = (1-x) mmol/g of zeolite

&) Zn = 0.9×10^{-3} mole/g of catalyst

Table 3.18. Activity and selectivity versus $ZnCl_2$ loading (contact time ≈ 1.04 h and T = 225 °C).

Zn_X loading* (0.45×10⁻³ mol/g)	Contact time (h)	Conversion (C atom %)	Product selectivity		mu/mo	Selectivity ratio	
			S_{iso}	S_{Crk}		R	(Iso/Crk)
Pt-$Zn_{0.9}$-HY catalysts (method of simultaneous incorporation)[&]							
------	1.06	52.5	94.7	5.3	0.17	17.8	9.4
(ZnF_2)	1.05	54.3	73.4	26.6	0.13	2.8	1.5
($ZnCl_2$)	1.04	63.1	65.2	34.8	0.14	1.9	1.2
($ZnBr_2$)	1.05	50.5	81.7	18.3	0.12	4.5	2.3
(ZnI_2)	1.02	54.2	74.0	26.0	0.12	2.8	1.5

*) (Zn_X) Zn loaded from ZnX_2 (X = F, Cl, Br and I) = 0.45 mmol/g of zeolite and (Zn_N) Zn loaded from $Zn(NO_3)_2$ = 0.45 mmol/g of zeolite

&) Zn = 0.9×10⁻³ mole/g of catalyst

Table 3.19. Activity and selectivity versus ZnX_2 (X = F, Br and I) loading (contact time ≈ 1.04 h and T = 225 °C).
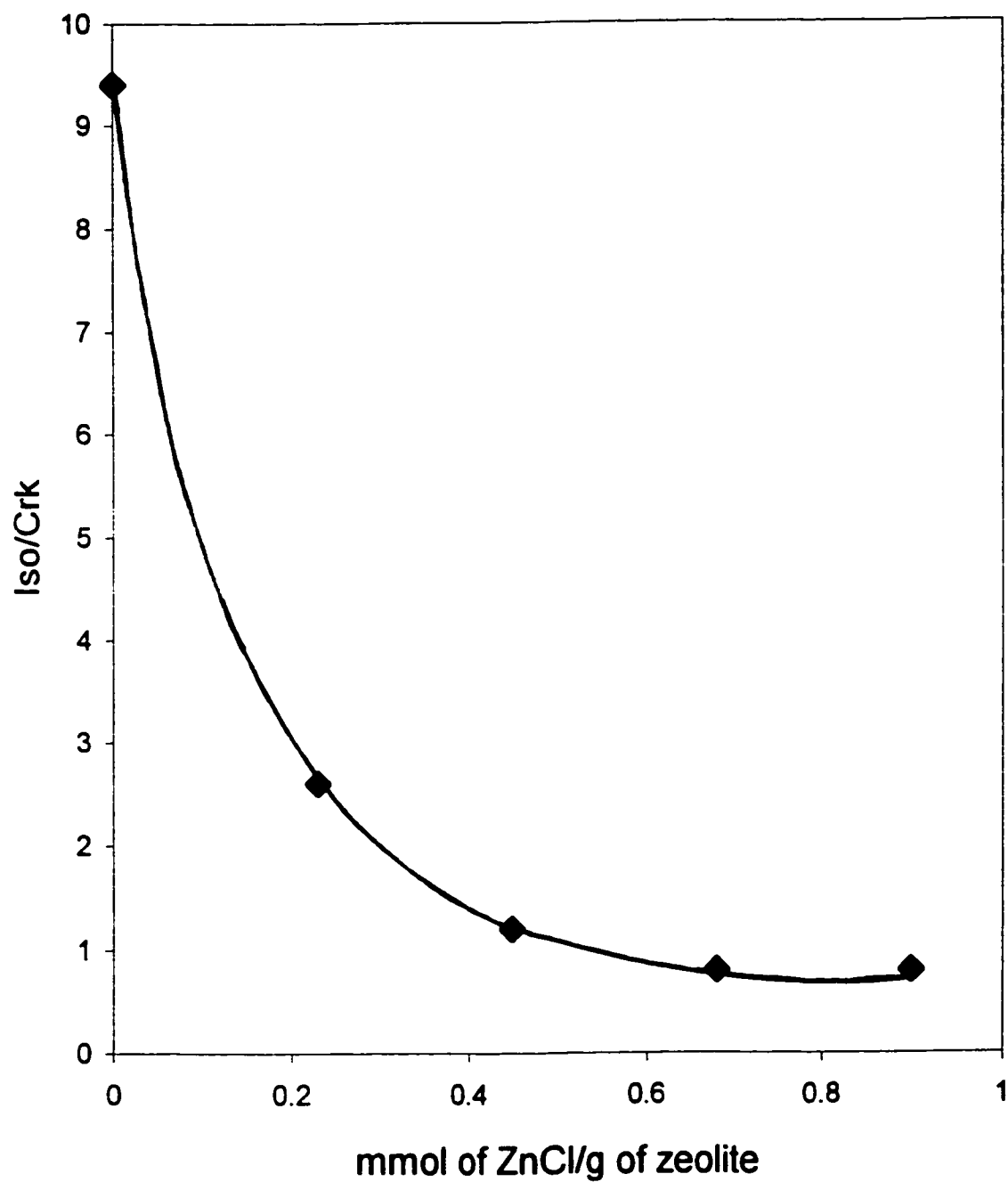
Figure 3.22. Composite selectivity ratio (Iso/Crk) versus ZnCl₂ loading at

T = 225 °C.

3.3.6.3 Effect of the incorporation of ammonium halide onto the trifunctional Pt-X-Zn$_{0.9}$-HY (X= F, Cl, Br or I) zeolite catalysts on *n*-heptane isomerization

These catalysts were prepared by immersing HY zeolite pellets in the solution of NH$_4$F, NH$_4$Cl, NH$_4$Br or NH$_4$I in water before loading of Zn and Pt (the same procedure as explained in section 2.1.3 part j).

The experimental set up, reaction conditions and the products analysis were similar to that of the reported elsewhere [121,143]. By loading of the halogen into the HY zeolite some of the OH⁻ groups on the surface of the zeolite are substituted by Cl⁻, Br⁻ or I⁻ which increase the acid strength on the surface of the zeolite. In the case of F⁻ loading, the results obtained was not satisfactory suggesting that the F⁻ loading damaged the framework of the zeolite catalyst. The results obtained show that the sample treated with Cl⁻ yielded more cracking products than that of the sample treated with I⁻ because of the higher "electron-withdrawing" properties of the bonded Cl species which result in stronger acid sites (Table 3.20). Surprisingly, I⁻ treated sample yielded higher conversion with lower cracking products. This is maybe due to formation of a special configuration of the active sites in the I⁻ treated trifunctional catalyst by replacement of some strong acid sites by I⁻ and the accessibility of these active sites located on the surface of this catalyst. However, the sample treated with Br⁻ yielded lower conversion than that of the Cl⁻ treated samples.

Treatment	Acidic Properties		Conversion (C atom %)	Product selectivity		Selectivity ratio	
	Density	Strength		S_{iso}	S_{Crk}	R	(Iso/Crk)
Pt-Zn$_{0.9}$-HY catalysts (method of simultaneous incorporation of Pt and Zn)							
0 (tri.)$^{\&}$	2.5	MS*	52.5	94.7	5.3	17.8	9.4
Cl⁻	1.9	SS	69.0	64.2	35.8	1.8	1.2
Br⁻	----	MS	67.9	86.1	13.9	6.2	4.2
I⁻	1.8	MS	55.0	90.2	9.8	9.2	5.1
0 (Bi.)$^{\$}$	2.5	MS	82.9	46.2	53.8	0.9	0.7

*) M = Medium, S = Strong

&) Trifunctional Pt-Zn$_{0.9}$-HY zeolite catalyst

$) Bifunctional Pt-HY zeolite catalyst

Table 3.20. Activity and selectivity versus halogen X⁻ (X⁻ = Cl⁻, Br⁻ or I⁻)

loading (contact time ≈ 1.04 h and T = 225 °C).

3.4 Kinetic studies

The purpose of this research work was comparative study of the kinetic behavior of the trifunctional (Pt-Zn$_y$-HY) and bifunctional (Pt-HY) zeolite catalysts in the hydroisomerization of n-heptane. Kinetic can be used to give support to a hypotheses of reaction mechanism. However, it cannot provide the final experimental evidence of such a mechanism [178].

When a catalytic reaction occurs on the heterogeneous catalysts, several physical and chemical steps take place in proper sequence during reaction. However, these steps have been broken down by Hill and Hougen and others on molecular scale as follow [179,180]:

i) Mass transfer of the reactants from the main body of the fluid to the gross exterior surface of the catalyst particle

ii) Molecular diffusion of the reactants from the exterior surface into the interior pore structure

iii) Chemisorption of at least one reactant on the catalyst surface

iv) Reaction on the surface of catalyst which this may involve several steps

v) Desorption of chemically adsorbed species from the surface of catalyst

vi) Transfer of products from the interior catalyst pores to the gross external surface of the catalyst by ordinary molecular diffusion

vii) Mass transfer of products from the exterior surface of the particle into the bulk of the fluid.

In addition, in the case of nonporous catalysts, steps (ii) and (vi) are absent. Steps (i), (ii), (vi) and (vi) are physical processes, while steps (iii) to (v) are basically chemical in character.

The mechanism of hydroisomerization of n-heptane and other long-chain paraffins over bifunctional catalysts includes competitive isomerization (primary and secondary) and cracking (β-scission) steps. As mentioned before, the formation of cracking products is significantly decreased by the addition of Zn⁺ ions (desorption-transfer promoting sites). However, on increasing the reaction temperature Zn loading must be increased in order to obtain the highest isomerization performance. This suggests that, at higher reaction temperature, more acid sites are activated and involved in the reaction, and more Zn species are needed to evacuate the intermediate carbocations from the acid sites (a higher N_{Zn}/N_{H^+} ratio). Hence, for production of branched paraffins from n-heptane, the best trifunctional catalyst configuration varies with reaction temperature.

In this research, we sought evidence of the concept of trifunctional catalyst by comparing the kinetic behavior of bifunctional (Pt-HY) zeolite catalyst to that of the trifunctional (Pt-Zn-HY) zeolite catalyst, in particular we focused on the effect of Zn species on the cracking (β-scission) activity, and the acidic properties of both catalysts.

The experimental set up and reaction conditions were similar to those reported in section 2.3, except the following reaction parameters:

i) the weight of catalyst used varied from 0.5 to 2.0 g

ii) contact time (gram of catalyst per g of n-heptane injected per hour) varied from 0.16 to 1.06 h

iii) reaction temperatures were 195 °C, 210 °C, 225 °C or 240 °C.

The preparation of bifunctional (Pt-HY) catalyst and the trifunctional (Pt-Zn_y-HY), catalysts testing, and product analysis were identical to those described in section 2.3. The total conversion of n-heptane and conversion to specific products P (P being mo, mu, cr, i.e. mono-branched heptanes, multi-branched heptanes, cracked products, respectively), and selectivity to product P were calculated using equations 2.6, 2.7 and 2.8 respectively.

The experimental data for total n-heptane conversion C_t and conversions C_{mo}, C_{mu} or C_{cr} (i.e. mono-branched heptanes, multi-branched heptanes and cracked products, respectively) for each catalyst at each reaction temperature were fit to a polynomial function $f(\tau)$ based on contact time (τ) using the non-linear regression simplex algorithm. The criteria for the choice of the polynomial function whose representative curve (total conversion C_t versus contact time τ) best fit the experimental points, were as follows: correlation factor higher than 0.95 (ideal fit = 1) and lowest degree of the polynomial function. The same procedure was used for C_{mo}, C_{mu} and C_{cr} (Figures 3.23-3.28). The following equation were used to calculate C_{mo}, C_{mu} and C_{cr}:

$$S_{mo} = [1/(1+(mu/mo))] \times S_{C7} \qquad (3.4)$$

$$C_{mo} = (C_t/100) \times S_{mo} \qquad (3.5)$$

$$S_{mu} = S_{C7} - S_{mo} \qquad (3.6)$$

$$C_{mu} = (C_t/100) \times S_{mu} \qquad (3.7)$$

$$S_{Cr} = 100 - S_{C7} \qquad (3.8)$$

$$C_{Cr} = (C_t/100) \times S_{Cr} \qquad (3.9)$$

where S_{mo} = selectivity to mono-branched C_7 products, S_{mu} = selectivity to multi-branched C_7 products, S_{cr} = selectivity to cracked products and S_{C7} = selectivity to C_7 isomers.

The polynomial function is expressed as below at a given reaction temperature T:

$$C_t = a + b\tau + c\tau^2 + d\tau^3 \ (\ 4 \ \text{coefficients maximum}) \qquad (3.10)$$

where C_t is the conversion expressed in % C-atoms.

In addition, in kinetic investigations for a static system, (τ) usually represents the reaction time over which the variation of reactant concentrations is followed. However, in catalytic reaction where a plug flow system is involved, (τ) represents the contact time for the reaction which is the average

time that a reactant molecule takes to pass through the catalyst bed.

The general form of the rate equation used is:

$$r = k\ P^n \tag{3.11}$$

where k, P and n are the rate constant, the partial pressure of reactant, and the order of reaction, respectively. Since P (for all runs) and n (for each catalyst) are constant, we have:

$$r = k \times P^n = d\ C_t/d\tau \tag{3.12}$$

$$k = P^{-n} \times r = P^{-n} \times d\ C_t/d\tau \tag{3.13}$$

For accuracy reasons, data for initial rates were used for determining the initial reaction rate by taking the derivative of the function $f(\tau)$ at zero contact time, resulting in the following equations for a reaction temperature T:

$$r_0 = \left[df(\tau)/d\tau\right]_{\tau = 0} \tag{3.14}$$

$$k = P^{-n} \times r_0 = P^{-n} \times \left[df(\tau)/d\tau\right]_{\tau = 0} = C \times r_0 \tag{3.15}$$

Where C is a constant and r_0 is the initial rate of reaction.

From these data, Arrhenius plots (ln r_0 versus $10^3/T$) were obtained. From the slope (- E_a / 10^3 R) the apparent activation energy E_a was evaluated. It is worth noting that the zero point was considered an experimental point because with no catalyst, the conversion of n-heptane was negligible within the range of reaction temperature investigated.

In general, the activation energy of a reaction could be determined using the Arrhenius equation(eq. 2.12), by knowing the reaction rate at various temperatures as follows:

$$k = A \exp(-E_a / RT)$$

where k is the rate constant, A is the pre-exponential factor, R is the gas constant and T is the reaction absolute temperature (in °K).

The rate of reaction can be determined as follows:

$$r = \text{rate} = k \text{ [reactant]} \qquad (3.16)$$

Assuming that the reaction is first order in reactant concentration.

In the case of n-heptane hydroisomerization the reaction rate could be expressed as consumption rate of n-heptane:

$$r = - d \text{ [}n\text{-heptane]} / d\tau \qquad (3.17)$$

Thus, the rate r_t was assumed to be as follows:

$$r_t = k_t \, [\textit{n}\text{-heptane}] \tag{3.18}$$

Since the various values of contact time τ were obtained by varying the weight of catalysts keeping the flow rate of $\textit{n}$-heptane and hydrogen constant, the rate constant can be determined as follows:

$$k_t = (\text{constant}) \, r_t = (\text{constant}) \, (d \, C_t/d\tau) = (\text{constant}) \, (b + 2c\tau + 3d\tau^2) \tag{3.19}$$

So that at zero contact time ($\tau = 0$) the determined rate constant was:

$$k_t^0 = (\text{constant}) \times b \tag{3.20}$$

The same treatment was applied to k_{mo}^0, k_{mu}^0 and k_{cr}^0.

where k_t^0, k_{mo}^0, k_{mu}^0 and k_{cr}^0 are the total, mono-branched C_7, multi-branched C_7 and cracking rate constants, respectively.
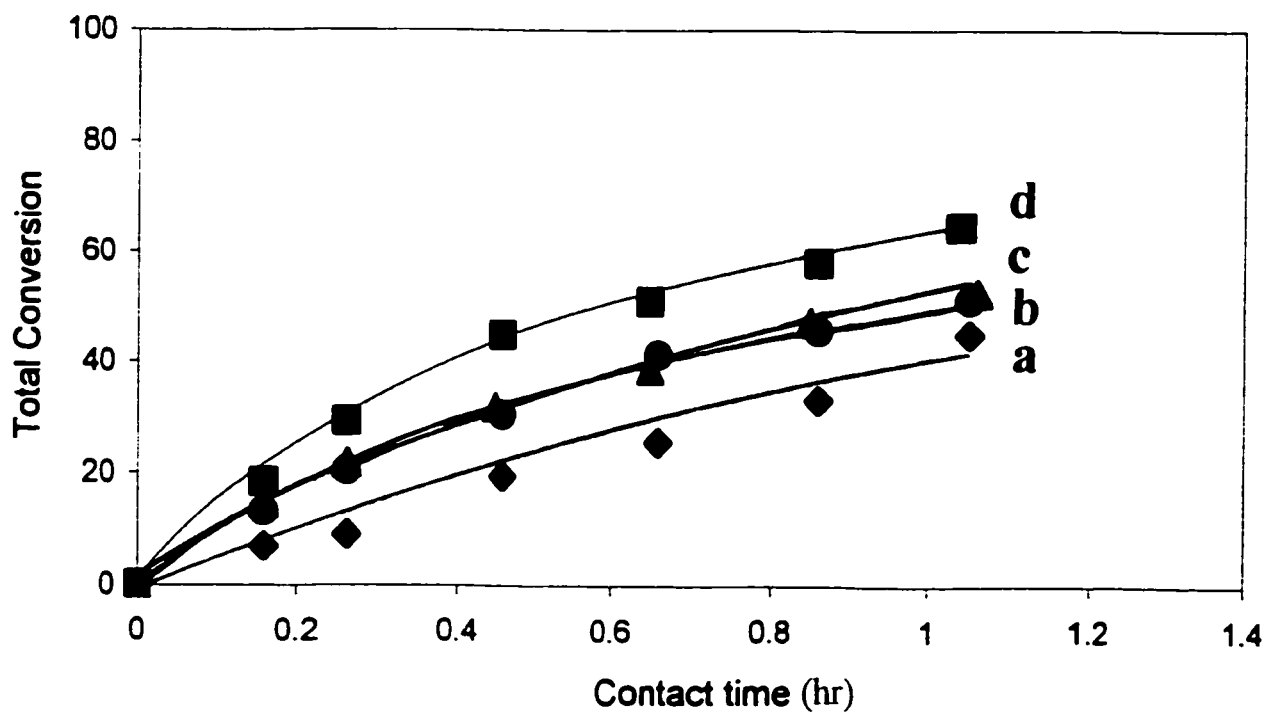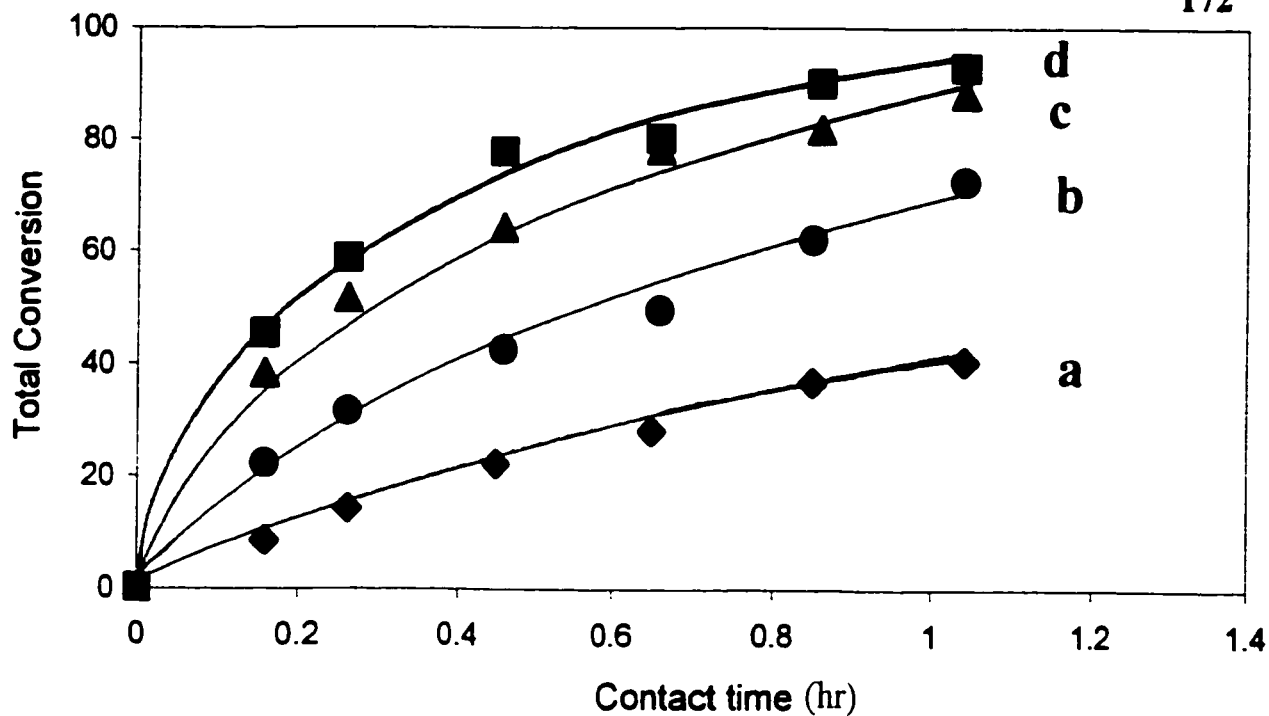
Figure 3.23. Total conversion versus contact time using bifunctional Pt-HY catalyst (A) and trifunctional Pt-Zn$_y$-HY catalyst (B) at: T = 195 °C (a, y = 0.55 mmol/g), 210 °C (b, y = 0.7 mmol/g), 225 °C (c, y = 0.9 mmol/g) and 240 °C (d,y = 1.2 mmol/g).
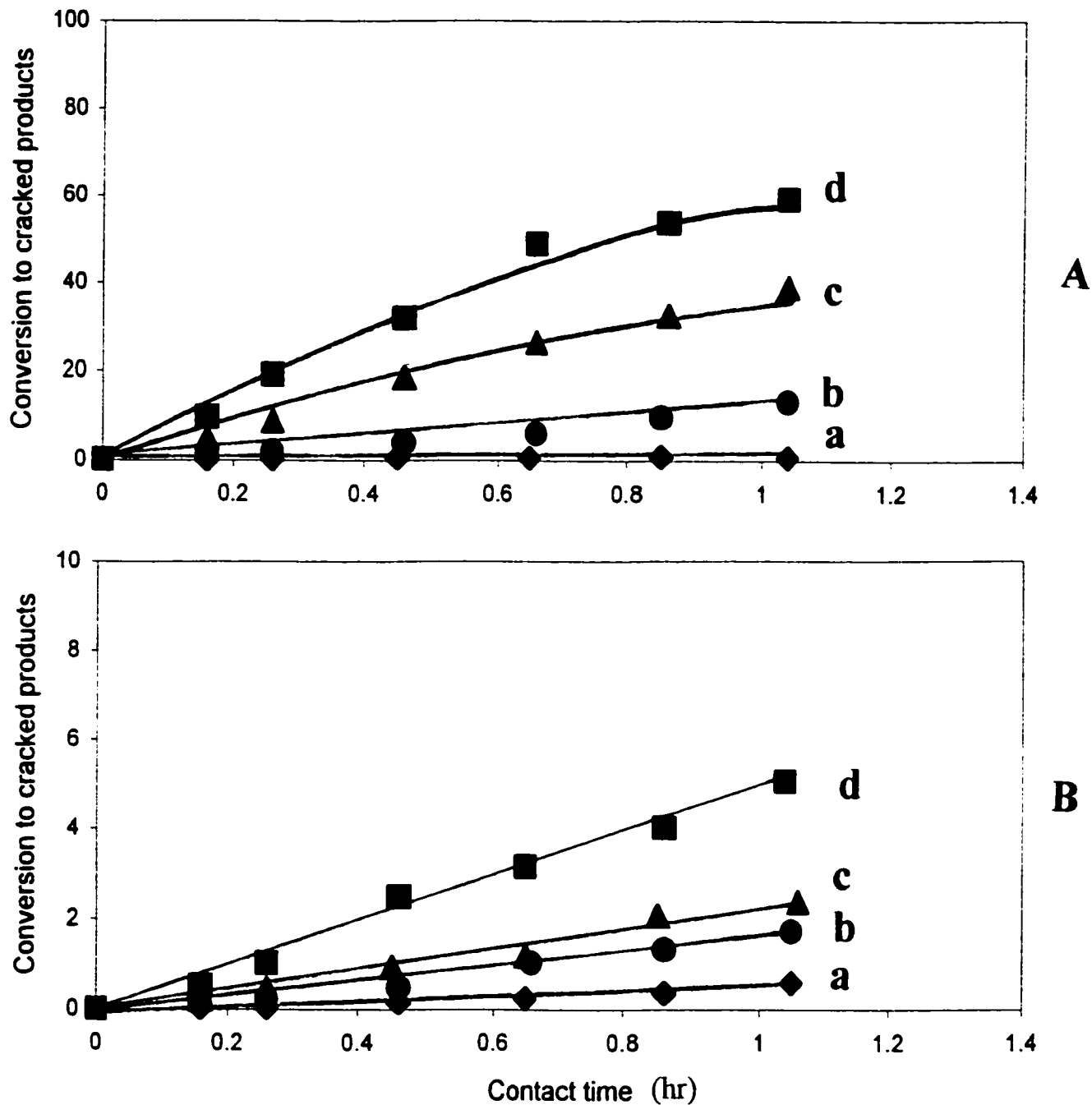
Figure 3.24. Conversion to cracked products versus contact time using bifunctional Pt-HY catalyst (A) and trifunctional Pt-Zn$_y$-HY catalyst (B) at: T = 195 °C (a, y = 0.55 mmol/g), 210 °C (b, y = 0.7 mmol/g), 225 °C (c, y = 0.9 mmol/g) and 240 °C (d, y = 1.2 mmol/g).
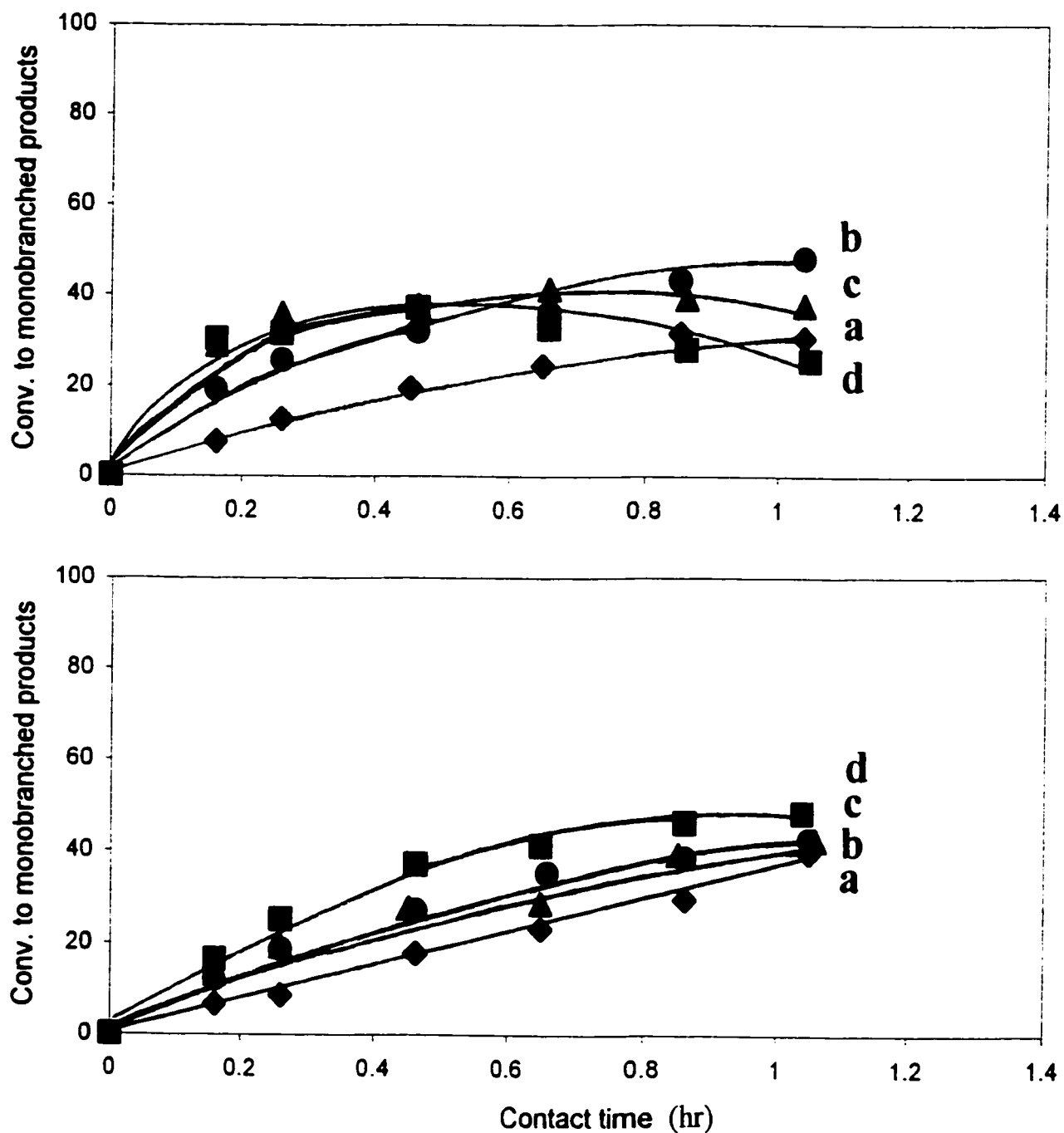
Figure 3.25. Conversion to mono-branched products versus contact time using bifunctional Pt-HY catalyst (A) and trifunctional Pt-Zn$_y$-HY catalyst (B) at: T = 195 °C (a, y = 0.55 mmol/g), 210 °C (b, y = 0.7 mmol/g), 225 °C (c, y = 0.9 mmol/g) and 240 °C (d, y = 1.2 mmol/g).
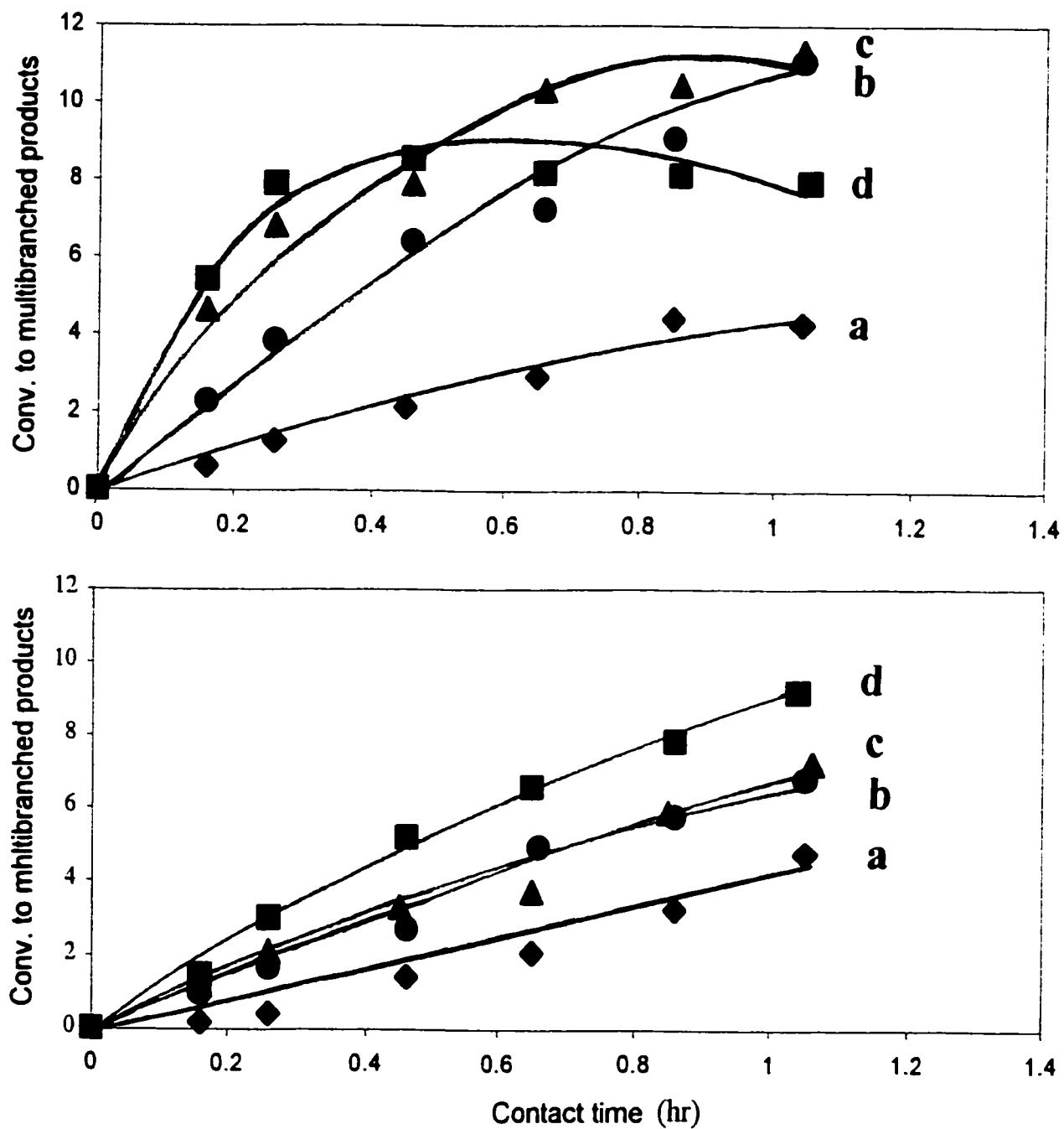
Figure 3.26. Conversion to multi-branched products versus contact time using bifunctional Pt-HY catalyst (A) and trifunctional Pt-Zn_y-HY catalyst (B) at: T = 195 °C (a, y = 0.55 mmol/g), 210 °C (b, y = 0.7 mmol/g), 225 °C (c, y = 0.9 mmol/g) and 240 °C (d, y = 1.2 mmol/g).
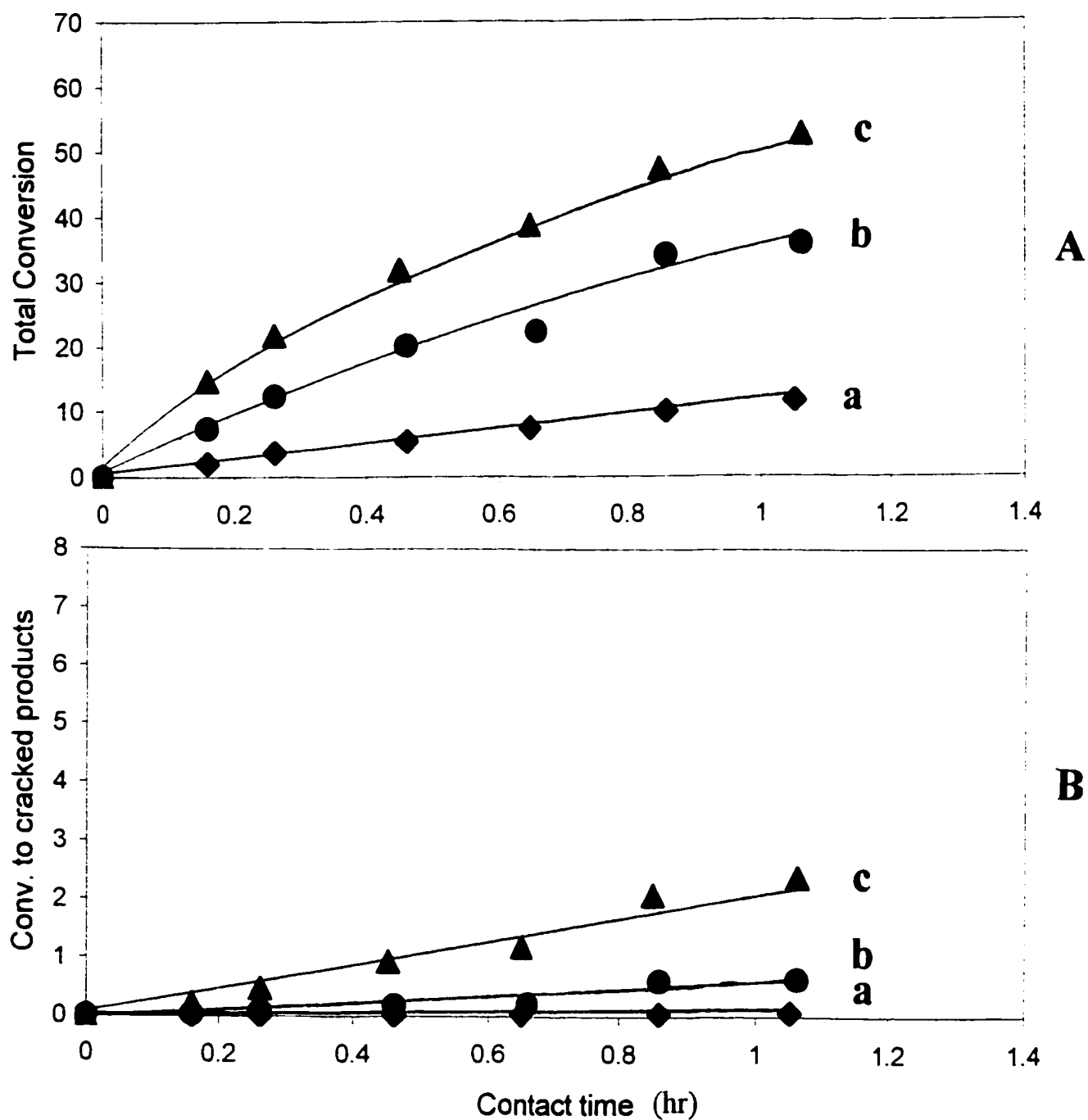
Figure 3.27. Total conversion (A) and conversion to cracked products (B) versus contact time using trifunctional Pt-$Zn_{0.9}$-HY catalyst at: T = 195 °C (a), 210 °C (b), and 225 °C (c).
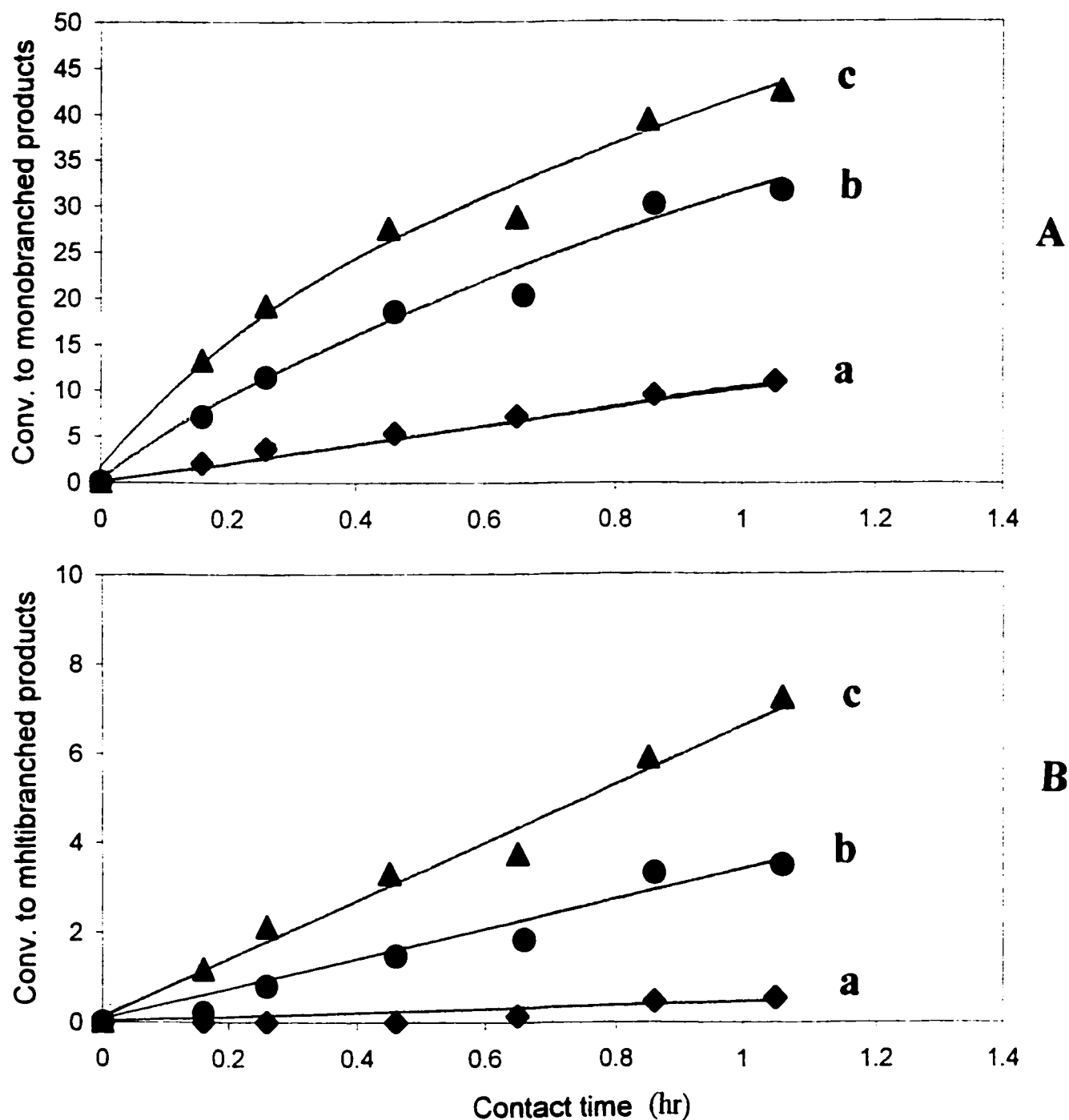
Figure 3.28. Conversion to mono-branched products (A) and conversion to multi-branched products (B) versus contact time using trifunctional $Pt-Zn_{0.9}-HY$ catalyst at: $T = 195\ °C$ (a), $210\ °C$ (b), and $225\ °C$(c).

From Figures 3.22-3.25 it is clear that the conversions C_t, C_{mo}, C_{mu} and C_{cr} decrease by using trifunctional Pt-Zn- HY catalyst (mainly C_{cr}) compared to the bifunctional Pt-HY zeolite catalyst.

As mentioned before, incorporation of Zn species in quite small amounts into the bifunctional Pt-HY zeolite did not significantly affect the surface acid density. The ammonia TPD profile and FT-IR of sorbed pyridine did reveal the presence of some weak Lewis acid sites due to incorporation of Zn^{2+} ions. On the other hand, the strength of surface Brønsted acid sites did not significantly changed upon Zn^{2+} incorporation. The FT-IR characteristic peaks of CO adsorbed on Brønsted acid sites (2117 cm^{-1} and 2173 cm^{-1}) did not undergo any noticeable shift and the peak of the acidic OH group (3610 cm^{-1}) also remained unchanged.

In addition, the incorporation of Zn^{2+} into the Pt-NaY zeolite did not change the dehydrogenation-hydrogenation property of this catalyst. Furthermore, varying the Pt loading from 0.5 wt % to 1.5 wt % did not result in any significant change in total conversion of n-heptane, or as product selectivity, thus, the dehydrogenation-hydrogenation of the olefinic species over the Pt-HY zeolite is not rate-determining step. All of these observations are evidence that the direct influence of the Zn^{2+} incorporated into the bifunctional Pt-HY on the acid sites of the zeolite and on Pt site is quite small.

Therefore, over Pt-HY zeolite catalyst, cracking (β-scission) is significant for the alkylcarbocations of both primary and secondary isomerizations which

are adsorbed on the Brønsted acid sites of the zeolite. Actually there are three types of alkylcarbocationic intermediate adsorbed on the zeolite acid sites as follow (Figure 3.29):

i) AH^+ which is obtained from protonation of the n-heptene (A) as transferred from dehydrogenation-hydrogenation (Pt) site

ii) $A'H^+$, this carbocation results from the primary isomerization of AH^+. The hydrogenation of the olefinic form of this type carbocation (as desorbed from Brønsted acid sites) on the Pt sites resulted in the mono-branched heptanes

iii) Finally, $A''H^+$ which is obtained by the secondary isomerization of $A'H^+$ carbocation.

After desorption of this type of carbocation ($A''H^+$) from Brønsted acid site as olefinic species and hydrogenation on the Pt site the multi-branched heptanes are obtained. Once again, it is should be remembered that the multi-branched heptane carbocations undergo β-scission much faster than the mono-branched heptane carbocations. However, to consider the quite simple mechanistic scheme of the overall reaction (Figure 3.29) it is useful to show the actual role of the Zn^{2+} incorporated into the bifunctional Pt-HY zeolite catalyst.

$$A'H_2 \text{ [mo]} \qquad A''H_2 \text{ [mu]}$$

$$+H_2 \quad | \quad Pt \qquad +H_2 \quad | \quad Pt$$

$$A' \qquad\qquad A''$$

$$196.6(Bi)^* \quad | \quad 93.4(Tri)^{\&} \quad 25.2(Bi)^* \quad | \quad 9.9(Tri)^{\&}$$

$$\begin{array}{c} -H_2 \\ AH_2 \rightleftharpoons A + H^+ \rightleftharpoons AH^+ \rightleftharpoons A'H^+ \rightleftharpoons A''H^+ \\ (Pt) \quad (Z) \qquad (Z) \qquad (Z) \end{array}$$

$$39.0(Bi)^* \qquad\qquad 0.6(Tri)^{\&}$$

$$[Cr]$$

or:

$$n\text{-heptane} \underset{Pt\,(\,-H_2\,)}{\rightleftharpoons} n\text{-heptene}$$

$$+H^+$$

mono-branched C_7 carbocations $\longrightarrow$ multi-branched C_7 carbocations

Pt (+H$_2$)   cracked products   Pt (+H$_2$)

mono and multi-branched heptanes

---
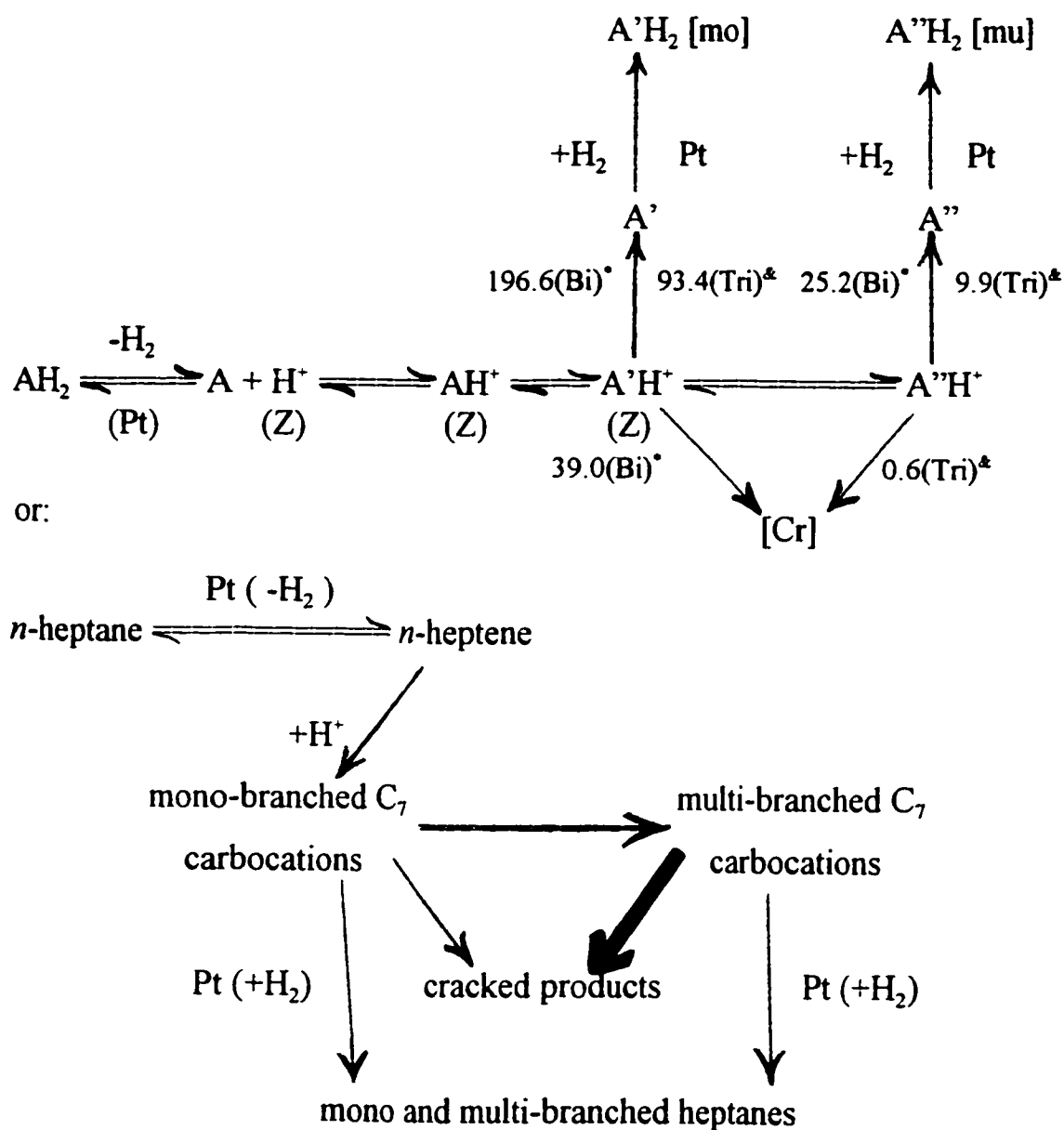
*) Obtained rate constants for bifunctional (Pt-HY) catalyst at 225 °C
&) Obtained rate constants for trifunctional (Pt-Zn$_{0.9}$-HY) catalyst at 225 °C

Figure 3.29. Simplified scheme of the reaction steps.

AH$_2$ = n-heptane; (Pt) = Pt site; H$^+$(Z) = H$^+$ bound to the zeolite (Z) structure (Brønsted acid site on the surface); [Cr], [mo] and [mu]: cracked products, product of mono-branched and multi-branched heptane, respectively

$$r_t = r_{mo} + r_{mu} + r_{cr} \qquad (3.21)$$

where r_{mo}, r_{mu} and r_{cr} are the rate of formation of the C_7 mono-branched isomers, the C_7 multi-branched isomers and cracking products (molecules having less than 7 carbons), respectively.

In Table 3.21 the values of rate constants of the n-heptane conversion over bifunctional Pt-HY zeolite catalyst are reported. These values were calculated at contact time $\tau = 0$ (initial rate). From this table the following were observed:

(i) In terms of rate constant, the equation $k_t^0 = k_{mo}^0 + k_{mu}^0 + k_{cr}^0$ was fully verified for all the reaction temperature tested (i.e. 195 °C, 210 °C, 225 °C and 240 °C)

ii) As expected, the values of all the rate constants increased with increasing of the reaction temperature

iii) The ratio of rate constants, k_{cr}^0 / k_t^0 (cracking to the total), increase rapidly from value of < 0.01 at T = 195 °C, to 0.27 at 240 °C while the ratio of rate constant k_{mu}^0 / k_t^0 (multi-branched to the total) remain constant.

From all of this it is clear that, surprisingly, at higher reaction temperatures, cracking affects the alkylcarbocation of the primary isomerization more than that of the secondary isomerization.

Reaction				Rate constants ([Constant] h^{-1})			
Temp.°C	k_t^0	k_{mo}^0	k_{mu}^0	k_{cr}^0	k_{mo}^0/k_t^0	k_{mu}^0/k_t^0	k_{cr}^0/k_t^0
240	319.4	203.5	38.1	86.6	0.64	0.12	0.27
225	261.5	196.6	25.2	39.0	0.75	0.10	0.15
210	159.3	133.1	12.2	4.2	0.84	0.08	0.03
195	62.0	54.7	7.0	0.4	0.88	0.11	<0.01

Table 3.21. Values of the rate constants of the bifunctional Pt-HY zeolite catalyst, determined at contact time $\tau = 0$, and their ratios.

In Table 3.22 the values of rate constants of the n-heptane conversion over trifunctional Pt-$Zn_{0.9}$-HY zeolite catalyst are reported. These values were calculated at contact time $\tau = 0$ (initial rate). From this table the following is observed:

(i) In terms of rate constant, the same equation (i.e. $k_t^0 = k_{mo}^0 + k_{mu}^0 + k_{cr}^0$) was obtained for all the reaction temperatures tested (i.e. 195 °C, 210 °C, and 225 °C). However their values are lower than those of the bifunctional Pt-HY zeolite catalyst

ii) As expected, with increasing reaction temperature the values of all rate constants increased

iii) Most importantly, cracking products are very low using this catalyst. Data obtained show that, the value of the ratio of the rate constants k_{cr}^0/k_t^0 was extremely low (almost zero) for all of reaction temperatures investigated (195 °C, 210 °C, and 225 °C)

On the other hand, the variations of the ratios k_{mo}^0/k_t^0 and k_{mu}^0/k_t^0 were quite moderate. The k_{mo}^0/k_t^0 ratio decreased with increasing of reaction temperature, while the k_{mu}^0/k_t^0 ratio increased. All of these mean that, over trifunctional Pt-$Zn_{0.9}$-HY zeolite catalyst, cracking was almost suppressed at reaction condition for n-heptane isomerization, which conversion to multi-branched heptanes increased with increasing reaction temperature.

Reaction	Rate constants ([Constant] h^{-1})						
Temp.°C k_t^0	k_{mo}^0	k_{mu}^0	k_{cr}^0	k_{mo}^0/k_t^0	k_{mu}^0/k_t^0	k_{cr}^0/k_t^0
225 104.2	93.4	9.9	0.6	0.90	0.10	<0.01
210 45.6	42.3	3.7	0.2	0.92	0.08	<<0.01
195 10.9	10.3	0.7	<0.1	0.94	0.06	<<0.01

Table 3.22. Values of the rate constants of the trifunctional $Pt-Zn_{0.9}-HY$ zeolite catalyst, determined at contact time $\tau = 0$, and their ratios.

Table 3.23 shows the values of rate constants for the n-heptane conversion over trifunctional Pt-Zn$_y$-HY (y = 0.55, 0.7, 0.9 and 1.2 mmol/g of zeolite) zeolite catalysts, which were calculated at contact time τ = 0 (initial rate). The Zn loadings were such that the catalysts provided the maximum performance of isomerization at the reaction temperature used [143]. These catalysts showed the same catalytic trends as the catalyst reported in (Table 3.22). Results obtained show that the cracking reaction was decreased and reduced almost to zero while, the ratios of $k_{mo}{}^0/k_t{}^0$ and $k_{mu}{}^0/k_t{}^0$ remained almost constant.

In Table 3.24 and 3.25 the product selectivities are reported at (equal) total conversion of 30 % for the bifunctional Pt-HY and of the trifunctional Pt-Zn$_y$-HY zeolite catalysts, respectively. The contact time which gives a total conversion (C_t) 30 % was determined graphically using the plot of total conversion versus contact time for each catalyst and each temperature. Then the corresponding conversion and product selectivities were determined using the fitted curves. Data reported in Table 3.24 and 3.25 show that the incorporation of Zn species into the bifunctional Pt-HY zeolite catalyst dramatically reduced the cracking and the secondary isomerization to lower value. At higher reaction temperature the negative effect of Zn on cracking is higher, the better the selectivity to isomerization.

Zn loading (mmol/g)	Reaction Temp.°C	k_t^0	k_{mo}^0	k_{mu}^0	k_{cr}^0	k_{mo}^0/k_t^0	k_{mu}^0/k_t^0	k_{cr}^0/k_t^0
						Rate constants ([Constant] h^{-1})		
1.2	240	145.3	124.9	14.3	1.3	0.86	0.10	0.01
0.9	225	104.2	93.4	9.9	0.6	0.90	0.10	0.01
0.7	210	83.6	74.9	6.8	1.6	0.90	0.08	0.02
0.55	195	41.4	36.3	5.0	0.0	0.88	0.12	0.00

Table 3.23. Values of the rate constants of the trifunctional Pt-Zn$_y$-HY (y = 0.55, 0.7, 0.9 and 1.2 mmol/g zeolite) zeolite catalyst which provide the maximum performance at their reaction temperature, which determined at contact time τ = 0, and their ratios.

Reaction	Contact	Product selectivity (C atom %)			Selectivity ratio
Temp.°C	time (h)	S_{mo}	S_{mu}	S_{Cr}	R
240	0.11	65.3	12.8	21.9	3.6
225	0.14	70.8	12.7	16.6	5.0
210	0.25	82.5	11.3	6.2	15.1
195	0.67	87.9	9.8	2.3	42.5

Table 3.24. Product selectivity reported for the bifunctional Pt-HY zeolite catalyst at contact time (τ) such that C_t (total Conversion) = 30 %.

Zn loading (mmol/g)	Reaction Temp.°C	Contact time (h)	Product selectivity (C atom %)			Selectivity ratio
			S_{mo}	S_{mu}	S_{Cr}	R
1.2	240	0.27	87.1	9.5	3.4	28.4
0.9	225	0.42	87.4	9.8	2.8	34.7
0.7	210	0.45	89.3	9.1	1.6	61.5
0.55	195	0.74	89.6	9.4	1.0	99.0

Table 3.25. Product selectivity reported for the trifunctional Pt-Zn$_y$-HY (y = 0.55, 0.7, 0.9 and 1.2 mmol/g zeolite) zeolite catalyst at contact time (τ) such that C$_t$ (total Conversion) = 30 %.

Table 3.26 details the Arrhenius treatment based on rate constants calculated at contact time ($\tau = 0$), plotted against the reciprocal of reaction temperature. The initial reaction rate (r_0) was calculated for bifunctional Pt-HY zeolite catalyst and trifunctional Pt-$Zn_{0.9}$-HY zeolite catalyst. Since no conversion was possible ($C_t = 0$) at zero contact time ($\tau = 0$) when the reactant was not in contact yet with the catalyst. Thus, the initial reaction rate was determined by taking the derivative of the fitting function $f(\tau)$ and extrapolating the conversion C_t to zero contact time:

$$r_0 = \lim \left[dC_t/d\tau \right]_{\tau \to 0} = \left[df(\tau)/d\tau \right]_{\tau \to 0} \qquad (3.22)$$

which then gave a constant value b, owing to the linearity of experimental C_t versus contact time τ.

$$r_0 = b \qquad (3.23)$$

Then the Arrhenius plot of the initial rates (in % C-atom h^{-1} g^{-1}) of n-heptane conversion versus the reciprocal of reaction temperature was obtained (Figure 3.30).

The apparent activation energy was calculated for both bifunctional Pt-HY zeolite catalyst and trifunctional Pt-$Zn_{0.9}$-HY zeolite catalyst. The obtained results showed that the activation energy of trifunctional Pt-$Zn_{0.9}$-HY zeolite catalyst was significantly higher than that of the bifunctional Pt-HY zeolite

catalyst. This does not mean that the energy barrier for the reaction was higher in the case of trifunctional catalyst. In fact, the key factor for the formation of cracking products and of the mono and multi-branched heptane is the residence time of the alkylcarbocation on the acid sites. The higher the residence time, the more extended the overall reaction and the more effective the cracking reaction [145].

However, the cracking reaction occurred at two different levels of A'H* and A''H*, which were significantly higher for the bifunctional Pt-HY zeolite catalyst (Tables 3.21 and 3.24) than for the trifunctional Pt-Zn-HY zeolite catalysts (Tables 3.22, 3.23 and 3.25). As mentioned before, the Zn^{2+} ions incorporated act as adsorption competitor the zeolite protonic sites for mentioned alkylcarbocations and effectively shortened the residence time of these species on acid sites, as a result, decreased the cracking activity and minor extent the activity of secondary isomerization [121,143].

Data reported in Table 3.26 clearly show that the mechanism of the *n*-heptane conversion over the Pt-HY zeolite catalyst in this research work was that of the bifunctional catalyst [99].

Catalyst	$k_t^{(*)}$	ln k_t	T (K)	1/T ($\times 10^{-3}$)	$E_a^{(\&)}$	Corr.$^{(S)}$
Pt-HY	261.5	5.5664	498.15	2.0074		
	159.3	5.0708	483.15	2.0698	94	0.99
	62.0	4.1271	468.15	2.1361		
Pt-Zn$_{0.9}$-HY	104.2	4.6463	498.15	2.0074		
	45.6	3.8199	483.15	2.0698	146	0.99
	10.9	2.3888	468.15	2.1361		

(*): $k_t = k_{total}$

(&): apparent activation energy expressed in kJ/mol

($): correlation factor

Table 3.26. Arrhenius plots for the bifunctional Pt-HY and trifunctional Pt-Zn$_{0.9}$-HY zeolite catalysts.
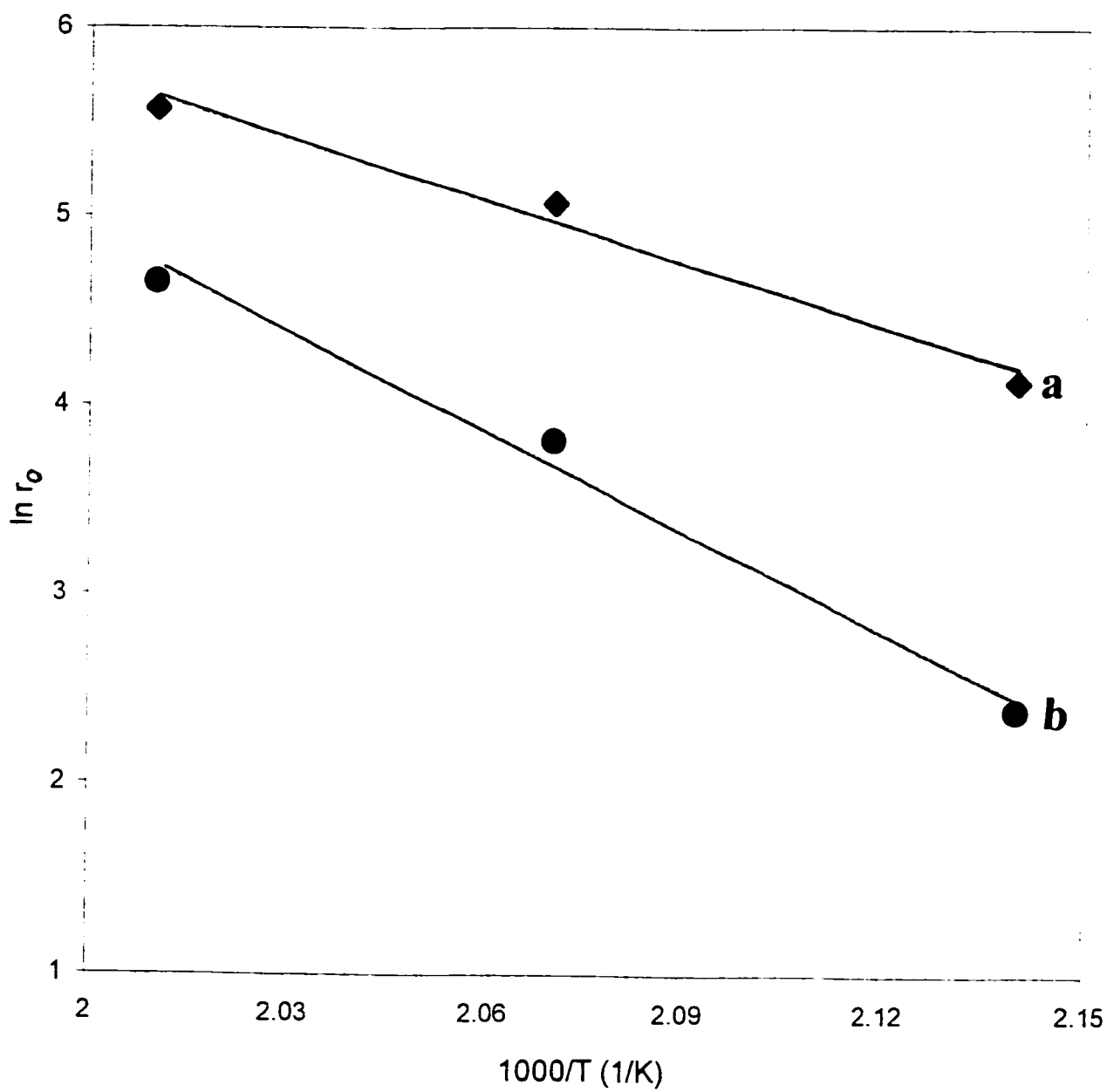
Figure 3.30.Arrhenius plots of the initial rates (in % C-atom h^{-1} g^{-1}) of n-heptane conversion obtained with the bifunctional Pt-HY (a) and trifunctional Pt-$Zn_{0.9}$-HY zeolite catalysts (b).

In fact, the value of the apparent activation energy found in this research work (94 kJ per mol) was close to those determined for this type of mechanism (105-135 kJ per mol), and far that reported for the monofunctional mechanism (40 to 50 kJ per mol) [99]. In addition, Travers et al [99] and Guisnet [180] observed a great influence of the n-Pt/n-A (n-Pt being the hydrogenation function and n-A the acid function) ratio on the bifunctional mechanism. They distinguished three cases: the first case corresponds to n-Pt/n-A ratio > 0.15 and the two other cases correspond to n-Pt/n-A < 0.15. Essentially, in the latter cases, the olefins can undergo one or more successive changes before arriving at a metallic site (mechanism b and c) [99], because the number of strong acid sites is higher than the number of hydrogenation sites. These changes may be a sequence of "desorption from the acid site of as an isoolefin A' and readsorption on another acid site resulting in further (secondary) isomerization and cracking" before adsorption on hydrogenation site (Figure 3.29). These situations are not different from the concept of longer residence time of intermediate carbocations on acid sites as mentioned in this thesis. In these situations which seem to coincide with that of the Pt-HY zeolite catalyst, the formation of cracking products may be important (Table 3.21). However, when n-Pt/n-A is high, "the probability that (desorbed) olefins encounter acid sites between two metallic sites is slight and side reactions are consequently reduced and a maximum in isomerization activity is obtained per acid site" (mechanism a) [99]. This explanation can be used for the behavior of Pt-Zn_y-HY zeolite catalysts on the isomerization n-heptane, where Zn^{2+} ions are sorption competitors to the acid sites, reducing the probability for the desorbed olefinic species to encounter other acid sites.

3.4.1 Conclusion

The kinetic behavior of the trifunctional Pt-Zn_y-HY zeolite catalysts showed a very significant difference to that of the bifunctional Pt-HY zeolite catalyst. The reported kinetic data indicated clearly a drastic reduction of cracking (β-scission) within the reaction temperature range 195 °C - 240 °C. The hypothesis reported in this research: competitive adsorption of intermediate alkylcarbocations by the Zn^{2-} ions resulting in shorter residence times of these former on the Brønsted acid sites is not different from the hypothesis of Travers et al [99], which gave a mechanism leading in the end to the same reducing effect on cracking.

3.5 Summary of the experimental evidence of the "trifunctional catalytic configuration":

In Table 3.27 are reported the various elements of experimental evidence that have been so far collected in support of the "trifunctional catalytic configuration" hypothesis. Detailed interpretations of some principal results are also given.

Finally, some focusing investigations are suggested in order to elucidate such an intriguing hypothesis.

Catalysts & techniques used	Results obtained	Interpretation
1) Catalysts: Pt & Me^{n+} loaded by (incipient wetness) impregnation, in quite small amounts (Catalytic testing)	performance in the isomerization of n-heptane: simultaneous loading >> sequential loading [121,143,181]	Pt & Me^{n+} should be at molecular distance of each other
2) Catalysts: Pt-HY and Pt-Al-HY with same Al^{3+} loading but the variable Pt content (Catalytic testing)	same catalytic behavior for both catalysts (plateau of conversion at 1 wt %)	Al^{3+} species do not significantly affect Pt sites
3) Catalysts : Pt-HY loaded with Cd^{2+}, Al^{3+}, Ni^{2+}, Zn^{2+} (Catalytic testing)	*performance in n-heptane isomerization : $Zn^{2+}> Ni^{2+}> Al^{3+}>> Cd^{2+}$ *same sequence for total conversion [121,143,181]	*potential exchange of Me^{n+} with zeolite acid sites, depending on the alkaline character of Me^{n+} (i.e. acid/base neutralization)[a] *free Me^{n+} having Lewis acid character (soft and hard) may interact with alkylcarbocations still adsorbed on the acid sites

4) Strong base probes: NH_3(TPD) and pyridine adsorption (FT-IR) Catalysts: Pt-Al-HY, Pt-Zn-HY and Pt-HY acid sites	*no significant change in the density of acid sites *presence of some Lewis acid sites of medium strength due to the incorporated Al^{3+} or Zn^{2-} [143]	*Al^{3+} or Zn^{2+} does not significantly exchange with the zeolite
5) Weak base probe: CO (DRIFTS technique) Catalysts: Pt-Zn-HY and Pt-HY	no shift of the charateristic bands of C=O (2117 and 2175 cm^{-1})	no significant effect of Zn^{2+} on the protonic acid sites (i.e. no significant modification of the acid strength)
6) Catalyst: Pt-Zn-HY	the incorporation of halide changes the Pt-Zn-HY back to the Pt-HY in terms of product selectivity, while the conversion remains unchanged. the sequence of such reverse effect is: $Cl^- > Br^- > I^-$ [181]	this shows that it is possible to affect the zeolite acid sites without affecting other sites (Pt and Zn^{2+}). As expected, owing to its lowest electronegativity, I^- does not significantly modify the catalytic performance of the Pt-Zn-HY
7) Catalyst: Pt-Zn-HY (Catalytic testing)	maximum isomerization activity with Zn^{2+} loading which has to increase with increasing reaction temperature [143]	*owing to the large difference in rate variation with reaction temperature: i.e. the rate of cracking increases more rapidly than that of isomerization. *The effect of Zn^{2+} is probably of physical nature; otherwise the maximum activity of isomerization would correspond to **only** one catalyst configuration, at all reaction temperatures

8) Catalysts: Pt-Zn-HY and Pt-HY (Kinetic study)	*higher isomerization activity for Pt-Zn-HY at equal conversion *lower value of apparent activation energy for Pt-Zn-HY [181]	*the change in the apparent activation energy may be ascribed to the variation of the the residence time of the alkylcarbocation on the acid sites [b] *the dramatic change in the rates of cracking and isomerization upon incorporation of Zn^{2+} may be interpreted in a similar way as in the case reported by Polanyi [c]

Table 3.27. Changes in catalytic and physical-chemical properties of the Pt-HY catalyst upon incorporation of Me^{n+} species [121,143,181].

[a] It is obvious that when the Me^{n+} species are incorporated into the Pt-HY catalyst, even by the technique of incipient wetness impregnation, these species undergo at first ion-exchange with the zeolite acid sites if they have some alkaline (strong base) properties. Hence, the incorporation of Na^+ ions leads to a general decrease of the catalyst activity without resulting in unusual product selectivity. On the other hand, non-alkaline ionic species may create Lewis acid sites whose effect on the isomerization performance seems to depend on the nature of the resulting Lewis acidity. Cd^{2+} which is softer than Zn^{2+} [174], shows lower isomerization-promoting effect.

[b] In our hypothesis, adsorption of the alkylcarbocation on the zeolite acid site (and its desorption) is the key factor for the formation of the reaction products: branched paraffins (isomerization) or cracking products. As shown by Iglesia et al [145], a shorter residence time of the alkylcarbocation on the acid site results in a higher production of branched paraffins while a longer residence time leads to more cracking produced. To confirm this statement, we can recall the classical formula of the apparent activation energy when adsorption is a significant factor:

$$E_a = E_2 + (\Delta U^o) \tag{3.24}$$

where E_2 and ΔU^o are the activation energy corresponding to the reaction of the adsorbed species and the standard molar internal energy change in the adsorption process, respectively [182].

By using the van't Hoff relationship which expresses the temperature dependence of the equilibrium constant for the adsorption process and the equation of the simple Langmuir isotherm, it can be seen that the value of ΔU^o depends, on the end, on the surface coverage. In fact, at high pressure of reactant, a catalyst shows a high surface coverage and its apparent activation energy is close to E_2 [182]. In contrast, the same catalyst exposed to a low pressure of reactant, shows a lower surface coverage and its apparent activation energy is given by equation 3.24 [182]. However, if we have two catalysts with two different surface configurations and we want to have the same surface coverage, we have to use two quite different pressures of reactants. The catalyst

which needs only a low pressure of reactant must show an apparent activation energy as depicted by equation (3.24) while the catalyst which requires much higher pressure to achieve the same surface coverage, must give a value of the apparent activation energy close to E_2.

In our case, since the alkylcarbocation remains adsorbed on the acid sites of the Pt-HY for a longer time than on those of the Pt-Zn-HY (the higher residence time resulting in higher surface coverage for Pt-HY), the apparent activation energy of the reaction over the catalysts tested are as follows:

For the Pt-HY catalyst: $(E_a)_{bi} = E_2 + (\Delta U^o)$
For the Pt-Zn-HY catalyst: $(E_a)_{tri} = E_2$

Therefore: $(E_a)_{bi} - (E_a)_{tri} = (\Delta U^o) < 0$ because (ΔU^o) is always negative [182].
So that: $(E_a)_{bi} < (E_a)_{tri}$
This is exactly the result obtained in our kinetic study: the apparent activation energy of the Pt-Zn-HY catalyst (146 KJ/mol) is larger than that of the Pt-HY catalyst (94 KJ/mol).

It is worth mentioning that a higher residence time on the acid sites may also mean a larger number of encounters between the alkylcarbocations and the acid sites, the former undergoing thus a sequence of adsorption/desorption processes [180].

[c] It was reported that in the presence of a "collision" partner on a solid surface, the reaction Na + Cl → NaCl went very quickly [183]. This species acts as an efficient means of energy transfer although the catalyst never binds strongly to the reactants. These observations which bear some similarities with our case of "trifunctional catalytic configuration", encourage us to pursue our effort to understand the exact role of Zn^{2+} on the Pt-HY catalyst.

Since our results all indicate that the key factor for having high isomerization performance is adsorption/desorption of the alkylcarbocation or shortening of its residence time on the acid site, it is very tempting to have direct experimental evidence by using various techniques of:

i) Macroscopic study (in-situ investigations of adsorption/desorption or reaction) [184]

ii) Investigation of diffusion at molecular level, such as the combination of nanosecond laser heating with Scanning Tunneling Microscopy (STM) [185]

Besides experimental techniques, theoretical studies similar to those developed at the University of Utah which make use of the ab initio embedded cluster method [186,187] can also be done.

CHAPTER IV

CONCLUSIONS

Safer ways to increase the octane number of gasolines may include alkylation of isobutane with butenes to yield branched C_8 octane-boosting additives or the isomerization of n-paraffins to isoparaffins, so that less polluting gasolines can be produced.

There are some abundant long chain n-alkanes in refinery stream fuels which have a lower octane number and a higher pour point. It would be thus desirable to convert these normal paraffins to their branched isomers (which have higher octane number). Novel classes of cation incorporated Pt-M-HY (M being cation such as Zn^{2+}, Al^{3+}, Cd^{2+}, Ni^{2+}, Cr^{3+} and some others) and bifunctional Pt-HY zeolite catalyst have been prepared and tested for hydroisomerization of n-Paraffins (using n-heptane as a model molecule). Among them, the Pt-Zn-HY zeolite catalyst showed higher isomerization properties. Their catalytic performance regarding the conversion of n-paraffins have been evaluated in relation to their physico-chemical properties as obtained by various characterization techniques.

In the hydroisomerization processes, n-paraffins are converted to olefinic species on Pt (hydrogenation-dehydrogenation) sites, these olefinic species are moved on Brønsted acid sites and catalyzed producing the intermediate carbocations (protonation). The intermediate carbocations after rearrangement or cracking, again are moved on Pt site producing new paraffins (hydrogenation).

The cracking of multi-branched carbocations is much faster than that of the mono-branched carbocations. The cage of the zeolite, particularly the supercage of the faujasite type zeolites (such as Y zeolite), has an effect on both the adsorption of n-paraffins and the formation of the specific branched intermediate carbocation configuration.

The modified zeolite catalysts showed superiority over the parent bifunctional Pt-HY zeolite catalyst in term of isomerization of n-heptane. This is due to the desorption-transfer promoting behavior of the mentioned cations, as a result, the residence time of intermediate alkylcarbocations on Brønsted acid sites decrease by rapid removal of them from these sites. By decreasing the residence time of intermediate alkylcarbocation on Brønsted acid sites the isomerization products increased significantly and cracked products decreased. Such behavior was ascribed to the formation of new desorption-transfer promoting sites.

A hypothetical triangular "acid/dehydro-hydrogenation/desorption-transfer promoting" site configuration (trifunctional catalyst) was proposed. The obtained data from characterization study such as BET, XRD, FTIR and NH_3-TPD show that cationic species do not significantly effect the pore size distribution, the surface area, the crystallinity, the dehydrogenation-hydrogenation properties of (Pt) site and the density and strength of Brønsted acid site. No significant ion-exchange was observed upon Zn^{2+}, Al^{3+}, Cd^{2+}, Ni^{2+} and Cr^{3+} loading at the reaction conditions. These species only create some Lewis acid sites of which the Lewis acid character appeared to play an

important role in the enhancement of the isomerization activity. The Zn^{2+} and other ions incorporated act as adsorption competitor to the zeolite protonic sites for alkylcarbocations and effectively shortened the residence time of these species on acid sites, as a result, decreased the cracking activity, where the effect of Zn^{2+} was higher than the other cations. In addition the simultaneous incorporation of Zn^{2+} and the other cations with Pt species gave better results than that of the sequential loading.

On the other hand, with increasing reaction temperature, more acid sites are activated and involved in the reaction, thus, each reaction temperature needed a specific Zn^{2+} loading in order to provide the best isomerization activity, and a higher amount of zinc was required at higher reaction temperature where the cracking activity is stronger.

The kinetic studies showed that the behavior of the trifunctional Pt-Zn$_y$-HY was significantly different than that of the bifunctional Pt-HY zeolite catalyst. All kinetic data showed a drastic reduction of cracking (β-scission) within the temperature range of 195 °C - 240 °C. From kinetic method and the reaction mechanism, the initial rate of isomerization to multi-branched and mono-branched products and that of the cracking for the conversion of n-heptane have been calculated. The results obtained further demonstrate that the hydroisomerization and hydrocracking of n-paraffins over acidic zeolite catalysts are a multi-step process. A catalytic cracking is endothermic reaction and is very rapid at higher reaction temperature. This type of reaction occurs via β-scission of alkylcarbocation which its reaction rate depends on the branching

configuration of the original alkylcarbocation. With increasing of branching the stability of alkylcarbocation increases, as a result, its residence time on the acid site increases and undergo further β-scission.

The apparent activation energy for over all reactions was found to be different for bifunctional Pt-HY zeolite catalyst and the trifunctional Pt-Zn$_{0.9}$-HY zeolite catalyst; specifically, higher for the later.

The final product distribution depends on the reaction conditions and the structure of the catalyst. At higher reaction temperature the conversion of n-heptane was high but cracking was significant, at lower reaction temperature the cracking was not significant but the conversion of n-heptane was low. It is seen that higher isomerization performance can be achieved by using the trifunctional Pt-Zn-HY zeolite catalyst at lower reaction temperature and longer contact time.

REFERENCES

References:

1. J. G. Speight, *The Chemistry and Technology of Petroleum*, March Dekker, Inc., New York, (1980) 1.

2. J. E. Johnson and F. M. Peterson, *Chemtech*, 296, May, (1991).

3. H. H. Schobert, *The Chemistry of Hydrocarbon Fuels*, Butterworths, London, (1990) 184.

4. J. H. Gary, *Petroleum Refining: Technology and Economics*, Marcel Dekker, Inc., New York, (1994) 3.

5. E. M. Goodgar, *Hydrocarbon Fuels*, Macmillan Press LTD, New York, (1975) 131.

6. J. G. Speight, *the Chemistry and Technology of Petroleum*, Marcel Dekker, Inc., New York, (1980) 428.

7. J. Scherzer, *Octane-Enhancing Zeolitic FCC Catalysts*, Marcel Dekker, Inc., New York, (1990) 7.

8. D. E. Gushee, *Chemitech*, July (1992) 406.

9. H. L. Brockwell, P. R. Sarathy and R. Trotta, *Hydrocarbon Processing*, 70, September (1991) 133.

10. H. H. Schobert, *The Chemistry of Hydrocarbon Fuels*, Butterworth & Co (Publisher) Ltd, (1990) 313.

11. D. N. Nakamura, *Hydrocarbon Processing*, 74, January (1995) 15.

12. S. Romanow-Garcia, *Hydrocarbon Processing*, 78, January (1999) 15.

13. H. Lerner, *Handbook of Petroleum Refining Processes*, McGraw-Hill Companies, Inc., New York, (1996) 1.3.

14. J. Weitkamp and Y. Traa, *Catalysis Today*, 49, (1999) 193.

15. L. D. Holtermann, *US Patent* No. 5,166,112, (1992).

16. T. S. Bakas, *US Patent* No. 4,665,272, (1987).

17. W. G. Skeels, *US Patent* No. 5,095,169, (1992).

18. J. Scherzer, *Octane-Enhancing Zeolitic FCC Catalysts*, Marcel Dekker, Inc., New York, (1990) 1.

19. J. G. Speight, *The Chemistry and Technology of Petroleum*, March Dekker, Inc., New York, (1980) 303.

20. H. H. Schobert, *The Chemistry of Hydrocarbon Fuels*, Butterworth & Co (Publisher) Ltd, (1990) 211.

21. R. A. Meyers, *Handbook of Petroleum Refining Processes*, McGraw.Hill Companies, (1997) 7.43.

22. D. Decroocq, *Catalytic Cracking of Heavy Petroleum Fractions*, Editions Technip, Paris, (1984) 7.

23. J. B. Hill and J. G. Moxey, *Petroleum Products Handbook*, Edit by V.B. Guthrie, McGraw-Hill Companies, New York, (1960) 4 - 4.

24. J. M. Thomas, *Angew. Chem. Int. Engl.*, **33**, (1994) 913.

25. W. G. Skeels, *US Patent* No. 5,744,673, (1998).

26. G. D. Pirngruber, K. Seshan and J. A. Lercher, *J. Catal.*, **186**, (1999) 188.

27. M. Duagl, G. Sankear, R. Raja, and J. M. Thomas, *Angew. Chem. Int. Engl.*, **39**, (2000) 2310.

28. R. Raja, G. Sankear, and J. M. Thomas, *Angew. Chem. Int. Engl.*, **33**, (2000) 2313.

29. D. W. Breck, *Zeolite Molecular Sieves: Structure, Chemistry and Use*, John Wiley & Sons, Inc., New York, (1974) 4 .

30. D. E. W. Vaughan, *Chemical Engineering Progress, Feb., (1988) 25.*

31. E. M. Flanigen, B. M. Lok, P. L. Patton and S. T. Wilson, *Stud. Surf. Sci. Catal.*, **28**, (1986) 103.

32. G. C. Edwards, J. P. Gilson and C. V. McDaniel, U.S. Patent No. 4,764,269 (1988).

33. R. J. Pellet, P. K. Coughlin, M. T. Staniulis, G. N. Long and J. Rabo, U.S. Patent No. 4,734,185 (1988).

34. R. J. Pellet, P. K. Coughlin, M. T. Staniulis, G. N. Long and J. Rabo, U.S. Patent No. 4,791,083 (1988).

35. M. A. Uguina, G. Ovejero, R. V. Grieken, D. P. Serrano and M. Camacho, *J. Chem. Soc., Chem. Comm.*, **9**, (1994) 27.

36. D. Venkataraman, S. Lee, J. Zhang and J. S. Moore, *Nature*, **371**, (1994) 591.

37. G. Ertl, Edited by G. Ertl, H. Knözinger r, J. Weitkamp, *Handbook of Heterogeneous Catalysis* vol. 2, Wiley/VCH Verlag, Weinheim, (1997) 1986.

38. J. Yu, K. Tu and R. Xu, *Stud. Surf. Sci. Catal.*, **84**, (1994) 315.

39. G. Alberti, F. Marmottini, S. Murcia-Mascaros and R. Vivani, *Angew. Chem. Int. Ed. Engl.*, **33**, (1994) 1594.

40. J. A. Martens, B. Verlinden, M. Mertens, P. J. Grobet and P. A. Jacobs M. L. Occelli and H. E. Robson, *Zeolite Synthesis*, American Chemical Society, Washington, DC (1989) 305.

41. G. Leofanti, M. Padovan, G. Tozzola and B. Venturelli, *Catalysis Today*, **41**, (1998) 207.

42. M. E. Davis, *Ind. Eng. Chem., Res.* **30**, (1991) 1675.

43. J. Chen, R. H. Jones, S. Natarajam, M. B. Hursthos and J. M. Thomas, *Angew. Chem. Int. Ed. Engl.*, **33**, (1994) 639.

44. N. Y. Chen and T. F. Degnan, *Chemical Engineering Progress*, (1988) 32.

45. C. B. Khouw and M. E. Davis, Edited by M. E. Davis and S. L. Suib, *Selectivity in Catalysis*, American Chemical Society, Washington, DC, (1993) 206.

46. J. R. Anderson, K. Foger, T. Mole, R. A. Rajadhyaksha and J. V. Saders, *J. Catal.*, **58**, (1979) 114.

47. C. N. Satterfield, *Heterogeneous Catalysis in Industrial practice*, McGraw-Hill Companies, New York, (1991) 209.

48. A. Dyer, *An Introduction to Zeolite Molecular Sieves*, John Wiley & Sons, Inc., New York, (1988) 121.

49. R. Szostak, *Molecular Sieves Principles of Synthesis and Identification*, Van Nostrand Reinhold Company, New York, (1989) 26.

50. P. A. Jacobs, R. von Ballmoos, *J. Phys. Chem.*, **86**, (1982) 3050.

51. W. O. Haag, R. M. Lago and P. B. Weisz, *Nature*, **309**, (1984) 589.

52. J. B. Uytterhoeven, L. G. Cristner and W. K. Hall, *J. Phys. Chem.*, **69**, (1965) 2117.

53. C. T. Chu and C. D. Chang, *J. Phys. Chem.*, **89**, (1985) 1569.

54. D. C. Harris, *Quantitative Chemical Analysis*, W. H. Freeman and Company, New York, (1995) 598.

55. W. J. Price, *Analytical Atomic Absorption Spectroscopy*, Heyden & son Ltd, New York, (1972) 8.

56. Z. Sarbak, *Applied Catal.* **117**, (1999) 85.

57. S. Suvanto, T. A. Pakkanen and L. Backman, *Appl. Catal. A: General.* **177**, (1999) 25.

58. M. L. Occelli, S. Biz, A. Auroux and P. S. Iyer, *Appl. Catal. A: General*, **179**, (1999) 117.

59. S. Huber and H. Knözinger, *Appl. Catal. A: General*, **17**, (1999) 239.

60. D. Barthomeuf *J. Phys. Chem.*, **83**, No. 2 (1979) 249.

61. W. K. Hall, Edited by G. Ertl, H. Knözinger, J. Weitkamp, *Handbook of Heterogeneous Catalysis* vol. 2, Wiley/VCH Verlag, Weinheim, (1997) 692.

62. E. Iwamatsu, E. Hayashi, Y. Sanada, S. Ahmed, S. Ahmed Ali, A. K. K. Lee, H. Hamid and T. Yoneda, *Appl. Catal. A: General*, **179**, (1999) 139.

63. H. Knözinger, Edited by G. Ertl, H. Knözinger, J. Weitkamp, *Handbook of Heterogeneous Catalysis* vol. 2, Wiley/VCH Verlag, Weinheim, (1997) 707.

64. M. A. Makarova, K. M. Al-Ghefaili and J. Dwyer, *J. Chem. Soc., Faraday Trans*, **90**, (1994) 383.

65. M. A. Makarova, A. F. Ojo, K. Karim, M. Hunger, and J. Dwyer, *J. Phys. Chem.*, **98**, (1994) 3619.

66. L. Kubelkova, S. Beran and J. A. Lercher, *Zeolites*, **9**, (1993) 539.

67. F. Wakabayashi, J. N. Kondo, A. Wada, K. Domen and C. Hirose, *J. Phys. Chem.*, **97**, (1993) 10761.

68. F. Wakabayashi, J. N. Kondo, K. Domen and C. Hirose, *J. Phys. Chem.*, **99**, (1993) 10573.

69. N. Y. Topsoe, K. Pedersen and E. G. Derouane, *J. Catal.*, **70**, (1981) 41.

70. B. C. Gates, *Catalytic Chemistry*, John Wiley & Sons, Inc. New york, (1992) 268.

71. R. Szostak, *Molecular Sieves Principles of Synthesis and Identification*, Van Nostrand Reinhold, USA, (1989) 40.

72. C. N. Satterfield, *Heterogeneous Catalysis in Induistrial practice*, McGraw-Hill Companies, New York, (1991) 244.

73. E. G. Derouane and Z. Gabelica, *J. Catal.*, **65**, (1980) 486.

74. J. Scherzer, *Octane-Enhancing Zeolitic FCC Catalysts*, Marcel Dekker, Inc., New York, (1990) 43.

75. J. F. Le Page, *Applied Heterogeneous Catalysis*, Editions Technip, Paris, (1987)113.

76. D. W. Breck, *Zeolite Molecular Sieves: Structure, Chemistry and Use*, John Wiley & Sons, Inc., New York, (1974) 529.

77. K. S. W. Sing and J. Rouquerol, Edited by G. Ertl, H. Knözinger, J. Weitkamp, *Handbook of Heterogeneous Catalysis* vol. 2, Wiley/VCH Verlag, Weinheim, (1997) 427.

78. D. W. Breck, *Zeolite Molecular Sieves: Structure, Chemistry and Use*, John Wiley & Sons, Inc., New York, (1974) 593.

79. S. J. Gregg and K. S. W. Sing, *Adsorption, Surface Area and Porosity*, 2nd ed., Academic Press, London, (1982) 37.

80. J. H. de Boer, *The Dynamical Character of Adsorption*, Oxford University Press, London, (1968) 84.

81. S. Brunauer, P. H. Emmett and E. Teller, *J. Amer. Chem. Soc.* **60**,(1938) 309.

82. W. Adamson, *Physical Chemistry of Surface*, John Wiley & Sons, Inc., New York, (1990) 591.

83. Y. Chu, Z. Wei, S. Yang, C. Li, Q. Xin and E. Min, *Appl. Catal. A: General*, **176**, (1999) 17.

84. A. P. Bolton, Edited by J. A. Rabo, *Zeolite Chemistry and Catalysis*, American Chemical Society, Washington, DC, (1976) 729.

85. J. Scherzer, *Octane-Enhancing Zeolitic FCC Catalysts*, Marcel Dekker, Inc., New York, (1990) 21.

86. C. N. Satterfield, *Heterogeneous Catalysis in Induistrial practice*, McGraw-Hill Companies, New York, (1991) 230.

87. D. W. Breck, *Zeolite Molecular Sieves: Structure, Chemistry and Use*, John Wiley & Sons, Inc., New York, (1974) 92.

88. M. I. Levinbuk, M. L. Pavlov, L. M. Kustov, J. P. Fraissard, T. V. Vanisa, A. V. Kazakov, Y. I. Azimova and Y. Y. Smorodinskaya, *Appl. Catal. A: General*, **172**, (1998) 177.

89. J. Scherzer, U.S. Patent No. 4,477,336 (1984).

90. P. S. Iyer, J. Scherzer and Z. C. Mester, *ACS Symposium Series*, **368**, (1988) 48.

91. A. P. Bolton, *J. Cata.*, **22**, (1971) 9.

92. J. Weitkamp, *Ind. Eng. Chem. Prod. Res. Dev.*, **21**, (1982) 550.

93. J. A. Martens, R. Parton, L. Uytterhoeven and P. A. Jacobs, *Appl. Catal. A: General*, **76**, (1991) 95.

94. B. A. Orkin, *Ind. Eng. Chem. Res. Dev.* **8**, (1969) 154.

95. J. M. Campelo, F. Lafont and J. M. Marins, *Zeolits*, **15**, (1995) 97.

96. A. K. Aboul-Gheit, S. A. Ghoneim and A. A. Al-Owais, *Applied Catalysis A: General*, **170**, (1998) 277.

97. L. O. Almanaza, T. Narbeshuber, P. d'Araujo, C. Naccache and Y. B. Taarit, *Applied Catalysis A: General*, **178**, (1999) 39.

98. S. J. Miller, *Microporous Materials*, **2**, (1994) 439.

99. C. Travers, Edited by P. Leprine, *Conversion Processes*, Edition Technique Paris, (2001) 229.

100. J. F. Joly, Edited by P. Leprine, *Conversion Processes*, Edition Technique Paris, (2001) 257.

101. S. Matar and L. F. Hatch, *Chemistry of Petrochemical Processes*, Butterworth-Heinemann MA, (2001) 180.

102. P. Travers, Edited by P. Leprine, *Conversion Processes*, Edition Technique Paris, (2001) 291.

103. P. A. Jacobs and J. A. Martens, *Applied Catalysis*, **8**, (1983) 123.

104. W. Souverijns, J. A. Martens, G.F. Froment and P.A. Jacobs, *J. Catal.*, **174**, (1998)177 .

105. H. Vinek, A. Lugstein and A. Jentys, *Applied Catalysis A: General*, **166**, (1998) 29.

106. A. Lugstein, A. Jentys and H. Vinek, *Applied Catalysis A: General*, **176**, (1999) 119.

107. G. L. Frischkorn, P. J. Kuchar, and R. K. Olson, *Energy prog.* **8**, (1988) 154.

108. F. G. Ciapetta and J. B. Hunter, *Ind. Eng. Chem.* **45**, (1953) 147.

109. D. M. Brouwer and J. M. Oelderik, Preprints Div. of petroleum Chem., ACS meeting San Francisco, April 1968, *Rec. Trav. Chem.* **87**, (1968) 721.

110. P. Mériaudeau, Vu. A. Tuan, G. Sapaly, Vu. T. Nghiem and C. Naccache, *Catalysis Today*, **49**, Issue 1-3, (1999) 285.

111. R. J. Taylor and R. H. Petty, *Appl. Catal. A: General*, **119**, (1994) 121.

112. J. M. Campelo, F. Lafont and J. M. Marinas, *Applied Catalysis A: General*, **170**, (1983) 139.

113. E. Blomsma, J. A. Martens, and P. A. Jacobs, *J. Catal.* **165**, (1997) 241.

114. M. L. Coonradt, and W. E. Garwood, *Ind. Eng. Chem. Prod. Res. Dev.* **3**, (1962) 38.

115. P. B. Weizs, *Adv. Catal.* **13**, (1962) 137.

116. A. Chauval and G. Lefevre, *Petrochemical Processes 1, Synthesis-Gas Derivatives and Major Hydrocarbons*, Editions Technip, Paris, France, (1986) 165.

117. J. A. Martens and P. A. Jacobs, Edited by J. B. Moffat, *Theoretical Aspects of Heterogeneous Catalysis*, Van Nostrand Reinhold, New York, (1990) 52.

118. D. M. Brouwer, *Chemistry and Chemical Engineering of Catalytic Processes*, NATO ASI Ser. E. No. 39 (R. Prins, and G.C.A. Schuit, eds.), Rockville: Sijthoff and Noordhoff, (1980) 137.

119. J. Weitkamp, P. A. Jacobs, J. A. Martens, *Applied Catal.* **8**, (1983) 123.

120. G. A. Olah, G. k. Surya Prakash and J. Sommer, *Superacids*, John Wiley & Sons, Inc., New York, (1985) 133.

121. R. Le Van Mao and M. A. Saberi, *Appl. Catal. A: General.* **199**, (2000) 99.

122. R. Le Van Mao and M. A. Saberi, J. A. Lavings, S. Xiao and G. Dénès, *Mat. Res. Soc. Symp. Proc.* Vol. **497**, (1998) 183.

123. S. Xiao and R. Le Van Mao, *Microporous Mater.* **4**, (1995) 435.

124. S. Xiao, R. Le Van Mao and G. Dénès, *J. Mater. Chem.* **5** (6), (1995) 1251.

125. M. A. Camblor, J. Perez-Pariente, V. Fornes, *Zeolites*, **12**, (1992) 280.

126. V. Jorik, *Zeolites*, **13**, (1993) 187.

127. G. Bergert, Edited by G. Ertl, H. knÖzinger, J. Weitkamp, *Handbook of Heterogeneous Catalysis* vol. **2**, Wiley/VCH Verlag, Weinheim, (1997) 464.

128. J. Scherzer, *Catal. Rev. Sci. Eng.*, **31** (3), (1989) 215.

129. S. Xiao, R. Le Van Mao and G. Dénès, *J. Mater. Chem.*, **5** (8), (1995) 1251.

130. I. Langmuir, *J. Amer. Chem. Soc.*, **40**, (1918) 1361.

131. D. H. Everett and J. C. Pwol, *J. Chem. Soc. Faraday Trans*, **72**, (1976) 619.

132. M. G. White, *Heterogeneous Catalysis*, Prentice Hall Inc, (1991) 66.

133. B E. Spiewak, R. D. Cortright and J. A. Dumesic, Edited by G. Ertl, H. knÖzinger, J. Weitkamp, *Handbook of Heterogeneous Catalysis* vol. **2**, Wiley/VCH Verlag, Weinheim, (1997) 698.

134. C. V. Hidalgo, H. Itoh, T. Hattori, M. Niwa and Y. Murakami, *J. Cata.*, **85**, (1981) 41.

135. R. L. V. Mao, T. M. Nguyen and J. Yao, *Appl. Cata.*, **61**, (1990) 161.

136. J. A. Gadsden, *Infrared Spectra of Minerals and Related Inorganic Compounds*, Butterworth & Co (Publishers) Ltd, (1975) 3.

137. W. R. Moser, C. C. Chian and R. W. Thompson, *J. Cata.*, **115**, (1989) 532.

138. V. L. Zholobenko, L. M. Kustov, V. Yu. Borovkov and V. B. Kazansky, *Zeolites*, **8**, (1988) 175.

139. M. A. Makarova, V. L. Zholobenko, K. M. Al-Ghefaili, N. E. Thompson, J. Dewing and J. Dwyer, *J. Chem. Soc. Faraday Trans*, **90**(7), (1994) 1047.

140. M. W. Anderson and J. Klinowski, *Zeolites*, **6**, (1986) 455.

141. T. R. Hughes and H. M. White, *J. Phys. Chem.*, **71**, (1967) 2192.

142. N. Y. Topsoe, F. Joensen and E. G. Derouane, *J. Catal.*, **110**, (1988) 404.

143. M. A. saberi, R. Le Van Mao, M. Martin and A. W. H. Mak, *Appl. Catal. A: General.* **214**, (2001) 229.

144. M. Steijns, G. Froment, P. A. Jacobs, J. Uytterhoeven and J. Weitkamp, *Ind. Eng. Chem. Prod. Res. Dev.*, **20**, (1981) 654.

145. E. Iglisia, S. L. Soled and G. M. Kramer, *J. Catal.*, **144**, (1993) 238.

146. P. E. Eberly, Edited by J. A. Rabo, *Zeolite Chemistry and Catalysis*, American Chemical Society, N. Y. (1976) 392.

147. I. E. Maxwell and W. H. J. Stork, *Stud. Surf. Sci. Catal.*, **58**. (1991) 571.

148. P. B. Weisz, *Adv. Catal.*, **13**, (1962) 137.

149. A. A. Lopéz, A. Asensio and A. Corma, *J. Catal.*, **69**, (1981) 274.

150. P. G. Smirniotis and E. Ruckenstein, *J. Catal.*, **140**, (1993) 526.

151. J. Leglise, A. Chambellan and D. Cornet, *Appl. Catal.*, **69**, (1991) 15.

152. R. Le Van Mao, *Microporous and Mesoporous Materials*, **28**, (1999) 9.

153. M. Y. wen, I. Wender, J. W. Tierney, *Energy Fuels*, **4** (1990) 372.

154. B. Parlitz, E. Schreier, H. L. Zubowa, R. Eckelt, E. Lieske, G. Lischke and R. Fricke, *J. Catal.*, **155** (1995) 1.

155. K. Nakamoto, *Infrared Spectra of Inorganic and coordination Compounds*, Wily-interscience, New York, (1986).

156. E. P. Parry, *J. Cata.*, **2**, (1963) 371.

157. B. Parlits, E. Schreier, H. L. Zubowa, R. Eckelt, R. Eckelt, E. Lieske, G. Lischke and R. Fricke, *J. Catal.* **155** (1995) 1.

158. R. Le Van Mao, T. S. Le, M. Fairbaim, A. Muntasar, S. Xiao and G. Dénès, *Appl. Catal. A: General*, **185**, (1994) 41.

159. G. Ghiotti, E. Garrone, C. Morterra, F. Boccuzzi, *J. Phys. Chem.*, **83**, (1979) 2863.

160. M. I. Zaki and H. knÖzinger, *Mater. Chem. Phys.*, **17**, (1987) 201.

161. A. Zecchina, E. Garrone, E. Guglieminotti, *in Catalysis*, (Eds: G. C. Bond, G. Webb), The Royal Society of Chemistry, London, vol. **6**, (1983) 90.

162. G. Busca, *Catal. Today*, **41**, (1999) 191.

163. A. Zecchina, C. Lamberti and S. Bordiga, *Catal. Today*, **41**, (1999) 169.

164. E. A. Paukshtis and E. N. Yurchenko, *Russ. Chem. Rev.*, **52**, (1983) 42.

165. H. knÖzinger, *in Elementry Reaction Steps in Heterogeneous Catalysis* (Eds: R. W. Joyner, R. A. van Snten), Kluwer, Dordrecht, (1993) 267.

166. H. knÖzinger, *in Acid-Base Catalysis* (Eds: K. Tanabe, H. Hattori, T. Yamaguchi, T. Tanaka), Verlag Chemei, Weinheim, (1989) 147.

167. M. I. Zaki and H. knÖzinger, *J. Catal.*, **119**, (1989) 311.

168. V. B. Kazansky, *Catal. Today*, **51**, (1999) 419.

169. G. C. Bond, Edited by G. Ertl, H. knÖzinger, J. Weitkamp, *Handbook of Heterogeneous Catalysis* vol. **2**, Wiley/VCH Verlag, Weinheim, (1997) 752.

170. B. C. Gates, *Catalytic Chemistry*, John Wiley & Sons, Inc. New york, (1992) 397.

171. R. Le Van Mao and M. A. Saberi, Presented at the 17th North American Catalysis society, Toronto, June 3-8 (2001).

172. M. C. Day Jr. and J. Selbin, in: *theoretical Inorganic Chemistry*, Reinhold, New York, (1969) 376.

173. R. G. Pearson, J.A.C.S. 85 (22) (1963) 3533.

174. R. G. Pearson, *Chem. in Britain*, **3**, (1967) 103.

175. G. A. Somorjai, *Catal. Today*, **18**, (1993) 113.

176. S. Savitz, A. L. Myers and R. J. Gorte, *Micropor. Mesopor. Mater.*, **37**, (2000) 33.

177. E. G. Derouane and C. D. Chang, *Micropor. Mesopor. Mater.*, **35/36**, (2000) 425.

178. K. J. Laidler, J. H. Meiser and B. C. Sanctuary, *physical chemistry*, Houghton Mifflin Company, Boston, MA, (2002) 419.

179. C. G. Hill, *an Introduction to Chemical Engineering Kinetics and reactor Design*, John Wiley & Sons, Inc. New york, (1977) 178.

180. M. Guisnet, F. Alvarez, G. Gianetto and G. Perot, Catal. Today 1 (1987) 415.

181. M.A. Saberi, R. Le Van Mao, *Appl. Catal A : General* (2002), in press.

182. K. J. Laidler, *in Chemical Kinetics*, Harper Collins, New York, (1987) 230.

183. M. Polanyi, in Atomic Reactions, Williams-Norgate (London) (1932), cited by R.I. Masel, *in Chemical Kinetics and Catalysis*, Wiley-Interscience, New York, (2001) 738.

184. J. Happel, *in Isotopic assessment of Heterogeneous Catalysis*, Academic Press, Orlando, (1986) 10.

185. M. Durr, A. Biedermann, Z. Hu, U.Hofer, T.F. Heinz, Science, **296**, (2002) 1838.

186. V. Stefanovich and T.N. Truong, *J. Phys. Chem. B*, **102**, (1998) 3018.

187. J. M. Vollmer, E.V. Stefanovich, T.N. Truong, *J. Phys. Chem. B*, **103**, (1999) 9415.

APPENDICES

APPENDIX 1

X-RAY POWDER
DIFFRACTION (XRD) STUDY

The x-ray powder diffraction pattern was recorded for the samples of HY zeolite and modified bifunctional Pt-HY zeolite catalyst, as well as the trifunctional Pt-Zn$_y$-HY (y = 0.9 mmol/g of zeolite), Pt-I$_x$-Zn$_y$-HY (x = 5 mmol/g and y = 0.9 mmol/g of zeolite) and Pt-Al$_y$-HY (y = 0.37 mmol/g of zeolite) zeolite catalysts, by using the diffraction apparatus described in section 2.2.2. The experimental set up and procedures were the same as described in section 2.2.2. An external standard was used instead of internal standard because of the following reasons:

i) possible overlapping of some peaks of the internal standard material with that of the characteristic peaks of the samples

ii) possible occurrence of ion-exchange between cations of standard material and acid sites of zeolite samples during grinding.

The diffraction pattern obtained for each sample was then compared to that of the parent HY zeolite. The degree of crystallinity was determined according to a method similar to the ASTM D3906 as mentioned in ref. [128,129]. In accordance to this method, the sum of the heights of the five most intensive peaks with in the range of 2θ (from $5°$ to $35°$) of the modified zeolite catalysts divided by that of the parent HY zeolite which has been designated to be 100 % crystalline. X-ray diffraction pattern showed that there is minor change in the degree of crystallinity upon Pt loading, some change occurred upon zinc, iodine loading and no change occurred upon Al loading with respect to the parent HY zeolite (Table 3.28 and Figures 3.31 to 3.35).

sample	cation loading (mmol/g)	Si/Al	Degree of Crystallinity (%)
HY	0.00	2.5	100
Pt-HY*	0.00	2.5	99
Pt-Zn$_y$-HY*	0.9	2.5	91
Pt-I$_x$-Zn$_y$-HY*	0.9	2.5	89
Pt-Al$_y$-HY*	0.37	2.5	100

*) Pt = 1 wt. % and I = 5 mmol/g of the zeolite

Table 3.28. Degree of the crystallinity of the bifunctional Pt-HY, trifunctional Pt-Al$_y$-HY (y = 0.37 mmol/g of zeolite), Pt-Zn$_y$-HY (y = 0.9 mmol/g of zeolite) and Pt-I$_x$-Zn$_y$-HY (x = 5 mmol/g and y = 0.9 mmol/g of zeolite) zeolite catalyst using parent HY zeolite as standard which taken to be 100 % crystalline.
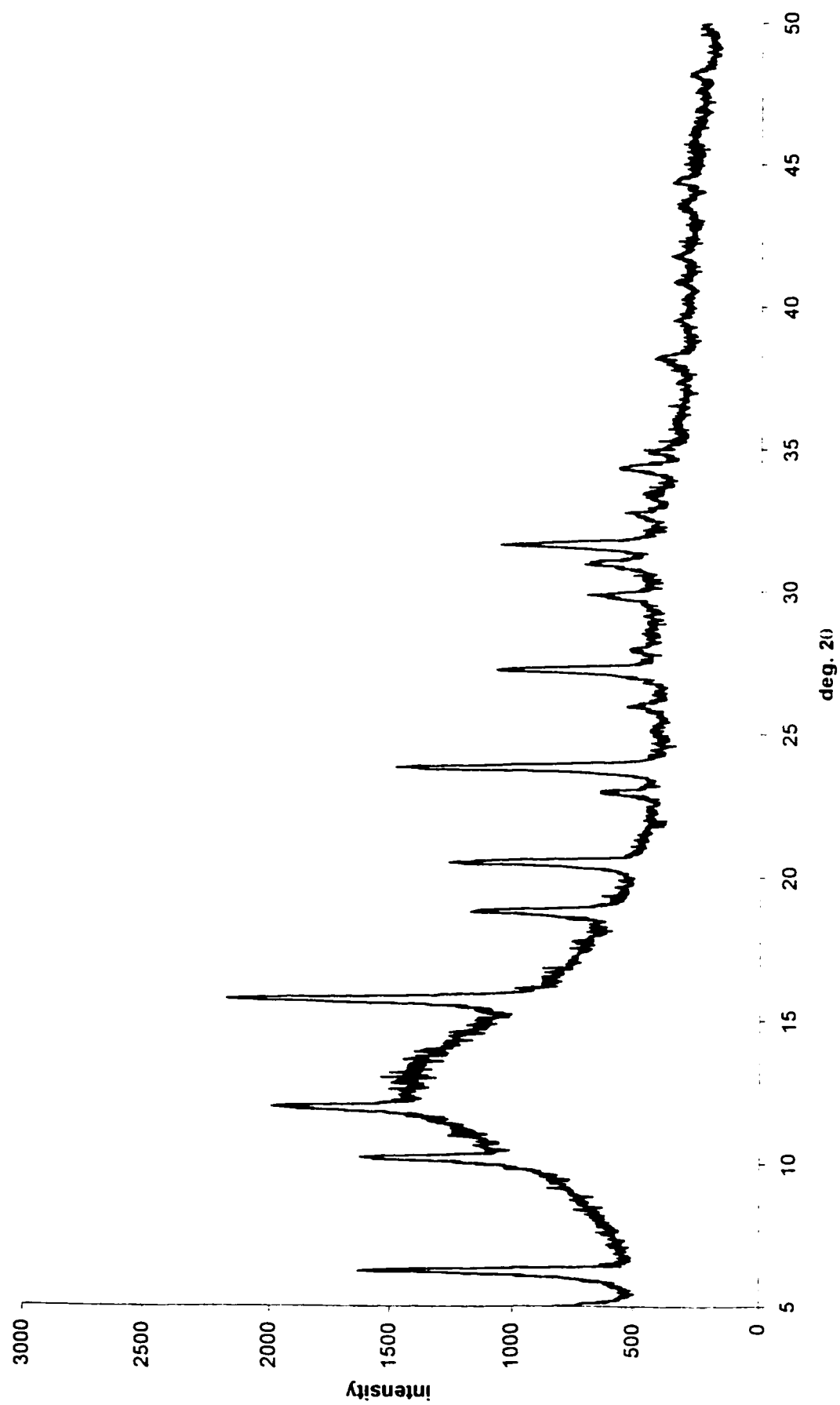
Figure 3.31. X-Ray powder diffraction pattern of the HY zeolite.
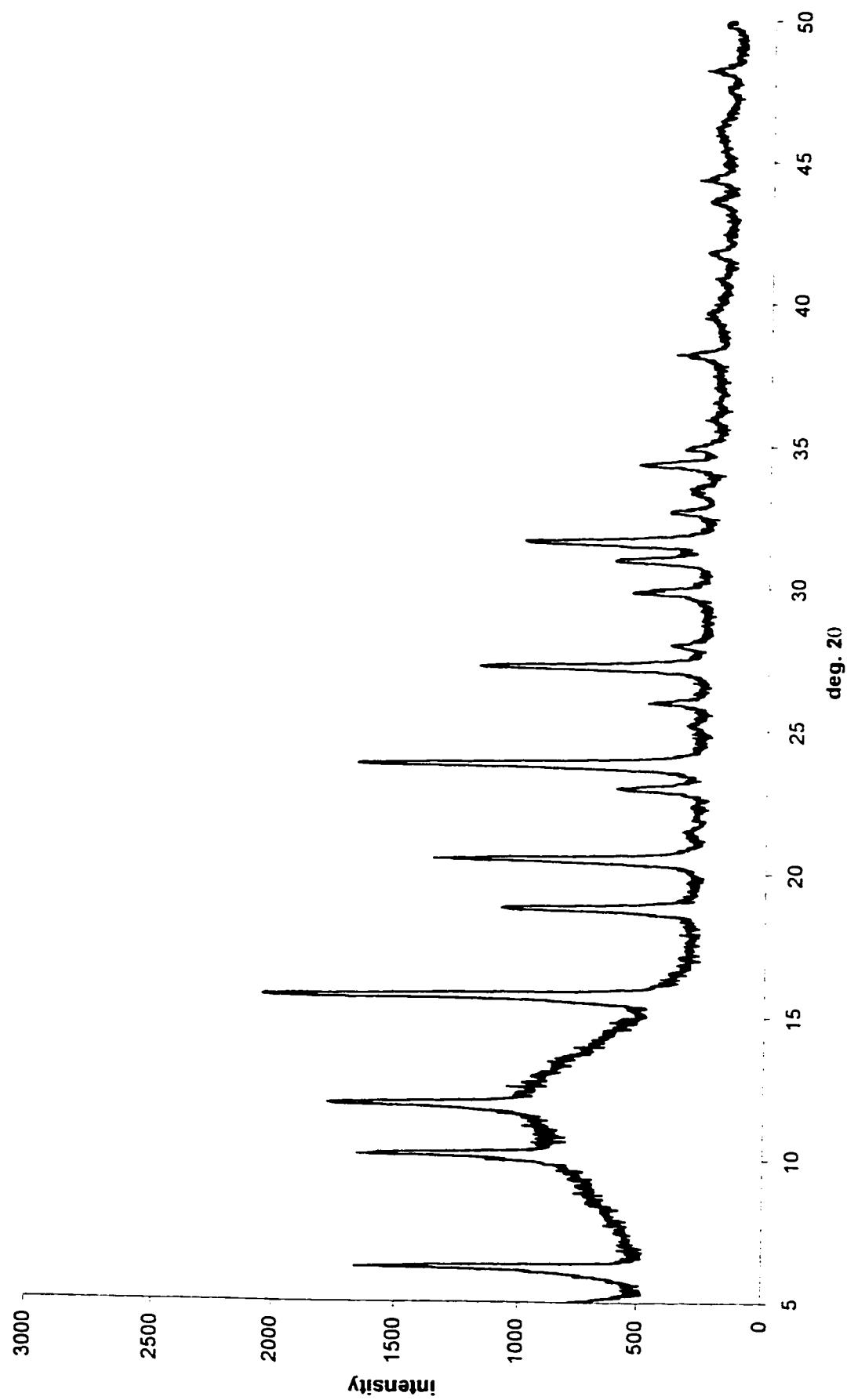
Figure 3.32. X-Ray powder diffraction pattern of the bifunctional Pt-HY zeolite.

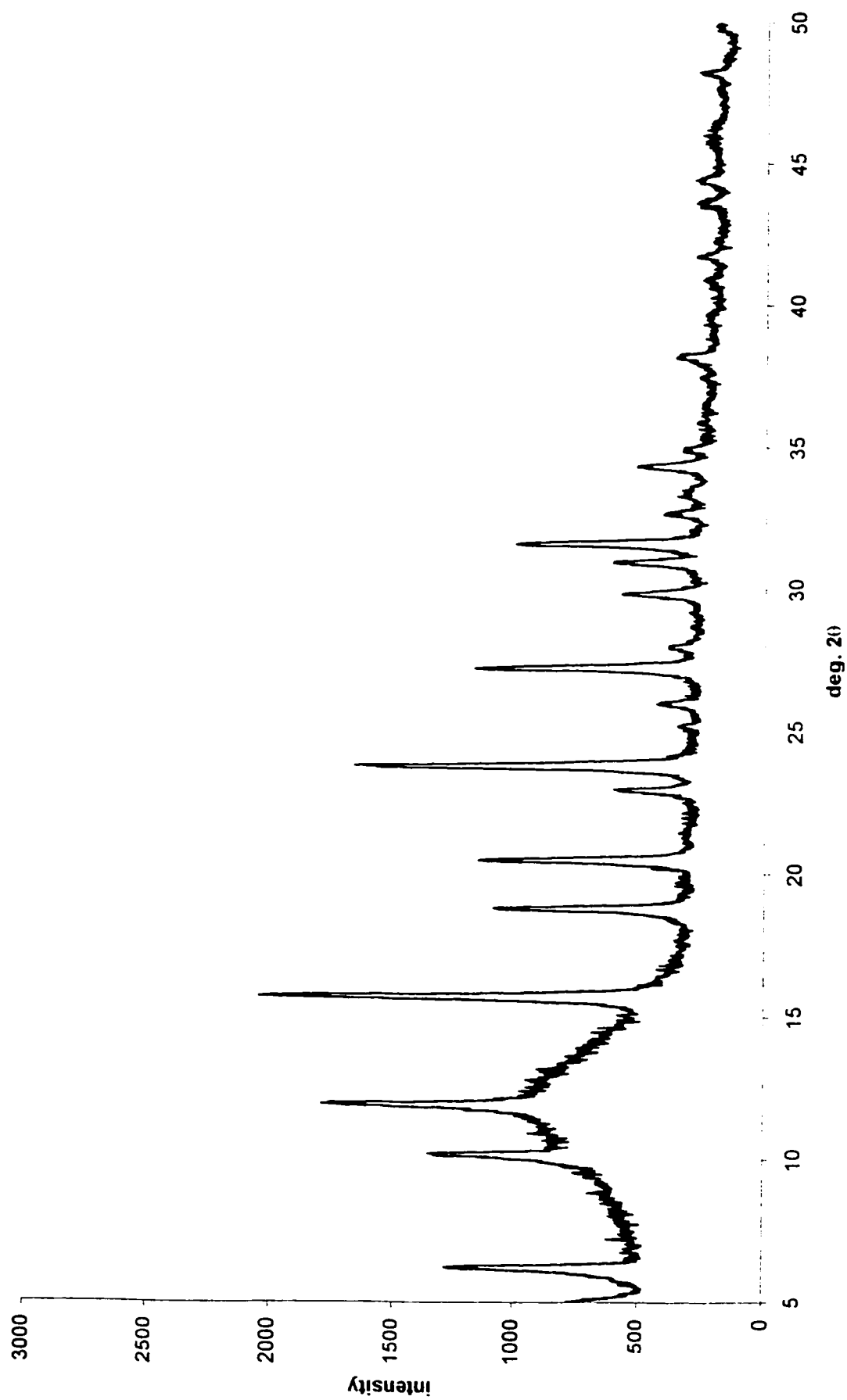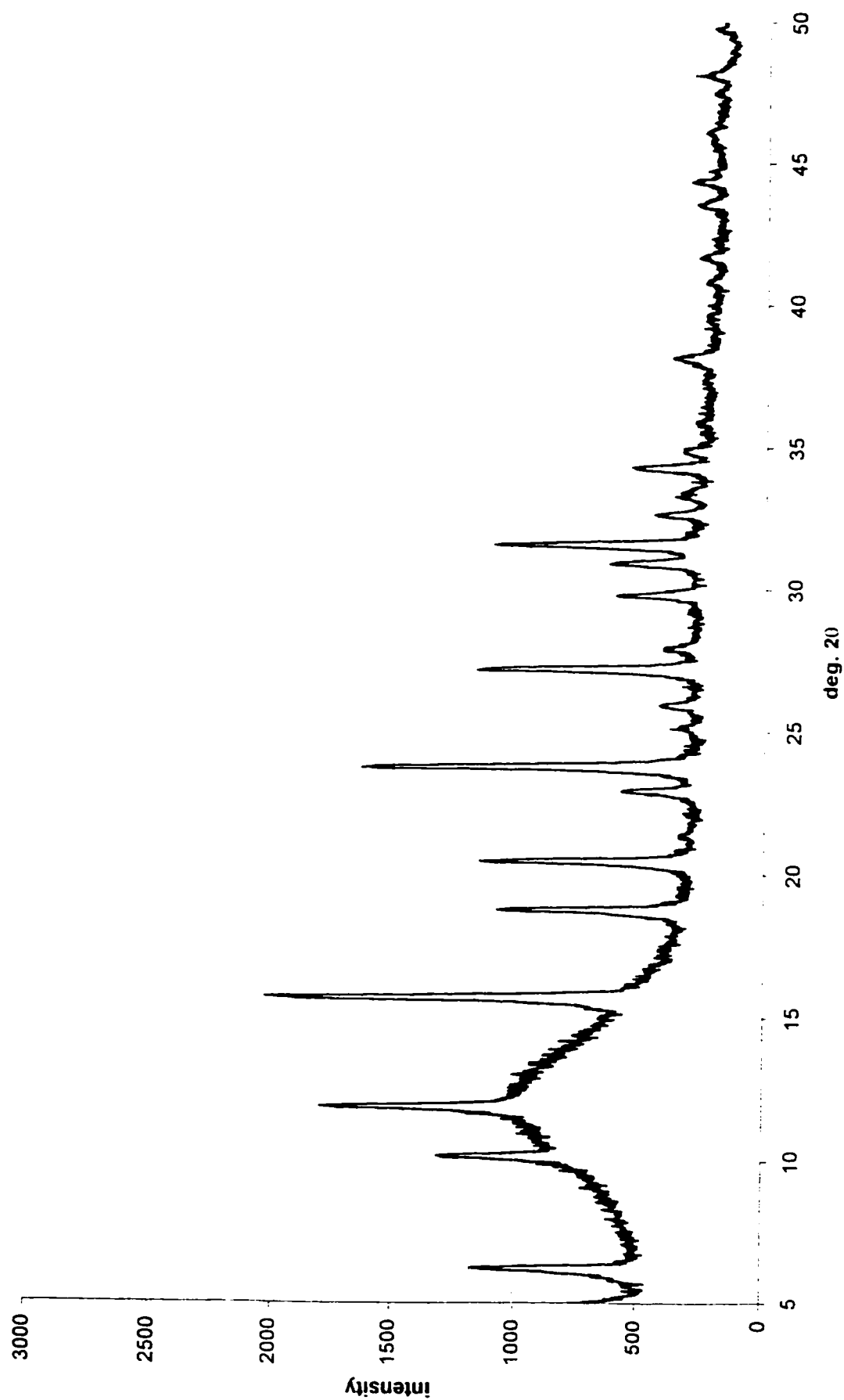Figure 3.33. X-Ray powder diffraction pattern of the trifunctional Pt-Zn$_{0.9}$-HY zeolite catalyst.

Figure 3.34. X-Ray powder diffraction pattern of the iodine treated trifunctional Pt-I$_{0.5}$-Zn$_{0.9}$-HY zeolite catalyst.
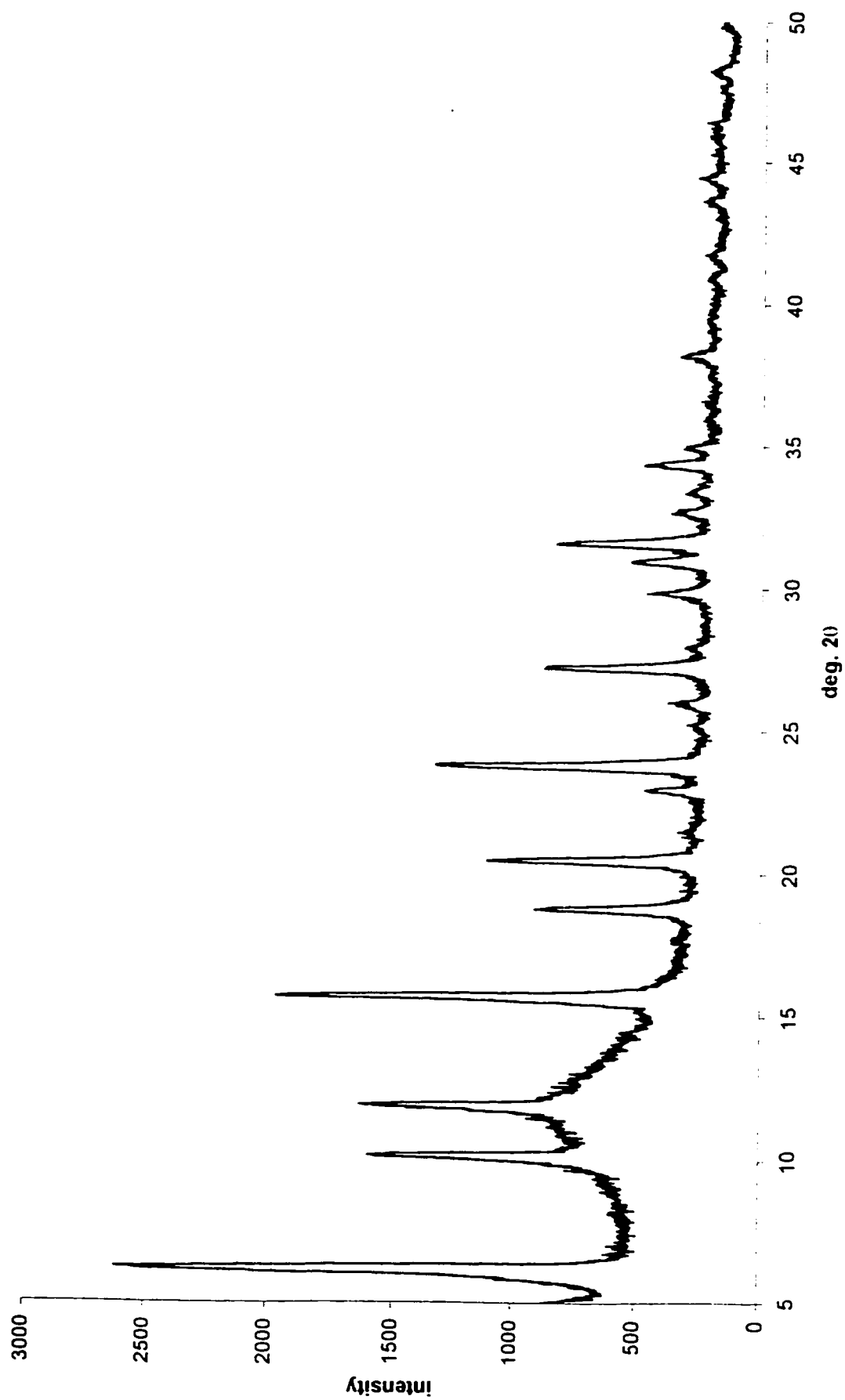
Figure 3.35. X-Ray powder diffraction pattern of the trifunctional Pt-Al$_{0.37}$-HY zeolite catalyst.

APPENDIX 2

PROGRAM IN GWBASIC FOR THE CALCULATION
OF *N*-HEPTANE CONVERSION

```
LIST 0-200
 ' REM **************************************************************
 .. REM HEPTANE Reaction Data Calaculated on Gas & Liquid Phase
 50 REM **************************************************************
 70 DIM NO$(24),NG$(34)
 80 DIM CO(24), CG(34)
 90 DIM FO(24), FG(34)
100 DIM T(34)
110 ' --------------------------------------------------------------
120 ' names and correction factors of the organic phase
130 ' --------------------------------------------------------------
140 DATA iso-Pentane,0.969,Pentane,1.157,Y-01,1.068,22-DMB,1.006,  c-C5,1.068
145 DATA 2-M-P,1.065,3-M-P,1.042,Hexane,1.078,M-cyc-P,1.114,M-b-C7,1.0
150 DATA Monobr-C7,1.078,c-C6,1.144,iso-Octane,0.957,Heptane,1.000,M-c-C6,1.004
155 DATA Mul-bC6,1.006,M-Heptane,0.958,Octane,0.929,Ethyl-Ben,1.05
160 DATA pm-xylene,0.994
165 DATA o-xylene,1.050
170 DATA iso-C9,1.008,nor-C9,1.006
171 DATA C9+,1.003
180 ' --------------------------------------------------------------
190 'NAMES AND CORRECTION FACTORS OF THE GASEOUS PHASE              LIST
200 ' --------------------------------------------------------------
206 ' --------------------------------------------------------------LIST
210 DATA methane,1.21,ethylene,1.34,ethane,1.28,prop lene,1.37
220 DATA propane,1.41,iso-butane,1.42,butylene,1.45
230 DATA n-Butane,1.10,t-Butene,1.54,22-m-P,1.05,c-Butene,1.05,  m-P
   5 DATA iso-Pentane,0.80,Y-02,0.68,Pentane,0.94,2-C5,0.87,  c-C5,1.05
240 DATA 2-c-C5,0.98,2-M-P,0.98,3-M-P,0.98,hexane,1.02,M-b-C7,1.0
245 DATA M-c-C6,1.07,Benzene,1.15,McC7,1.11,Cyc-C6,1.05,iso-Octane,1.  ,Heptane,
0.95
248 DATA MuB-C6,1.11,Toluene,1.15,m-Heptane,1.02,Octane,1.01,pm-xylene,1.18,22DM
B,1.00
250 REM **************************************************************
260 REM introduction
270 REM **************************************************************
280 FOR I=1 TO 24
290    READ NO$(I),CO(I)
300 NEXT
310 FOR I=1 TO 34
320    READ NG$(I),CG(I)
330 NEXT
340 REM **************************************************************
350 REM enter experimental data (area or area %)
360 REM calculation of moles of carbon
0

1LIST   2RUN

500 FOR I=1 TO 24
0
LIST 360-550
 360 REM calculation of moles of carbon
 370 REM part 1: organic phase
 380 REM **************************************************************
 390 INPUT "catalyst :";C$
 400 INPUT "run # : ";F1$
 410 INPUT "data performed :";D$
 420 INPUT "temperature reactor ii :";F1l$
 430 INPUT "Heptane Feed(WHSV):";P
```

```
450 INPUT "H2 feed (ml/min):":V
460 PRINT
470 PRINT "organic phase"
480 INPUT "weight of organic phase :":W
490 IF W > 0 THEN GOTO 750
500 FOR I=1 TO 24
510    T(I)=0
520    PO(I)=0
530 NEXT I
550 X=W/14.02
0

ILIST
LIST 550-750
550 X=W/14.02
560 PRINT "enter the area %"
570 S=0
580 FOR I=1 TO 24
590    PRINT NO$(I);
600    INPUT PO(I)
610    T(I) = PO(I)*CO(I)
620    S = S+T(I)
630 NEXT I
640 PRINT
650 PRINT
660 FOR I=1 TO 24
670    PRINT NO$(I),PO(I)
680 NEXT I
690 INPUT "areas ok ? or n:":A$
700 IF A$ = "n" THEN GOTO 560
710 PRINT
720 PRINT
730 REM ************************************************************************
740 LPRINT "catalyst:":C$
750 LPRINT "run # :":R1$, "date :":D$

0
list 750-950
750 LPRINT "run # :":R1$, "date :":D$
760 LPRINT "temperature (1) :":R1$:"c"
770 LPRINT "Heptane Feed (WHSV) = ":F:"hr-1"
780 LPRINT "N2 feed :":N$:"ml/min"
790 LPRINT "H2 feed :":V:"ml/min"
800 LPRINT
810 LPRINT "organic phase"
820 LPRINT "wt. organic phase :":W:"g."
830 LPRINT
840 LPRINT "compound","area %","correction","moles of carbon"
850 FOR I=1 TO 24
860    T(I) = T(I)/S
870    T(I) = T(I)*X
880 LPRINT NO$(I),PO(I),CO(I),T(I)
890    PO(I)=T(I)
900 NEXT I
910 LPRINT
920 LPRINT
940 LPRINT "organic phase";X; "c. atoms"
950 LPRINT


        CRUN

LIST 950-1150
950 LPRINT
960 REM ***********************************************************************
970 REM part 3: gaseous phase
```

```
980 REM ***********************************************
990 PRINT
1000 PRINT "gaseous phase"
1010 PRINT "enter aerage  area %"
1020 S=0
1030 FOR I=1 TO 34
1040    PRINT NG$(I);
1050    INPUT PG(I)
1060    T(I) = PG(I) * OG(I)
1070    S = S + T(I)
1080 NEXT I
1090 PRINT
1100 FOR I=1 TO 34
1110    PRINT NG$(I),PG(I)
1120 NEXT I
1130 INPUT "area % ok  y or n ";A$
1140 IF A$ = "n" THEN GOTO 990
1150 FOR I=1 TO 34
O

        2RUN
1150 FOR I=1 TO 34
1160    T(I)=T(I)*100/S
1170 NEXT I
1190 LPRINT "gas phase"
1200  D = 1.65143E-06
1210 LPRINT "c. atoms:";D
1240 INPUT "sample time minutes:";T1
1250 LPRINT "sample time:";T1;"minutes"
1260 INPUT "enter average volume from the bubble meter (in ml.) :";V3
1270 LPRINT "average bubble meter :";V3" ml."
1280 INPUT "enter calibration factor totalizer  20 : ";V4
1290 LPRINT "calibration factor totalizer :";V4
1300 INPUT "enter calibration factor mfm 20 :";V5
1310 LPRINT "calibration factor mfm :";V5
1320 T1 = V4 * T1 * V3 / V5
1330  T1 = T1 * D * (100 - T(34)) / T(34)
1340 LPRINT
1350 LPRINT  T1;" c. atoms"
1360 LPRINT
1370 LPRINT "compound","area %","correction","c. atoms"
1380 S=0
1390 FOR I=1 TO 33
O

1LIST   2RUN
O
LIST 1390-1590
1390 FOR I=1 TO 33
1400    S = S + T(I)
1410 NEXT I
1420 FOR I=1 TO 33
1430    T(I) =T(I) / S
1440    T(I) =T(I) * T1
1450    LPRINT NG$(I),PG(I),OG(I),T(I)
1460    PG(I) = T(I)
1470 NEXT I
1480 LPRINT
1500 REM ***************************************************
1510 REM part 4: conversion
1520 REM ***************************************************
1530 LPRINT
1540 LPRINT "conversion"
1550 LPRINT
1560 INPUT " Heptane injected by Syring ( g ):"; TP
1570 LPRINT " Heptane injected by Syring = "; TP; " g "
1580 LPRINT
```

```
1590 PI = (TR+T)/100.21
O

          /RUN
LIST 1590-1790
1590 PI = (TR+T)/100.21
 1600 LPRINT "Heptane Injected = "; PI; "C-atoms"
 1610 PR = PI - PO(14)+RG(28)
.1620 LPRINT "Heptane Reacted: "; PR; "C-atoms"
1630 LPRINT
1640 LPRINT "% Heptane Conversion:"; (PR/PI)*100
1650 LPRINT
1660 S=0
1670 FOR I =1 TO 24
1680    S=S+PO(I)
1690 NEXT I
1700 FOR I=1 TO 33
1710    S=S+RG(I)
1720 NEXT I
1730 LPRINT "% total hydrocarbons recovered:";S/(PI)*100;"%"
1740 LPRINT
1750 LPRINT
1760 REM ****************************************************************
1770 REM part 5: resume
1780 REM ****************************************************************
1790 LPRINT "resume"
O


1800 I =RG(15) +RG(2)
O
LIST 1790-1850
 1790 LPRINT "resume"
 1770 LPRINT
1800 P = S - RG(28) +PO(14)
1804 Q = P * 100 / S
1806 LPRINT "% Heptane Conversion Basing on Products == "; Q
1808 LPRINT
1810 LPRINT "  items ","yield","selectivity"
1812 LPRINT "+++++++++++++++++++++++++++++++++++++++++++++++++++++++++++"
1814 LPRINT
1820 LPRINT NG$(1),RG(1)*100/S,RG(1)*100/P
1822 LPRINT
1824 Z = RG(2) + RG(3)
1826 LPRINT "carbon-2:",Z *100/S,Z*100/P
1830 LPRINT NG$(2),RG(2)*100/S,RG(2)*100/P
1840 LPRINT NG$(3),RG(3)*100/S,RG(3)*100/P
1842 Z = RG(4) + RG(5)
1844 LPRINT
1846 LPRINT "carbon-3:",Z *100/S,Z*100/P
1850 LPRINT NG$(4),RG(4)*100/S,RG(4)*100/P
O


1LIST   2RUN
1940 LPRINT "Carbon-7:", Z*100/S, "--------"
1950 L = RG(28) + PO(14)
O
'IST 1850-1900
 .50 LPRINT NG$(4),RG(4)*100/S,RG(4)*100/P
1860 LPRINT NG$(5),RG(5)*100/S,RG(5)*100/P
1862 LPRINT
1864 Z =RG(6) + RG(7) + RG(8) + RG(9) +RG(11)
1866 LPRINT "carbon-4:",Z*100/S,Z*100/P
1868 LPRINT "nor-C4:",RG(8)*100/S,RG(8)*100/P
1870 LPRINT "iso-C4:",RG(6)*100/S,RG(6)*100/P
1872 LPRINT "un-C4:", (RG(7)+RG(9)+RG(11))*100/S, (RG(7)+RG(9)+..)*100/P
```

```
1874 LPRINT
1876 Z =PG(10)+PG(12)+PG(13)+PG(14)+PG(15)+PG(16)+PG(18)+RO(1)+PO(2)+PO(3)+RO(5)
1878 LPRINT "carbon-5:",Z*100/S,Z*100/P
1880 Z =PG(15)+PO(2)
1890 LPRINT "nor-C5:",Z*100/S,Z*100/P
1892 Z = PG(10)+PG(12)+PG(13)+PG(14)+PG(16)+RO(1)+PO(3)
1894 LPRINT "iso-C5:",Z*100/S,Z*100/P
1896 Z = PG(18)+RO(5)
1898 LPRINT "cyc-C5:",Z*100,S,Z*100/P
1900 LPRINT
0

1LIST  2RUN
LIST 1900-1984
1900 -1984
1902 Z =PG(17)+PG(19)+PG(20)+PG(21)+PG(22)+PG(26)+PG(24)+PO(4)+PO(6)+PO(7)+PO(8)
+PO(9)+PO(12)
1904 LPRINT "carbon-6:",Z*100/S,Z*100/P
1906 Z =PG(21)+ RO(8)
1908 LPRINT "nor-C6:",Z*100/S,Z*100/P
1910 Z = PG(17)+PG(19)+PG(20)+RO(4)+RO(6)+RO(7)
1912 LPRINT "iso-C6:",Z*100/S,Z*100/R
1914 Z =PG(23)+PG(26)+RO(9)+PO(12)
1916 LPRINT "cyc-C6:",Z*100/S,Z*100/R
1920 LPRINT
1922 LPRINT
1924 LPRINT
1930 Z =PG(22)+PG(25)+PG(28)+RO(10)+RO(11)+PO(14)
1940 LPRINT "Carbon-7:", Z*100/S, "--------"
1950 L = PG(28)+ RO(14)
1960 LPRINT "nor-C7:", L*100/S, "--------"
1970 B = PG(22)+ PO(11)
1980 LPRINT "i-5-17", B*100/S, B*100/P
1982 M = PG(25)+ PG(10)
1984 LPRINT "mu-b-C7", M*100/S, M*100/P
0

1LIST  2RUN  3 L O A D  "     4  S A V E "
LIST 1984-2000
1984 LPRINT "mu-b-C7", M*100/S, M*100/P
1986 LPRINT
1990 LPRINT
2000 OG = PG(27)+PG(29)+PG(31)+PG(32)+PG(34)+PG(30)+PG(33)
2010 G = PO(13)+PO(16)+PO(17)+PO(18)+PO(20)+PO(21)
2012 L = PO(19)+ PO(22)+ RO(23)+ RO(24)
2014 O = OG + G + L
2030 LPRINT "Others", O*100/S, O*100/P
2040 LPRINT
2050 LPRINT
2052 IS = B + M + O
2054 LPRINT "Isomerization:", IS*100/S, IS*100/P
2065 CR = P - IS
2070 LPRINT "Cracking", CR*100/S, CR*100/P
2080 LPRINT
2090 LPRINT " Ratio of", "Iso / Cracking = " , IS/CR
2100 LPRINT
2110 LPRINT
2112 LPRINT
2114 LPRINT "++++++++++++++++++++++++++++++++++++++++++++++++++++"
2120 STOP
0

1LIST  2RUN  3 L O A D  "     4  S A V E "
CONTS., "LPT1     7 T R "
```